



Numerical study of non-Newtonian fluids past a stretching cylinder



By

Muhammad Naseer

*Department of Mathematics
Quaid-I-Azam University
Islamabad, Pakistan
2017*

Numerical study of non-Newtonian fluids past a stretching cylinder



By

Muhammad Naseer

Supervised By

Prof. Dr. Muhammad Yousaf Malik.

*Department of Mathematics
Quaid-I-Azam University
Islamabad, Pakistan
2017*

Numerical study of non-Newtonian fluids past a stretching cylinder



By

Muhammad Naseer

DOCTOR OF PHILOSOPHY
IN

MATHEMATICS

Supervised By

Prof. Dr. Muhammad Yousaf Malik.

*Department of Mathematics
Quaid-I-Azam University
Islamabad, Pakistan
2017*

Dedicated

To

*My Father and
Mother*

Acknowledgement

*I start my acknowledgment to saying Thanks Almighty **Allah** for giving me strength, wisdom, confidence and perseverance to continue my studies, without His sufficient grace and mercy; I would not have been able to complete this work. After Almighty **Allah** I say thanks to the **Holly Prophet Hazrat Muhammad** (Peace be upon him) who emphasized the importance of knowledge by saying “Learn the knowledge from cradle to grave”.*

*Special thanks form the core of my heart to great teacher kind supervisor and Chairman of Mathematics Department, **Prof. Dr. Muhammad Yousaf** Malik for his encouragement and providing me with an excellent atmosphere for doing research. I am grateful to, **Prof. Dr. Sohail Nadeem**, **Prof. Dr. Tasawer Hayat**, **Prof. Dr. Muhammad Ayub** and all faculty members for providing me facilities and proper atmosphere to complete the research work.*

*I can't imagine completing my acknowledgement without considering my friends. So I want to thank **Prof. Dr. Rehmat Ellahi**, **Dr. Abdul Rehman**, and specially **Khalif-ur-Rehman**. I also thanks to my worthy colleagues **Iqbal Ahmed Azhar**, **Naveed Akmal**, **Muhammad Saleem Iqbal** and all others who supported me during my research period. Thanks for being around and sharing several good times together during my stay in the university.*

Muhammad Naseer

Author's Declaration

I **Muhammad Naseer** hereby state that my PhD thesis titled

Numerical study of non-Newtonian fluids past a stretching cylinder

is my own work and has not been submitted previously by me for taking any degree from the Quaid-i-Azam University Islamabad, Pakistan or anywhere else in the country/world.

At any time if my statement is found to be incorrect even after my graduate the university has the right to withdraw my PhD degree.

Student/Author Signature: _____

Name of Student: **Muhammad Naseer**

Date: **04-05-2017**

Plagiarism Undertaking

I solemnly declare that research work presented in the thesis titled “**Numerical study of non-Newtonian fluids past a stretching cylinder**” is solely my research work with no significant contribution from any other person. Small contribution/help wherever taken has been duly acknowledged and that complete thesis has been written by me.

I understand the zero tolerance policy of the HEC and **Quaid-i-Azam University** towards plagiarism. Therefore, I as an Author of the above titled thesis declare that no portion of my thesis has been plagiarized and any material used as reference is properly referred/cited.

I undertake that if I am found guilty of any formal plagiarism in the above titled thesis even afterward of PhD degree, the University reserves the rights to withdraw/revoke my PhD degree and that HEC and the University has the right to publish my name on the HEC/University Website on which names of students are placed who submitted plagiarized thesis.

Student/Author Signature: _____

Student Name : **Muhammad Naseer**

Certificate of Approval

This is to certify that the research work presented in this thesis entitled **Numerical Study of Non-Newtonian Fluids Past a Stretching Cylinder**, was conducted by **Mr Muhammad Naseer** under the supervision of **Professor Dr Muhammad Yousaf Malik**. No part of this thesis has been submitted anywhere else for any other degree. This thesis is submitted to the department of Mathematics, Quaid-i-Azam University, Islamabad in partial fulfillment of the requirements for the degree of Doctor of Philosophy in the field of Mathematics from the Department of Mathematics, Quaid-i-Azam University, Islamabad, Pakistan.

Student Name: **Mr Muhammad Naseer**

Signature:

External Committee:

a) External Examiner 1:

Signature

Dr. Nazir Ahmad Mir

Designation: Professor

Office address: Department of Basic Sciences,
Riphah International University, I-14 Hajj Complex, Islamabad.

b) External Examiner 2:

Signature

Dr. Muhammad Mushtaq

Designation: Assistant Professor

Office address: COMSATS, Institute of Information Technology
Park Road Chak Shehzad, Islamabad.

c) Internal Examiner:

Signature

Dr. Muhammad Yousaf Malik

Designation: Professor

Office address: Department of Mathematics,
Quaid-I-Azam University, Islamabad Pakistan.

d) Supervisor Name:

Signature

Dr. Muhammad Yousaf Malik

Designation: Professor

Office address: Department of Mathematics,
Quaid-I-Azam University, Islamabad Pakistan.

e) Name of Dean/HOD:

Signature

Dr. Muhammad Yousaf Malik

Designation: Professor

Office address: Department of Mathematics,
Quaid-I-Azam University, Islamabad Pakistan.

Numerical Study of Non-Newtonian Fluids Past a Stretching Cylinder

By

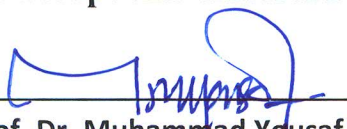
Muhammad Naseer

CERTIFICATE

A DISSERTATION SUBMITTED IN THE PARTIAL FULFILMENT OF THE
REQUIREMENTS FOR THE DEGREE OF DOCTOR OF PHILOSOPHY

We accept this dissertation as conforming to the required standard.

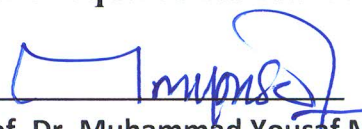
1.



Prof. Dr. Muhammad Yousaf Malik

(Supervisor)

2.



Prof. Dr. Muhammad Yousaf Malik

(Chairman)

3.

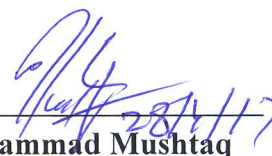


Professor Dr. Nazir Ahmad Mir

(External Examiner)

Department of Basic Sciences,
Riphah International University,
I-14 Hajj Complex, Islamabad.

4.



Dr. Muhammad Mushtaq

(External Examiner)

COMSATS, Institute of Information
Technology Park Road
Chak Shehzad, Islamabad.

Department of Mathematics
Quaid-I-Azam University
Islamabad, PAKISTAN
2017

Contents

1	Introduction	4
2	Boundary layer flow of a Casson nanofluid over a vertical exponentially stretching cylinder	14
2.1	Introduction	14
2.2	Mathematical formulation	14
2.3	Solution of the problem	15
2.4	Results and discussion	16
2.5	Conclusions	21
3	Numerical study of convective heat transfer in flow of power law fluid by an exponentially stretching cylinder	22
3.1	Introduction	22
3.2	Formulation	22
3.3	Solutions	23
3.4	Discussion	24
3.5	Conclusions	28
4	Boundary layer flow of an incompressible tangent hyperbolic fluid past a stretching cylinder	29
4.1	Introduction	29
4.2	Fluid model	29
4.3	Formulation	31

4.4	Solution	32
4.5	Results and discussion	33
4.6	Conclusions	36
5	Flow of Williamson fluid past a vertical exponentially stretching cylinder	37
5.1	Introduction	37
5.2	Mathematical formulation	37
5.3	Solution of the problem	38
5.4	Outcomes	39
5.5	Conclusions	43
6	Boundary layer flow of Williamson nanofluid past a vertical exponentially stretching cylinder	44
6.1	Introduction	44
6.2	Formulation	45
6.3	Solution of the problem	46
6.4	Results and discussion	47
6.5	Conclusions	52
7	Dual stratified mixed convection flow of Eyring-Powell fluid past an inclined stretching cylinder with heat generation/absorption effect	53
7.1	Introduction	53
7.2	Formulation	54
7.2.1	Flow analysis	54
7.2.2	Heat and mass transfer analysis	57
7.3	Results and discussion	58
7.3.1	Numerical solution	58
7.3.2	Velocity profiles	63
7.3.3	Temperature profile	66
7.3.4	Concentration profile	68
7.4	Conclusions	71

8	Boundary layer flow of second grade fluid past a vertical exponentially stretching cylinder	72
8.1	Introduction	72
8.2	Mathematical formulation	72
8.3	Solution of the problem	73
8.4	Homotopy solution	74
8.4.1	Zeroth-order deformation problems	75
8.4.2	mth-order deformation problems	75
8.5	Discussion	76
8.6	Conclusions	81

Chapter 1

Introduction

The unavailability of a solitary stress tensor that can be used to model all the non-Newtonian fluids diversifies the field of fluid mechanics from other disciplines. For flow problems allied with diverse fluid models the attained mathematical formalisms consists of a set of coupled highly non-linear partial differential equations. In numerous situations, the exact solution for such system, for a wide range of the involved physical parameters is yet a dream for the researchers even after putting enormous labor. The concept of boundary layers has overcome this exertion in various circumstances. The idea was first socialized by Ludwig Prandtl when he presented his paper at the 3rd International Congress of Mathematicians in Heidelberg, Germany in 1904 [1]. Since then, the theory is applied to virtually all the available non-Newtonian fluid models for diverse problems of fluid flowing under different physical constraints and the highly nonlinear coupled system of partial differential equations is abridged into a much simple one by systematically negating the less contributing slice. Mathematically, the role of the boundary layer is often to reduce the original elliptic nature scheme of partial differential equations into a more simple parabolic nature. The sensitivity of boundary layer theory is exceedingly enhanced by Blasius by adding the essence of transformed domain similarity solutions for the problem of viscous fluid flow past a flat plate [2]. Together, the boundary layer approximations and the similarity transformations has become a strong tool for the researchers and have been successfully applied on almost every available fluid model. Abel *et al.* [3] inspected the boundary layer flow of a second grade fluid past a stretched surface. Sahoo and Do [4] have probed into the effects of magnetic field and the partial slip on the flow and heat transfer of an electrically

conducting third grade fluid flow due to a linearly stretched surface. In another work, Sahoo and Poncet [5] have inspected the effects of slip and magnetic field on the flow and heat transfer of an incompressible, electrically conducting fourth grade fluid, flowing past an infinite porous plate. Nadeem *et al.* [6] have studied the magnetohydrodynamic effects over the boundary layer flow of a Casson fluid, for the case when the fluid is flowing in two lateral directions past a porous linearly stretched surface. Khan and Khan [7] have presented the solutions of the steady boundary layer flow of Williamson fluid, flowing under four different situations, namely the Blasius flow, the Sakiadis flow, the stretching and the stagnation point flows. Tonekaboni et al. [8] have presented the similarity solutions for three different cases of the boundary layer flow of non-Newtonian viscoelastic Walters' B fluid flow, namely stagnation-point flow problem, the Blasius flow problem and the Sakiadis flow problem. Hayat et al. [9] have presented the solutions for the problem of boundary layer flow and heat transfer for the Eyring Powell fluid flowing over a moving surface with convective boundary conditions by means of homotopy analysis method. Rehman and Nadeem [10] have discussed the problem of nanoparticles effects over the boundary layer flow of a micropolar fluid flowing over a vertical slender cylinder. Wang and Chen [11] have discussed the problem of steady laminar boundary layer flow of a non-Newtonian power-law fluid flowing past a semi-infinite symmetric structure with a wavy surface and a uniform wall temperature such that the axis of symmetry is aligned with the oncoming uniform stream. Khan et al. [12] have examine the influence of magnetic field and chemical reaction over the boundary layer flow of an electrically conducting non-Newtonian couple stress fluid flowing over sheet that is stretched along its surface with a non-linear surface stretching velocity. Nadeem et al. [13] have discussed the effects of magnetohydrodynamics and nanoparticles for the boundary layer flow of non-Newtonian Maxwell fluid flowing past a stretching sheet. Akber et al. [14] have analyzed the problem of boundary layer flow of tangent hyperbolic fluid towards a stretching sheet. Malik et al. [15] have studied the boundary layer flow and heat transfer in Sisko fluid flowing over a nonisothermal nonlinearly stretching surface with convective boundary condition under the influence of a uniform transverse magnetic field. Hayat et al. [16] have presented the analysis for momentum and thermal boundary layers arising from the motion of Carreau fluid flowing above a stretching sheet with convective boundary conditions. Hamad et al. [17] have studied the dynamics of the thermal boundary layer flow of a steady, incompressible non-

Newtonian Jeffrey fluid near the stagnation point on a stretching sheet taking into account the thermal jump condition at the surface of the sheet. Hayat and Mumtaz [18] have presented an analysis for the hydromagnetic boundary layer flow of a non-Newtonian Johnson-Segalman fluid flowing over a semi-infinite expanse of electrically conducting rotating plate in the presence of a transverse magnetic field. Phan-Thien [19] has obtained the solutions for the boundary layer stagnation point flows of an Oldroyd-B fluid flow for the case of plane stagnation point and axi-symmetric stagnation flows. Ravindran et al. [20] analyzed the occurrence of boundary layers due to the flow of a Burgers' fluid flow in an orthogonal rheometer. Pai and Kandasamy [21] have studied the momentum boundary layer profile due to the entrance region flow of a Herschel-Bulkley fluid flowing through an annular cylinder. Nirmalkar et al. [22] have studied the boundary layer creeping flow of a Bingham plastic fluid flowing past a two dimensional cylinder of square cross-section.

The study of stretching sheet was initiated by Crane [23]. Since then, the study of fluid past a stretching surface has become a problem of concentration for researchers due to its inclusive usage in wire drawing, polymer processing, glass blowing, metal spinning, manufacturing, cooling of metallic plates, extrusion of polymers, purification of liquefied metal from non-metallic inclusion, manufacturing process of artificial films and fibers, polymeric sheets, crystal growing and hot rolling. It is also used to assemble car body works in automobiles and to manufacture aircraft fuselages in aeronautics. It is experimentally validated that at high temperature; material passes through extrusion in liquefied state. This elongation of material is approximately proportional to the distance from the stagnation point. Particularly, for the flow problem over an exponentially stretching surface, the annealing and thinning of copper wires, the final product depends on the heat transfer rate at the surface of the stretching continuous object with exponential variations of stretching velocity and temperature distribution. During such practices, the kinematics of stretching and the heating/cooling have a crucial impact on the quality of the final products [24]. Mahapatra and Gupta [25] have debated the stagnation point flow of viscous fluid over a flat deformed sheet. They perceived a boundary layer immediate to the stretching surface and also observed that the configuration of this boundary layer rests on the ratio of the velocity of the stretching surface to that of the frictionless potential flow in the neighborhood of the stagnation point. Bachok et al. [26] explained the problem

of stagnation point flow over a stretching/shrinking sheet which is placed inside a nano fluid. The solution was carried for three specific water-based nano particles that are copper, alumina and titania. According to their results skin-friction coefficient has the largest magnitude for copper while the least for alumina while the local Nusselt numbers have the largest values for copper while the least for titania. Chiam [27] studied the problem of boundary layer flow and heat transfer of an electrically conducting fluid over a non-isothermal stretching sheet under the influence of a transverse magnetic field. Salleh et al. [28] have provided numerical solutions using Keller-box technique for the problem of boundary layer flow and heat transfer over a stretching sheet with Newtonian heating. They examined the influence of Prandtl number over the temperature profiles and the heat transfer coefficient. They were of the view that the thermal boundary layer thickness has a strong dependence upon the Prandtl number and that the temperature profile decreases with an increase in the Prandtl number. Mukhopadhyay [29] has numerically analyzed the problem of boundary layer flow and heat transfer towards a porous exponentially stretched sheet in presence of a magnetic field with partial slip conditions for the velocity and temperature functions at the surface of the sheet. She concluded that the surface shear stress is an increasing function of the magnetic field parameter and that the thermal boundary layer thickness is an increasing function of both the magnetic field parameter and the non-dimensional radiation parameter. In another effort, Mukhopadhyay [30] has presented the numerical results for the problem of steady, incompressible magnetohydrodynamic boundary layer flow and heat transfer of a viscous fluid flowing over a porous surface that is stretched with some exponential velocity along the surface of the object and is embedded in a thermally stratified medium. She obtained the result that the velocity field is suppressed by both the magnetic field parameter and the suction parameter. She also commented that the rate of heat transfer is a decreasing function of the non-dimensional stratification parameter. Fang and Zhong [31] have presented closed form analytic solutions for the boundary layer flow over a stretching/shrinking sheet with different stretching/shrinking velocity distributions assumed at the surface of the cylinder. They considered the surface stretching velocities to be linear, bilinear, nonlinear exponential, quadratic, power-law and periodic functions of the distance over the points on the surface of the cylinder from that of the stagnation point.

They commented that solution for such a problem is important for the case when mass

transfer at the wall is a function of the surface stretching velocity of the wall. Bhargava et al. [32] have studied the problem of steady incompressible boundary layer flow of the non-Newtonian micropolar fluid flow, heat and mass transfer over a nonlinear stretching Sheet. The problem was solved numerically with the help of finite difference and the finite element methods. Their work showed that the solutions obtained with both the methods were in contract. They concluded that the convective parameter can adeptively be used for stability of the temperature distribution. In another work, Fang et al. [33] analyzed the slip flow of viscous fluid flowing over a stretching/shrinking surface. They solved the problem for Wu's second order slip flow model. Merkin and Kumaran in their work [34] have examined the problem of unsteady, 2D laminar, incompressible, boundary layer flow of a viscous fluid flowing over an impulsively stretching/shrinking sheet. The fluid was assumed to be under the influence of a constant transverse magnetic field. Different solutions were obtained depending upon distinct values of the magnetic parameter, that is, the strength of the imposed magnetic field relative to the stretching velocity of the surface. In [35], Yacob et al. have commented over the melting effects over the boundary layer flow and heat transfer of a non-Newtonian micropolar fluid flowing over a stretching/shrinking sheet. They observed that the presence of melting route has decreased the friction and the heat transfer rate at the solid-liquid interface. Zheng et al. [36] have analyzed the problem of boundary layer for the flow and radiative heat transfer of an incompressible non-Newtonian micropolar fluid flowing over a stretching/shrinking sheet with nonlinear power-law surface stretching velocity and temperature functions. They applied the homotopy analysis method to obtain the dual solutions associated with the problem and included a detailed analysis of the effects of power-law index on the velocity and radiative temperature fields. Ishak et al. [37] have obtained numerical solutions through the Keller-box technique for the problem of flow and heat transfer of steady, incompressible boundary layer viscous fluid flowing outside a stretching permeable hollow cylinder with suction/injection. Their important observation was that the skin friction coefficient remains unchanged with varying Prandtl numbers and that skin friction reduces when the fluid flow is influenced by injection. They also predicted that in case of feeble injection, water is a healthier cooling mediator than air.

Ishak [38] has also numerically analyzed the effects of thermal radiation and magnetohydro-

dynamic on the two dimensional boundary layer flow and heat transfer of a steady, incompressible viscous fluid flowing over an exponentially stretching sheet. His conclusion was that both the magnetic and the radiation parameters have an inverse behavior on the temperature function. Govardhan and Kishan [39] have investigated the magnetohydrodynamic effects on the problem of boundary layer flow and heat transfer of unsteady, incompressible non-Newtonian micropolar fluid flowing over a stretching surface, when the sheet is stretched in its own plane linearly with the distance along the surface of the sheet. The problem was solved numerically with the help of Adams-Predictor Corrector technique for both the transient and the steady state flow outlines. They commented that the microrotation influence is more evident for $n = 1/2$ as compared with $n = 0$. The microrotation function has a parabolic distribution for $n = 0$, while for $n = 1/2$, the distribution is always decreasing. Due to impulsive motion, they found the skin friction coefficient having large magnitude values for small time at start of the motion. The skin friction coefficient magnitude values have a monotonic decrease till they reached the steady state values. Ahmad and Asghar [40] have obtained the exact analytic solutions for the flow and heat transfer of non-Newtonian second grade fluid flowing over a stretching surface with arbitrary velocity and appropriate wall transpiration. They considered the surface stretching velocities at the surface of the sheet to be linear, quadratic and polynomial functions of the length of the surface from the stagnation point. Weidman and Magyari [41] have obtained an exact solution of the Crane-type boundary layer partial differential equations arising from the problem of steady, incompressible viscous fluid flow encouraged by a planar stretching surface having an appropriate distribution of wall transpiration. They concluded that for any type of surface stretching velocity, the Crane-type boundary layer equations can be generated if the stretching sheet is permeable and an appropriate dissection of the wall transpiration subsists. Phakirappa et al. [42] have debated on the flow pattern of boundary layer viscous fluid and heat transfer in presence of a porous medium when the flow happens due to a non-isothermal stretching sheet with free convection and a temperature gradient reliant heat sink along with internal heat generation and suction/injection beneath the influence of a transverse magnetic field. Their attained exact solutions for the velocity and temperature profiles were in terms of the Kummer's function. Mahmoud et al. [43] have studied the impact of radiation and a uniform magnetic field on the hydromagnetic boundary layer flow and heat

transfer of an electrically conducting non-Newtonian micropolar fluid flows over a continuously moving stretching surface embedded in a non-Darcian porous medium. On the basis of the numerical solutions that were obtained, they were of the view that both the linear and angular velocity functions were in inverse proportion to the magnetic parameter and the Darcy number and that the radiation parameter increase the rate of heat transfer at the surface of the sheet. Gang et al. [44] have presented the exact solutions of the Navier-Stokes equations appearing from the boundary layer flow of a viscous fluid on an expending cylinder, where the surface stretching velocity of the cylinder was assumed to be proportional to the axial distance from the origin and a decreasing function of time. The radius of the cylinder was taken as a time dependent entity that fetched the impact of unsteady expansion of the cylinder in the analysis. Attia [45] has discussed the steady, laminar incompressible fluid flow problem of stagnation point boundary layer flow of micropolar fluid flowing over a permeable stretching surface with heat generation/ absorption with constant wall and stream temperatures. His numerical solution based on the finite difference approximation indicated that the velocity boundary layer thickness is a decreasing function of the stretching velocity of the surface of the sheet. Bidin and Nazar [46] have carried an analysis for the problem of steady laminar incompressible two dimensional boundary layer flow and heat transfer of a viscous fluid flow over a stretching sheet with thermal radiation. The surface stretching velocity is assumed to be an exponential function of the distance on the surface from the stagnation point. Their analysis was based on the implicit finite difference scheme, the Keller-box technique. Rosali et al. [47] have numerically analyzed the boundary layer flow of non-Newtonian micropolar fluid flow towards a permeable stretching/shrinking sheet in a porous medium with suction/injection. They showed that by increasing the permeability parameter, the skin friction coefficient enhances. Turkyilmazoglu [48] has studied the magnetohydrodynamic, steady laminar boundary layer flow of a viscous fluid flowing through a radially stretchable rotating disk in presence of a uniform vertical magnetic field with viscous dissipation and Joule heating. The problem is a generalization of the classical von Karman pump problem. Their analysis showed a strong dependence of the viscous and thermal boundary layer thicknesses over the rotation strength of the disk and the magnetic field strength. They concluded that the role of Joule heating is that to enhance the temperature distribution near the wall. Seddeek [49] has studied the magnetohydrodynamic hall and

ion-slip current effects over the steady boundary layer flow of a non-Newtonian fluid flow and heat transfer of a stretching sheet with suction and blowing. They included an interesting comment in their conclusion that unclean fluids may be preferable over the clean fluids in industrial applications where control of convective heat transfer is important. Kameswaran et al. [50] have analyzed the homogeneous-heterogeneous effects over the flow of boundary layer viscous nano fluid flowing over a stretching or shrinking sheet in a porous medium. The analysis was carried for the copper-water and the silver-water nano fluids such that the diffusion coefficients of the reactant and the auto catalyst are equal. They concluded that the nano particle volume fraction decreases the velocity profile and that the nano particle concentration at the surface is a decreasing function of the strength of the heterogeneous reaction for both copper-water and silver-water nano fluids. It was also mentioned that for the shrinking sheet problem, the velocity profile is a decreasing function of the increasing values of the nano particle volume fraction for both the copper-water and silver-water nano fluids. Ibrahim and Shankar [51] have investigated the problem of boundary layer flow and heat transfer of a viscous nano fluid flowing over a permeable stretching sheet with slip boundary condition and thermal radiation. The flow was also assumed to be under the influence of a uniform magnetic field. They included a detailed analysis for the effects of radiation, Brownian motion, thermophoresis parameter and nanoparticle fraction on the boundary layer flow and heat transfer due to nano fluids. They concluded that the boundary layer thickness is a decreasing function of the magnetic field strength, the thermal boundary layer thickness is a decreasing function of the slip parameter while an increasing function of the radiation parameter, the magnetic field parameter and the thermophoresis parameter. Bachok and Ishak [52] have analyzed the problem of boundary layer flow and heat transfer of steady, laminar incompressible viscous fluid flow due to a stretching cylinder with prescribed surface heat flux. They commented that both the shear stress at the surface and the heat transfer rate at the surface are increasing functions of the curvature parameter. Makinde et al. [53] analyzed the combined effects of the buoyancy force, convective heating, Brownian motion, thermophoresis and magnetic field over the stagnation point boundary layer flow and heat transfer due to nano fluid flowing towards a stretching sheet. Ibrahim et al. [54] have discussed the effect of magnetic field on stagnation point flow and heat transfer of nano fluid flowing towards a stretching sheet. Two important works about fluid flow over

stretching surfaces are cited in [55-58].

The present dissertation is centered mainly for the boundary layer flow of non-Newtonian fluid and heat transfer analysis by a stretching cylinder. Flow caused is by an exponentially stretching cylinder. The structure of thesis is arranged in eight chapters. The chapter wise arrangement is given below:

Literature review is presented in chapter 1. Chapter 2 describes flow of Casson fluid past an exponentially stretching cylinder. Nano fluid is considered. Numerical solution by Runge-Kutta Fehlberg technique is developed. Contents of this chapter are published in “**Applied NanoScience**”

Chapter 3 contains a study of heat transfer in boundary layer flow power law fluid past a vertical stretching cylinder. Further, the solution of the problem is obtained using the Runge-Kutta Fehlberg technique. Contents of this chapter are published in “**Applied and Computational Mathematics**”

Chapter 4 presents an analysis for boundary layer flow and heat transfer for hyperbolic tangent fluid. Stretching cylinder is examined. This problem is solved with the help of Runge-Kutta-Fehlberg method. Contents of the chapter are published in “**Alexandria Engineering Journal**”

The steady boundary layer flow of Williamson fluid past a stretching cylinder is examined in chapter 5. The obtained modeled equations are solved numerically with the help of Keller box method. Chapter 6 addresses Williamson material with Brownian motion and thermophoresis.

Chapter 7 is developed to study the effects of double stratification effect in mixed convection boundary layer flow of Eyring-Powell fluid by an inclined stretching cylinder. Numerical solutions of resulting intricate non-linear boundary value problem are computed successfully by utilizing fifth order Runge-Kutta algorithm with shooting technique. Contents of this chapter are published in “**AIP Advances**”.

Finally, chapter 8 gives the solution for steady boundary layer flow of a second grade fluid past a vertical stretching cylinder. Heat transfer is discussed. The obtained system of equations subject to the boundary conditions are solved with the help homotopy analysis method (HAM). The effects of different parameters, like Reynolds numbers, Prandtl numbers and the natural convection parameter are studied. The skin friction coefficient and Nusselt numbers

are presented for different parameters.

Chapter 2

Boundary layer flow of a Casson nanofluid over a vertical exponentially stretching cylinder

2.1 Introduction

The effects of Casson nanofluid due to a vertically exponential cylinder are studied in this chapter. Similarity solution of the boundary layer flow is computed by choosing suitable transformation. The governing partial differential equations and boundary conditions are reduced to a system of nonlinear ordinary differential equations. The solutions of the problems are obtained by using the numerical technique known as Runge Kutta Fehlberg method. Velocity and temperature profiles are presented through graphs. The important physical quantities such as the skin friction coefficient and the local Nusselt number are computed to examine the behavior of different parameters.

2.2 Mathematical formulation

Consider the problem of natural convection boundary layer flow of Casson nanofluid induced by a vertical circular cylinder of radius a . The cylinder is assumed to be stretched exponentially along the axial direction with velocity U_w . The temperature at the surface of cylinder is assumed

T_w and the uniform ambient temperature is taken as T_∞ such that the quantity $T_w - T_\infty > 0$ in case of the assisting flow while $T_w - T_\infty < 0$ in case of the opposing flow, respectively. Under these assumptions, the boundary layer equations of motion, heat transfer and nanoparticle concentration are

$$u_r + \frac{u}{r} + w_z = 0, \quad (2.1)$$

$$\begin{aligned} uw_r + ww_z &= \nu(1 + \frac{1}{\beta})(w_{rr} + \frac{1}{r}w_r) + g\beta(T - T_\infty)(1 - \phi_\infty) \\ &\quad + \frac{1}{\rho}(\rho^* - \rho)(\phi - \phi_\infty), \end{aligned} \quad (2.2)$$

$$uT_r + wT_z = \alpha(T_{rr} + \frac{1}{r}T_r) + \frac{\rho^*c_p^*}{\rho c_p}(D_T T_r \phi_r + \frac{D_T}{T_\infty} T_r^2), \quad (2.3)$$

$$w\phi_\infty + u\phi_r = D_B(\phi_{rr} + \frac{1}{r}\phi_r) + \frac{D_T}{T_\infty}(T_{rr} + \frac{1}{r}T_r), \quad (2.4)$$

where the velocity components along r and z directions are u and w respectively. ρ is the density, ν is the kinematic viscosity, p is the pressure, g is the gravitational acceleration along z - axis, β is the coefficient of thermal expansion, T is the temperature and α is the thermal diffusivity. The corresponding boundary conditions for the problem are

$$u(a, z) = 0, \quad w(a, z) = U_w \quad w(r, z) \longrightarrow 0 \text{ as } r \longrightarrow \infty, \quad (2.5)$$

$$T(a, z) = T_w(z), \quad T(r, z) \longrightarrow T_\infty \text{ as } r \longrightarrow \infty, \quad (2.6)$$

$$\phi(a, z) = \phi_w(z), \quad \phi(r, z) \longrightarrow \phi_\infty \text{ as } r \longrightarrow \infty, \quad (2.7)$$

where $U_w = 2ake^{z/a}$ is the fluid velocity at the surface of the cylinder.

2.3 Solution of the problem

We have the following similarity transformations:

$$u = -\frac{1}{2}U_w \frac{f(\eta)}{\sqrt{\eta}}, \quad w = U_w f'(\eta), \quad (2.8)$$

$$\theta = \frac{T - T_\infty}{T_w - T_\infty}, \quad \eta = \frac{r^2}{a^2}, \quad h = \frac{\phi - \phi_\infty}{\phi_w - \phi_\infty} \quad (2.9)$$

where the characteristic temperature and nanoparticles concentration difference is calculated from the relations $T_w - T_\infty = ce^{z/a}$ and $\phi_w - \phi_\infty = e^{z/a}$. With the help of transformations (2.8) and (2.9), Eqs. (2.1) to (2.4) take the form

$$(1 + \frac{1}{\beta})(\eta f''' + f'') + \text{Re}(ff'' - f'^2) + \text{Re} \lambda(1 - \phi_\infty)(\theta + N_r h) = 0 \quad (2.10)$$

$$\eta \theta'' + \theta' + \text{Re} \text{Pr}(f\theta' - f'\theta) + \eta \theta'(N_b h' + N_t \theta') = 0 \quad (2.11)$$

$$\eta h'' + h' + \frac{N_t}{N_b}(\eta \theta'' + \theta') + \text{Re} Le(fh' - f'h) = 0 \quad (2.12)$$

in which $\lambda = g\beta a(T_w - T_\infty)/U_w^2$ is the natural convection parameter, $\text{Pr} = \nu/\alpha$ is the Prandtl number, $Le = \nu/D_B$ is the Lewis number, $N_r = (\rho^* - \rho)(\phi_w - \phi_\infty)/\rho\beta(T_w - T_\infty)(1 - \phi_\infty)$ is the buoyancy ratio, $N_b = \rho^* C_p^* D_B(\phi_w - \phi_\infty)/\rho C_p \alpha$ is the Brownian motion parameter, $N_t = \rho^* C_p^* D_T(\phi_w - \phi_\infty)/\rho C_p \alpha T_\infty$ is the thermophoresis parameter and $\text{Re} = aU_w/4\nu$ is the local Reynolds number. The boundary conditions in nondimensional form become

$$f(1) = 0, \quad f'(1) = 1, \quad \theta(1) = 1, \quad h(1) = 1, \quad (2.13)$$

$$f' \longrightarrow 0, \quad \theta \longrightarrow 0, \quad h \longrightarrow 0, \quad \text{as} \quad \eta \longrightarrow \infty. \quad (2.14)$$

The important physical quantities such as the shear stress at the surface τ_w , the skinfriction coefficient c_f , the heat flux at the surface of the cylinder q_w and the local Nusselt number Nu are

$$\tau_w = \tau_{rz} \big|_{r=a}, \quad q_w = -k\tau_r \big|_{r=a}, \quad (2.15)$$

$$c_f = \frac{\tau_w}{\rho U_w^2}, \quad Nu_z = \frac{ae^{z/a} q_w}{k(T_w - T_\infty)} \quad (2.16)$$

The numerical solution of the present problem is computed by using Runge-Kutta-Fehlberg method.

2.4 Results and discussion

Here, the effect of the various parameters such as the Reynolds number Re , the Casson fluid parameter β , the Brownian motion parameter N_b , the thermophoresis parameter N_t , the buoy-

ancy ratio parameter N_r , the Prandtl number Pr and the natural convection parameter λ on the nondimensional velocity, temperature and concentration profiles are presented graphically and through tabular values. *Fig.2.1* shows the effect of Casson fluid parameter β on the velocity profile f' . From *Fig.2.1*, it is observed that for increasing the value of β , the velocity profile decreases. *Fig.2.2* shows the influence of mixed convection parameter λ on the velocity profile f' . It is noticed that the velocity increases for large mixed convection parameter. That is, the mixed convection parameter λ is directly proportionally to the velocity profile f' for constant values of other parameters. Similar pattern is observed for the buoyancy ratio N_r in *Fig.2.3*. In *Fig.2.4* by increasing the value of Reynolds number Re , the velocity profile decreases. *Figs.2.5* and *2.6* show a very slow increase in temperature profile by increasing the values of Brownian motion parameter N_b and the thermophoresis parameter N_t . *Figs.2.7* and *2.8* reflect similar behaviour of temperature profile, i.e. by increasing the value of Reynolds number Re and the Prandtl number Pr , the temperature profile decreases rapidly. In *Fig. 2.9*, it is clear that by increasing the value of Lewis number Le , the nano concentration profile decreases instantly. *Fig.2.10* shows slow effect of Reynolds number Re on nano concentration profile by increasing Reynolds number Re . Table 2.1 shows the boundary derivatives for the velocity profile at the surface of the cylinder that corresponds to the skin friction coefficient for different values of β and λ . Tabulated values indicate that the magnitude of the boundary derivative increases with the increase in β and it decreases by increasing the values of λ . Table 2.2 illustrates the values for local Nusselt numbers for different values of Re and Pr . It is noticed that local Nusselt number increases when Re and Pr are increased.

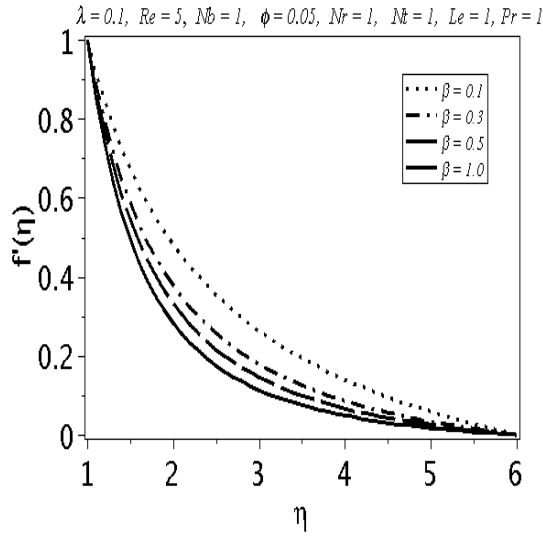


Fig.2.1 Influence of Casson fluid parameter on velocity profile

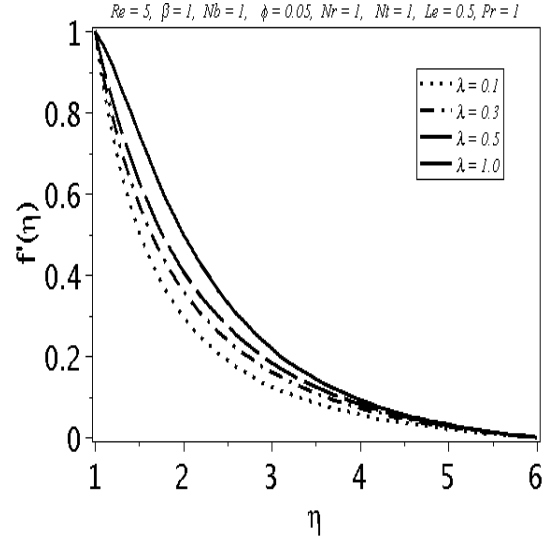


Fig. 2.2 Influence of natural convection parameter on velocity profile

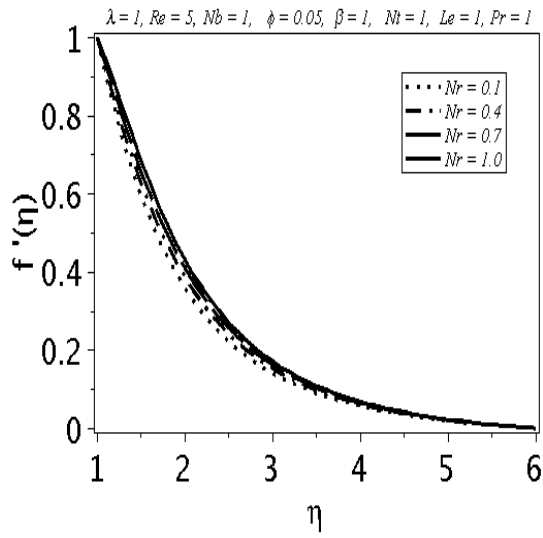


Fig.2.3 Influence of buoyancy ratio parameter on velocity profile

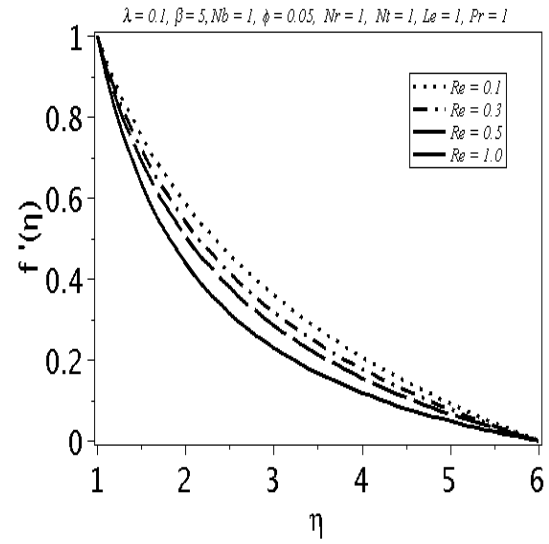


Fig.2.4 Influence of Reynolds numbers on velocity profile

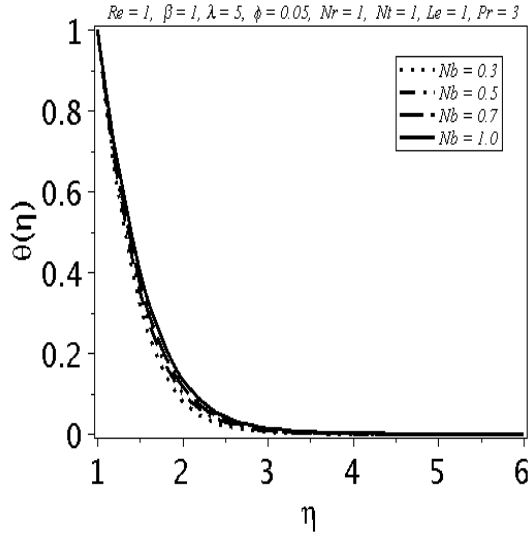


Fig.2.5 Influence of Brownian motion parameter on temperature profile

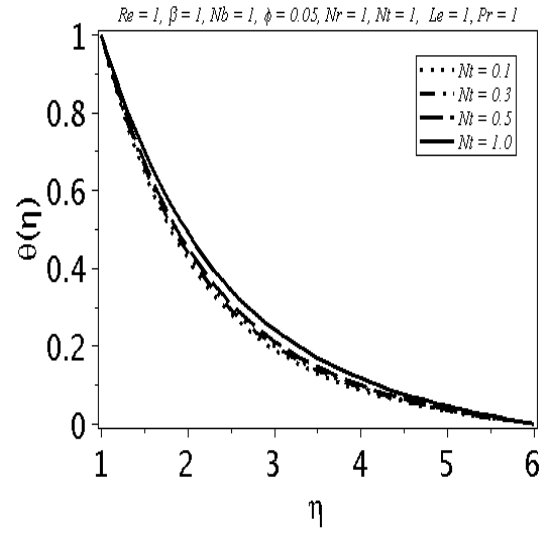


Fig.2.6 Thermophoresis parameter on temperature profile

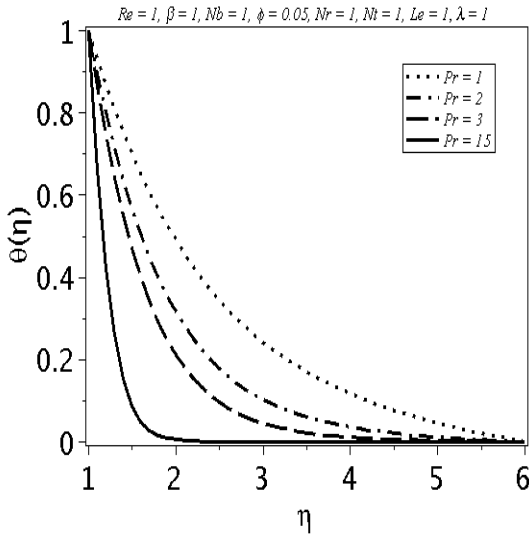


Fig.2.7 Influence of Prantdle numbers on temperature profile

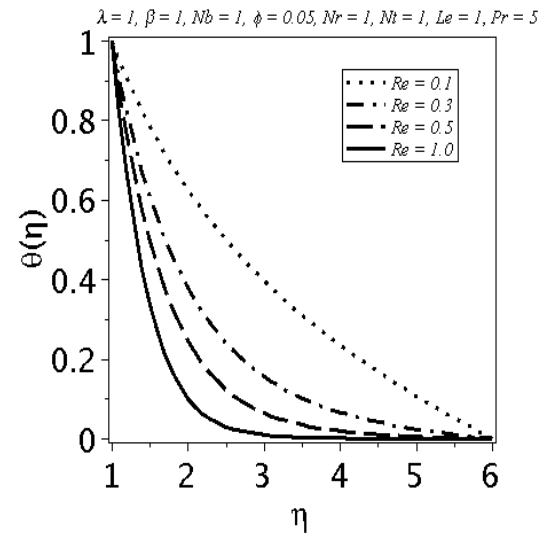


Fig.2.8 Influence of Reynold numbers on temperature profile

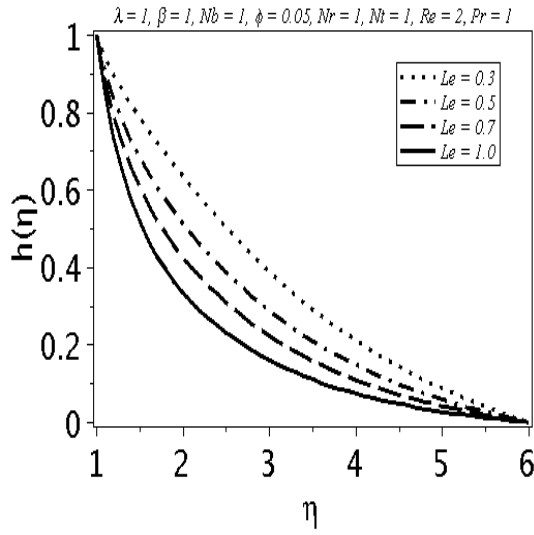


Fig.2.9 Influence of Lewis number on concentration profile

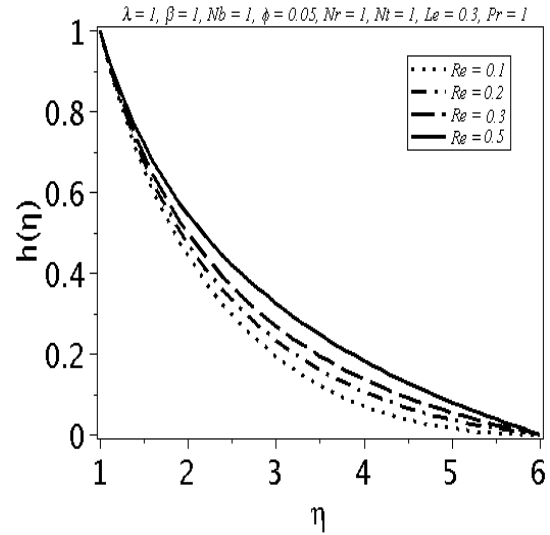


Fig.2.10 Effect of variation of Reynolds number on concentration profile.

Table 2.1 Skin friction coefficient at the surface of the cylinder for $\lambda \backslash \beta$

$\lambda \backslash \beta$	0.1	0.3	0.5	0.7	1.0
0.2	0.5333	0.6479	0.7154	0.7608	0.8071
0.4	0.5141	0.6021	0.6516	0.6840	0.7161
0.6	0.4950	0.5572	0.5895	0.6095	0.6283
0.8	0.4761	0.5130	0.5288	0.5369	0.5431

Table 2.2 Local Nusselt number.

Pr \ Re	0.1	0.2	0.3	0.4	0.5
1	0.2442	0.3094	0.3700	0.4260	0.4776
3	0.3826	0.5627	0.7173	0.8505	0.9668
5	0.5118	0.7844	1.0058	1.1904	1.3489
7	0.6327	0.9814	1.2546	1.4790	1.6714
15	1.0499	1.6121	2.0318	2.3762	2.6739

2.5 Conclusions

This study was focused on natural convection boundary layer flow of a Casson nanofluid. Numerical solution of the problem is obtained with the help of Runge-Kutta-Fehlberg method. Main findings of present analysis are listed below:

- Velocity profile increases by increasing buoyancy ratio parameter N_r and natural convection parameter λ but it decreases when Casson fluid parameter β and Reynold number Re are enhanced.
- Temperature profile increases for larger Brownian motion parameter N_b whereas thermophoresis parameter N_t decreases by increasing Reynold number Re and Prandtl number Pr .
- Nano concentration profile increases on increasing Reynold number Re and it decreases by increasing Lewis number Le .
- Skin friction coefficient decreases on increasing natural convection parameter λ and it increases for increasing Casson fluid parameter β .
- Local Nusselt number increases for larger Reynold number Re and Prandtl number Pr .

Chapter 3

Numerical study of convective heat transfer in flow of power law fluid by an exponentially stretching cylinder

3.1 Introduction

This chapter focuses on flow of power law fluid model due to vertical exponentially stretching cylinder with heat transfer. The governing partial differential equations are transformed to a system of ordinary differential equations. For numerical solution, Runge-Kutta-Fehlberg method is used. The effects of variation in physical parameters on velocity and temperature are highlighted through graphs. The important physical quantities, such as the skin friction coefficient and the local Nusselt number are computed.

3.2 Formulation

Here, the problem of natural convective boundary layer flow of a power law fluid flowing by a vertical circular cylinder of radius a is under consideration. The cylinder is assumed by an exponentially stretching sheet. The sheet stretches with velocity U_w . The temperature at the surface of the cylinder is assumed to be T_w and the uniform ambient temperature is taken as T_∞ such that the quantity $T_w - T_\infty > 0$ for assisting flow whereas $T_w - T_\infty < 0$ for opposing

flow, respectively. Under these assumptions the boundary layer equations of motion and heat transfer are

$$u_r + \frac{u}{r} + w_z = 0, \quad (3.1)$$

$$uw_r + ww_z = \frac{k}{\rho} \left(\frac{w_r^n}{r} + nw_r^{n-1}w_{rr} \right) + g\beta(T - T_\infty), \quad (3.2)$$

$$uT_r + wT_z = \alpha \left(T_{rr} + \frac{1}{r}T_r \right), \quad (3.3)$$

In above equations, the velocity components along the (r, z) axes are (u, w) , ρ is fluid density, k is the consistency coefficient, p is pressure, g is the gravitational acceleration along the z -direction, β is the coefficient of thermal expansion, T is the temperature and α is the thermal diffusibility. The corresponding boundary conditions are expressed as follows:

$$u(a, z) = 0, \quad w(a, z) = U_w \quad w(r, z) \longrightarrow 0 \text{ as } r \longrightarrow \infty, \quad (3.4)$$

$$T(a, z) = T_w(z), \quad T(r, z) \longrightarrow T_\infty \text{ as } r \longrightarrow \infty. \quad (3.5)$$

Here, $U_w = 2ake^{z/a}$ denotes the fluid velocity at the surface of cylinder.

3.3 Solutions

We write

$$u = -\frac{1}{2}U_w \frac{f(\eta)}{\sqrt{\eta}}, \quad w = U_w f'(\eta), \quad (3.6)$$

$$\theta = \frac{T - T_\infty}{T_w - T_\infty}, \quad \eta = \frac{r^2}{a^2}, \quad (3.7)$$

where the characteristic temperature difference is calculated from the relations $T_w - T_\infty = ce^{z/a}$. With the help of transformations (3.6) and (3.7), Eqs. (3.1) to (3.3) become

$$(n+1)\eta^{\frac{n-1}{2}}(f'')^n + 2n\eta^{\frac{n+1}{2}}f'''(f'')^{n-1} + \text{Re}_a(ff'' - f'^2) + \text{Re}_a\lambda\theta = 0 \quad (3.8)$$

$$\eta\theta'' + \theta' + \frac{1}{2}\text{Re Pr}(f\theta' - f'\theta) = 0, \quad (3.9)$$

in which $\lambda = g\beta a(T_w - T_\infty)/U_w^2$ is the natural convection parameter, $\text{Pr} = k/\rho\alpha$ is the Prandtl number, $\text{Re}_a = \rho a^n U_w^{2-n}/k$ is the local Reynolds number and $\text{Re} = a\rho U_w/4k$ is the Reynolds number. The boundary conditions are reduced to

$$f(1) = 0, \quad f'(1) = 1, \quad \theta(1) = 1, \quad (3.10)$$

$$f' \longrightarrow 0, \quad \theta \longrightarrow 0, \quad \text{as } \eta \longrightarrow \infty. \quad (3.11)$$

The skin friction coefficient c_f and the local Nusselt number Nu_z are

$$\tau_w = \tau_{rz} \big|_{r=a}, \quad q_w = -k\tau_r \big|_{r=a}, \quad (3.12)$$

$$c_f = \frac{\tau_w}{\rho U_w^2}, \quad Nu_z = \frac{ae^{z/a} q_w}{k(T_w - T_\infty)} \quad (3.13)$$

3.4 Discussion

Our interest in this section is to investigate the effects of the Reynolds number Re , the local Reynolds number Re_a , the power law index n , the Prandtl number Pr and the natural convection parameter λ over the nondimensional velocity and temperature profiles. For this purpose, the graphs and tables will be prepared. *Fig. 3.1* shows the effects of natural convection parameter λ on the velocity profile f' when $n = 1$. From *Fig. 3.1* it is observed that by increasing the values of natural convection parameter λ the velocity profile increases. *Fig. 3.2* shows the influence of local Reynolds number Re_a over the velocity profile f' when $n = 1$. It is observed that for larger local Reynolds number Re_a the velocity profile f' decreases. *Figs. 3.3* and *3.4* show the effects of variation in Prandtl number Pr and Reynolds number Re on temperature profile when $n = 1$. Here, the temperature profile decreases when Prandtl number Pr and Reynolds number Re are increased. The effects of natural convection parameter λ on the velocity profile f' are shown in *Fig. 3.5* when $n = 2$. The velocity profile f' decreases by increasing the values of natural convection parameter λ . *Fig. 3.6* shows opposite behavior of velocity profile f' when $n = 2$, that is, the velocity profile increases by increasing the local Reynolds number Re_a . The temperature profiles presented in *Figs. 3.7* and *3.8* have similar behavior both for $n = 1$ and $n = 2$. The values of skin friction coefficient and local Nusselt number at the surface of the

cylinder are presented in Tables 3.1 and 3.2. Table 3.1, indicates that skin friction coefficient increases upon increasing local Reynolds number Re_a but for fixed value of Prandtl number Pr . the local Nusselt number decreases for larger Reynolds number Re .

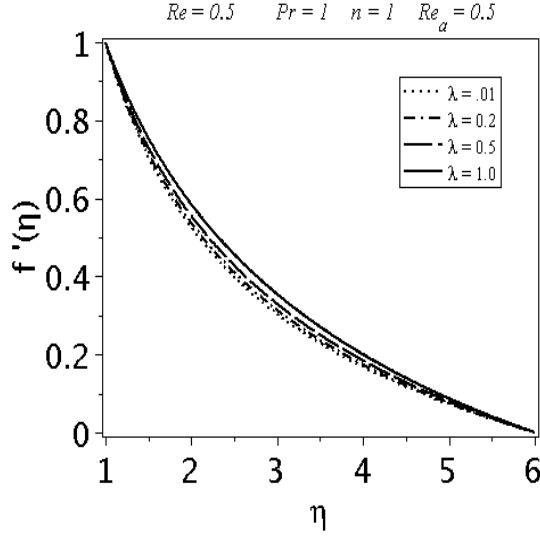


Fig. 3.1. Plots of velocity profile f' for natural convection parameter λ .

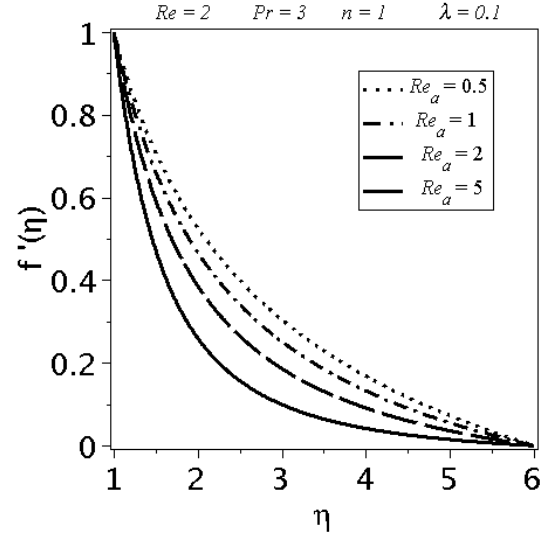


Fig.3.2 Plots of velocity profile f' for local Reynolds number Re_a .

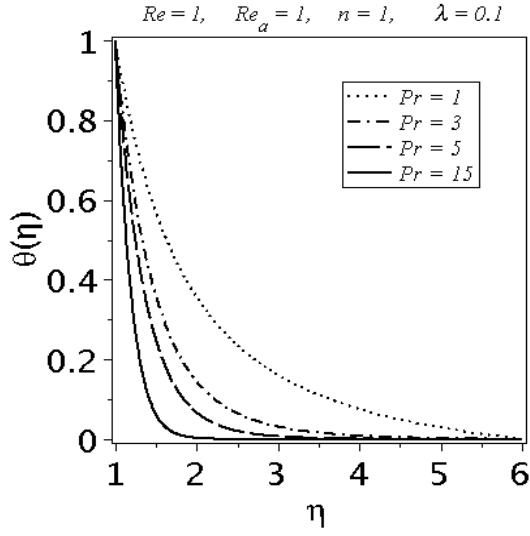


Fig.3.3 Influence of Prandtl number on temperature profile

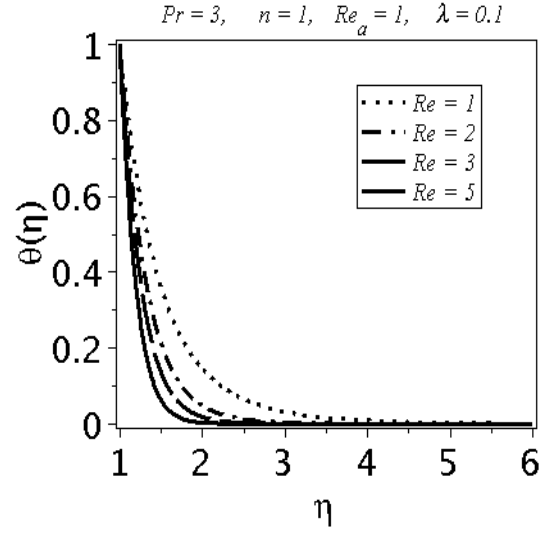


Fig.3.4 Influence of Reynolds number on temperature profile

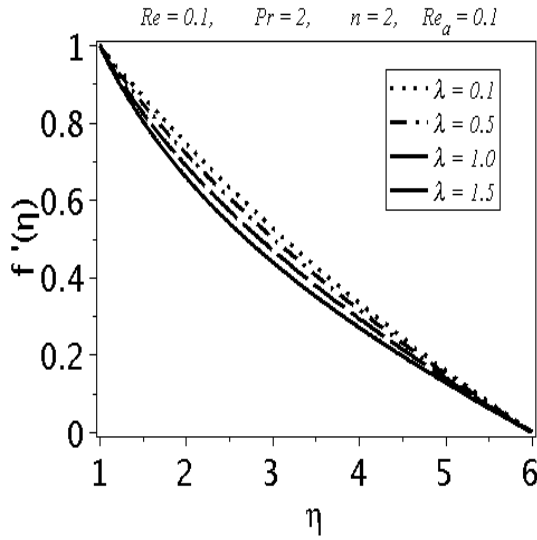


Fig.3.5 Influence of natural convection parameter on velocity profile

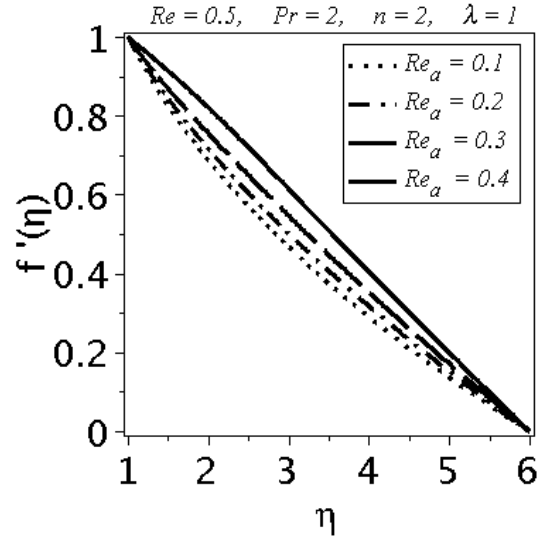


Fig.3.6 Influence of local Reynolds number on velocity profile

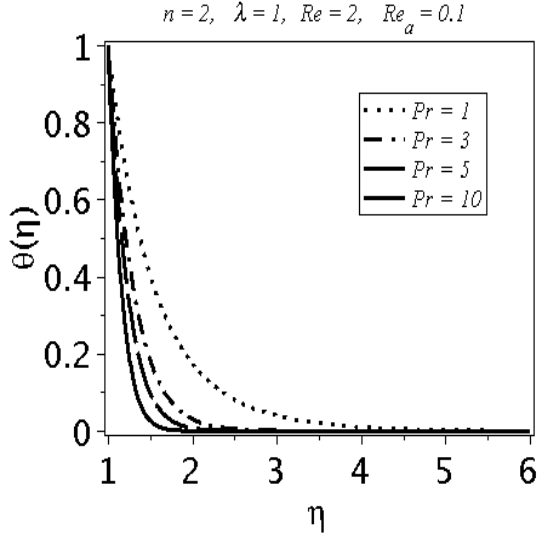


Fig.3.7 Influence of Prandtl number on temperature profile

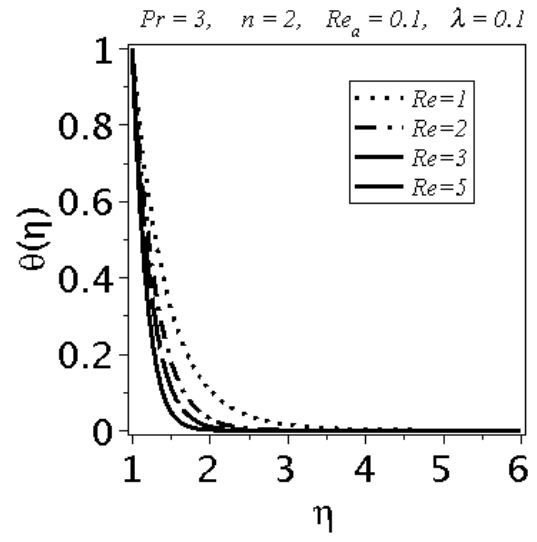


Fig.3.8 Influence of Reynolds number on temperature profile

Table 3.1 Skin friction coefficient at the surface.

$\lambda \backslash Re_a$	0	0.1	0.2	0.3	0.4
1	0.9859	0.9903	0.9953	1.0011	1.0078
3	1.2212	1.2366	1.2544	1.2754	1.3012
5	1.4494	1.4755	1.5065	1.5452	1.5972
10	1.9274	1.9809	2.0499	2.1505	2.3941
15	2.3145	2.3968	2.5121	2.7246	2.9537

Table 3.2 Local Nusselt number.

Pr \ Re	0.0	0.1	0.2	0.3	0.4
1	1.1971	1.1967	1.1962	1.1957	1.1952
7	1.7912	1.7890	1.7866	1.7838	1.7808
10	3.5901	3.5808	3.5699	3.5566	3.5396
15	5.5503	5.5360	5.5182	5.4944	5.4580
25	6.6652	6.6491	6.6285	6.5999	6.5508

3.5 Conclusions

This study is proposed just to address the flow of power law fluid model past a vertical exponentially stretching cylinder with heat transfer. Main results are mentioned below:

- The velocity profile gives opposite behavior for $n = 1$ and 2. That is, the fluid velocity increases for $n = 1$ and it decreases for $n = 2$ when natural convection parameter λ enhances.
- On increasing local Reynolds number Re_a the fluid velocity decreases for $n = 1$ but it increase when $n = 2$.
- The temperature profile decreases both for $n = 1$ and 2 when Reynold number Re and Prandtl number Pr are increased.
- Skin friction coefficient enhances on increasing natural convection parameter λ and local Reynold number Re_a .
- Local Nusselt number increases on increasing Prandtl number Pr but it decreases for larger Reynold number Re .

Chapter 4

Boundary layer flow of an incompressible tangent hyperbolic fluid past a stretching cylinder

4.1 Introduction

The tangent hyperbolic fluid is a four constant pseudoplastic fluid model capable of relating the shear thinning phenomenon. It is a material which measures the fluid resistance when flow decreases with an increasing rate of shear stress. Modelled partial differential equations are transformed to system of ordinary differential equations by applying transformations. Numerical solution has been computed by using Runge-Kutta-Fehlberg method. The fluid velocity and temperature profiles are presented for different values of physical parameters. Furthermore, the skin friction coefficient and Nusselt number are described for the influential variables.

4.2 Fluid model

The continuity and momentum equations are

$$\operatorname{div} \mathbf{V} = 0,$$

$$\rho \frac{d\mathbf{V}}{dt} = \text{div } \boldsymbol{\tau} + \rho \mathbf{b},$$

where ρ is the density, \mathbf{V} is the velocity, $\boldsymbol{\tau}$ is the Cauchy stress tensor, \mathbf{b} represents the specific body force and d/dt represents the material time derivative. The constitutive equations of hyperbolic tangent fluid model [8] are given as

$$\boldsymbol{\tau} = -p\mathbf{I} + \mathbf{S},$$

$$\mathbf{S} = [\eta_\infty + (\eta_0 + \eta_\infty) \tanh(\Gamma \bar{\dot{\gamma}})^n] A$$

in which p is the pressure, \mathbf{I} is the identity tensor, $\boldsymbol{\tau}$ is the extra stress tensor, A is second invariant strain tensor, η_0 and η_∞ are the limiting viscosities at zero and at infinite shear rate, $\Gamma > 0$ is the time constant and $\bar{\dot{\gamma}}$ is defined as

$$\bar{\dot{\gamma}} = \sqrt{\frac{1}{2} \sum_i \sum_j \dot{\gamma}_{ij} \dot{\gamma}_{ji}} = \sqrt{\frac{1}{2} \Pi},$$

where

$$\begin{aligned} \Pi &= \sum_i \sum_j \dot{\gamma}_{ij} \dot{\gamma}_{ji} = \text{tr}[(\text{grad } V) + (\text{grad } V)^t]^2 \\ V &= [u(r, z), 0, w(r, z)] \end{aligned}$$

and

$$\bar{\dot{\gamma}} = \sqrt{(u_r^2 + w_z^2) + \frac{1}{2}(u_z + w_r)^2 + \frac{2u^2}{r^2}}$$

We consider the case for which $\eta_\infty = 0$ and $\Gamma \bar{\dot{\gamma}} < 1$. Therefore, the component of extra stress tensor can be written as

$$\mathbf{S} = \eta_0 (\Gamma \bar{\dot{\gamma}})^n A = \eta_0 [1 + n [\Gamma \bar{\dot{\gamma}} - 1] A$$

4.3 Formulation

Consider the problem of natural convection boundary layer flow of a hyperbolic tangent fluid flow caused by a vertical circular cylinder of radius a . The cylinder is assumed exponentially stretching with velocity U_w . The temperature at the surface of the cylinder is assumed to be T_w and the uniform ambient temperature is taken as T_∞ such that the quantity $T_w - T_\infty > 0$ in case of the assisting flow while $T_w - T_\infty < 0$ for opposing flow respectively. Under these assumptions the boundary layer equations of motion and heat transfer are

$$u_r + \frac{u}{r} + w_z = 0, \quad (4.1)$$

$$uw_r + ww_z = g\beta(T - T_\infty) + \nu[(1 - n)(w_{rr} + \frac{1}{r}w_r) + \frac{n\Gamma}{2}w_r(2w_{rr} + \frac{1}{r}w_r)] \quad (4.2)$$

$$uT_r + wT_z = \alpha(T_{rr} + \frac{1}{r}T_r), \quad (4.3)$$

where the velocity components along the r -, z -axes are u and w , ρ is density, ν is the kinematic viscosity, p is pressure, g is the gravitational acceleration along z - direction, β is the coefficient of thermal expansion, T is the temperature, η_∞ is the infinite shear rate viscosity, η_0 is the viscosity at zero shear rate, Γ is the time constant, n is the power law index and α is the thermal diffusivity. The corresponding boundary conditions for the problem are

$$u(a, z) = 0, \quad w(a, z) = U_w \quad w(r, z) \longrightarrow 0 \text{ as } r \longrightarrow \infty, \quad (4.4)$$

$$T(a, z) = T_w(z), \quad T(r, z) \longrightarrow T_\infty \text{ when } r \longrightarrow \infty, \quad (4.5)$$

in which $U_w = 2ake^{z/a}$ (k is dimensional constant) is the fluid velocity at the surface of the cylinder.

4.4 Solution

We write

$$u = -\frac{1}{2}U_w \frac{f(\eta)}{\sqrt{\eta}}, \quad w = U_w f'(\eta), \quad (4.6)$$

$$\theta = \frac{T - T_\infty}{T_w - T_\infty}, \quad \eta = \frac{r^2}{a^2}, \quad (4.7)$$

where the characteristic temperature difference is calculated from the relations $T_w - T_\infty = T_0 e^{z/a}$. With the help of transformations (4.6) and (4.7), Eqs. (4.1) to (4.3) are reduced to

$$2(1-n)(\eta f''' + f'') + nWe\sqrt{\eta}f''(4\eta f''' + 3f'') + \text{Re}(ff'' - f'^2) + \text{Re}\lambda\theta = 0, \quad (4.8)$$

$$\eta\theta'' + \theta' + \text{RePr}(f\theta' - f'\theta) = 0, \quad (4.9)$$

in which $\lambda = g\beta a(T_w - T_\infty)/U_w^2$ is the natural convection parameter, $\text{Pr} = \nu/\alpha$ is the Prandtl number, $We = 4\Gamma U_w/a$ is the Weissenberg number and $\text{Re} = aU_w/4\nu$ is the local Reynolds number. The boundary conditions in nondimensional form become

$$f(1) = 0, \quad f'(1) = 1, \quad \theta(1) = 1, \quad (4.10)$$

$$f' \longrightarrow 0, \quad \theta \longrightarrow 0, \quad \text{as } \eta \longrightarrow \infty. \quad (4.11)$$

The important physical quantities such as the shear stress at the surface τ_w , the skin friction coefficient c_f , the heat flux at the surface of the cylinder q_w and the local Nusselt number Nu_z are

$$\tau_w = \tau_{rz} \big|_{r=a}, \quad q_w = -k\tau_r \big|_{r=a}, \quad (4.12)$$

$$c_f = \frac{\tau_w}{\rho U_w^2}, \quad Nu_z = \frac{ae^{z/a}q_w}{k(T_w - T_\infty)} \quad (4.13)$$

The solution of the present problem is obtained numerically by using the Runge Kutta Fehlberg method.

4.5 Results and discussion

In this chapter, an analysis is carried out for natural convection boundary layer flow of a hyperbolic tangent fluid due to an exponentially stretched cylinder. It is assumed that the cylinder is stretched exponentially along its radial direction. Here, $U_w = 2ake^{z/a}$ is the assumed exponential stretching velocity at the surface of cylinder. For the solution of problem, the Runge-Kutta-Fehlberg method is used. The impact of different parameters, such as the Reynolds number Re , the Prandtl number Pr , the Weissenberg number We and the natural convection parameter λ on the non-dimensional velocity and temperature profiles are presented graphically (see *Figs.4.1 – 4.5*). Here, *Fig. 4.1* shows the influence of Weissenberg number We on the velocity function f' . From the graph it is clear that velocity profile decreases by increasing the values of Weissenberg number We . *Fig. 4.2* shows the effects of Reynolds number Re on the velocity f' . The velocity profile increases by increasing the values of Re . *Fig. 4.3* shows the influence of natural convection parameter λ on velocity profile when $n = 1$. From the graph, it is clear that by increasing the values of λ the velocity profile decreases. *Fig. 4.4* describes the impact of Prandtl number Pr on temperature profile. The temperature profile increases for larger values of Pr . *Fig. 4.5* shows the influence of Reynolds number Re on the temperature profile. The temperature profile increases when Re is enhanced. *Table. 4.1* shows the behavior of heat flux at the surface of the stretching cylinder for different values of Pr and Re when $n = 0.3$. Entries in *Table. 4.1* show that increase in both Pr and Re increases the heat flux at the surface. *Table. 4.2* shows magnitude of the velocity profile when $n = 0.3$. Entries in *Table. 4.2* depict that the magnitude of boundary derivative increases by increasing both the Weissenberg and the Reynolds numbers.

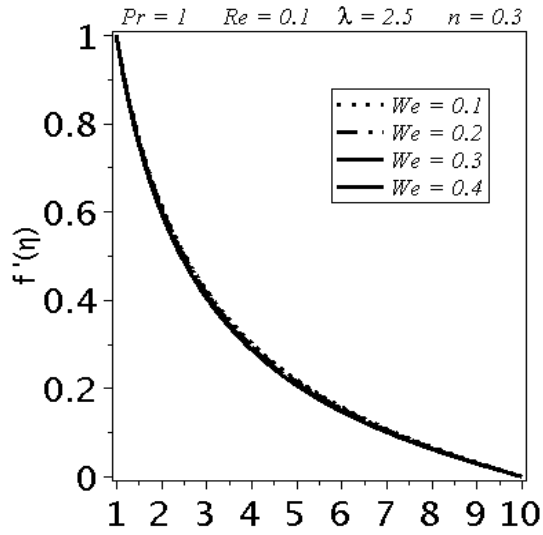


Fig.4.1 Influence of Wesonburg number
on velocity profile

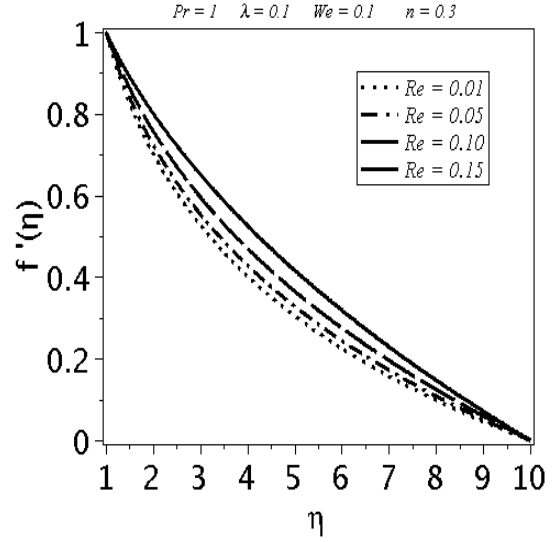


Fig.4.2 Influence of Reynolds number on
velocity profile

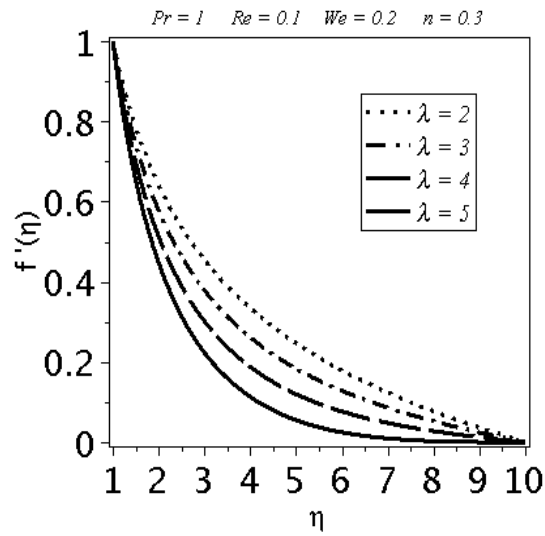


Fig.4.3 Influence of natural convection
parameter on velocity profile

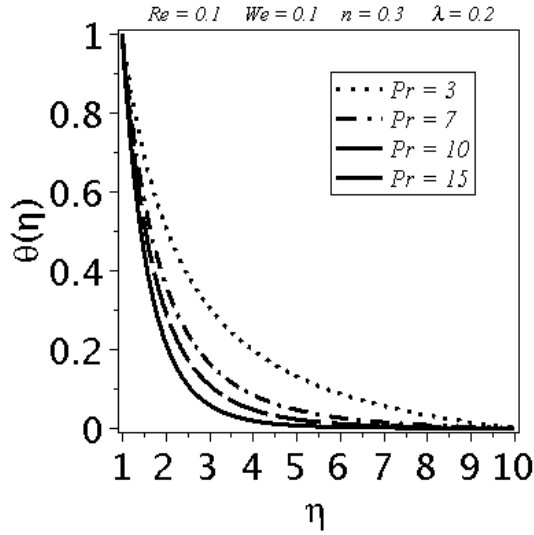


Fig.4.4 Influence of Prandtl number on temperature profile

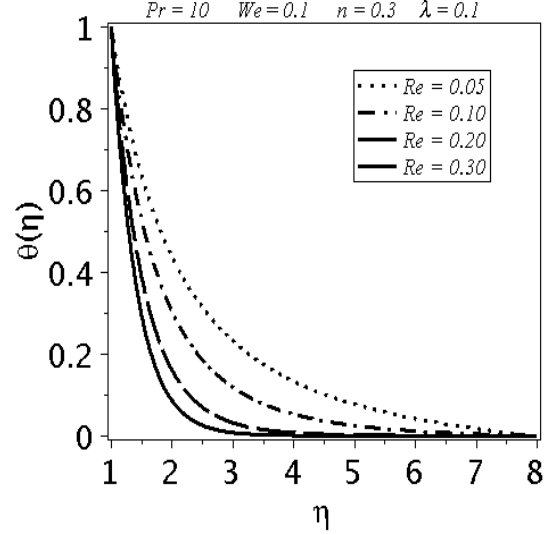


Fig.4.5 Influence of Reynolds number on temperature profile

Table 4.1 Local Nusselt number

Pr\Re	0.1	0.2	0.3	0.4	0.5	1.0
1	0.9613	0.9786	0.9963	1.0141	1.0323	1.1263
3	1.0610	1.0617	1.0624	1.0632	1.0639	1.0667
5	1.1578	1.1589	1.1601	1.1612	1.1624	1.1684
7	1.2517	1.2533	1.2548	1.2563	1.2579	1.2658
15	1.6018	1.6045	1.6071	1.6098	1.6125	1.6264

Table 4.2 Skin friction coefficient at the surface

We\Re	0.1	0.2	0.3	0.4	0.5	1.0
0.1	0.9621	1.0041	1.0450	1.0850	1.1240	1.3082
0.2	0.9767	1.0231	1.0687	1.1136	1.1580	1.3741
0.3	0.9943	1.0464	1.0982	1.1499	1.2017	1.4666
0.4	1.0163	1.0761	1.1366	1.1982	1.2612	1.6159

4.6 Conclusions

The following points are worth mentioning.

- Increase in natural convection parameter, Weissenberg number and Reynolds number reduces the fluid velocity.
- Increase in Prandtl and Reynolds numbers reduces the fluid temperature.
- Larger Prandtl and Reynolds numbers, give rise to heat flux at the surface.
- The magnitude of boundary derivative increases by increasing both the Weissenberg and the Reynolds numbers.

Chapter 5

Flow of Williamson fluid past a vertical exponentially stretching cylinder

5.1 Introduction

This chapter addresses the boundary layer flow of Williamson fluid occurred in many industrial processes and natural phenomena. Most of the interest in this subject is due to its applications. Flow caused is because of an exponentially stretching cylinder. The governing partial differential equations systems are reduced to nonlinear ordinary differential equations systems. Keller box technique is implemented for the numerical solution. The effects of different physical parameters (e.g. Reynold number Re , Prandtl number Pr , the natural convection parameter λ and Weissenberg number We) are presented through graphs. The skin friction coefficient is computed to see the effects of different parameters.

5.2 Mathematical formulation

Consider the problem of natural convection boundary layer flow of Williamson fluid due to a vertical circular cylinder of radius a . The cylinder is assumed stretched exponentially along the axial direction with velocity U_w . The temperature at the surface of the cylinder is assumed T_w

and the uniform ambient temperature is taken as T_∞ such that the quantity $T_w - T_\infty > 0$ in case of the assisting flow, while $T_w - T_\infty < 0$ in case of the opposing flow, respectively. The boundary layer flow under consideration are governed by

$$u_r + \frac{u}{r} + w_z = 0, \quad (5.1)$$

$$uw_r + ww_z = \frac{\nu}{r}(\Gamma w_r^2 + w_r) + \nu[w_{rr} + 2\Gamma w_{rr}w_r] + g\beta(T - T_\infty), \quad (5.2)$$

$$uT_r + wT_z = \alpha(T_{rr} + \frac{1}{r}T_r), \quad (5.3)$$

where the velocity components along the (r, z) axes are (u, w) , ρ is density, ν is the kinematic viscosity, p is pressure, g is the gravitational acceleration along the z - direction, β is the coefficient of thermal expansion, T is the temperature and α is the thermal diffusibility. The corresponding boundary conditions for the problem are

$$u(a, z) = 0, \quad w(a, z) = U_w \quad w(r, z) \longrightarrow 0 \text{ as } r \longrightarrow \infty, \quad (5.4)$$

$$T(a, z) = T_w(z), \quad T(r, z) \longrightarrow T_\infty \text{ as } r \longrightarrow \infty, \quad (5.5)$$

where $U_w = 2ake^{z/a}$ is the fluid velocity at the surface of the cylinder.

5.3 Solution of the problem

We consider

$$u = -\frac{1}{2}U_w \frac{f(\eta)}{\sqrt{\eta}}, \quad w = U_w f'(\eta), \quad (5.6)$$

$$\theta = \frac{T - T_\infty}{T_w - T_\infty}, \quad \eta = \frac{r^2}{a^2}, \quad (5.7)$$

where the characteristic temperature difference is calculated from the relations $T_w - T_\infty = ce^{z/a}$. With the help of transformations (5.6) and (5.7), Eqs. (5.1) to (5.3) are reduced to

$$\eta f''' + f'' + \text{Re}(ff'' - f'^2) + We\sqrt{\eta}f''(\eta f''' + f'') + \text{Re}\lambda\theta = 0 \quad (5.8)$$

$$\eta\theta'' + \theta' + \frac{1}{2}\text{RePr}(f\theta' - f'\theta) = 0, \quad (5.9)$$

in which $\lambda = g\beta a(T_w - T_\infty)/U_w^2$ is the natural convection parameter, $\text{Pr} = \nu/\alpha$ is the Prandtl number, $We = 4\Gamma U_w/a$ is the local Weissenberg number and $\text{Re} = aU_w/4\nu$ is the local Reynolds number. The boundary conditions now reduce to

$$f(1) = 0, \quad f'(1) = 1, \quad \theta(1) = 1, \quad (5.10)$$

$$f' \longrightarrow 0, \quad \theta \longrightarrow 0, \quad \text{as } \eta \longrightarrow \infty. \quad (5.11)$$

The important physical quantities, such as the shear stress at the surface τ_w , the skin friction coefficient c_f , the heat flux at the surface of the cylinder q_w and the local Nusselt number Nu_z are

$$\tau_w = \tau_{rz} \big|_{r=a}, \quad q_w = -k \tau_r \big|_{r=a}, \quad (5.12)$$

$$c_f = \frac{\tau_w}{\rho U_w^2}, \quad Nu_z = \frac{ae^{z/a} q_w}{k(T_w - T_\infty)} \quad (5.13)$$

Keller box Method is employed for the numerical solution.

5.4 Outcomes

In this section, the results are analyzed for the Reynolds number Re , the Weissenberg number We , the Prandtl number Pr and the natural convection parameter λ for the nondimensional velocity and temperature profiles. This objective is achieved through *Figs.*(5.1 – 5.8) and Tables 5.1 and 5.2. *Fig.*5.1 shows the effect of Prandtl number Pr on the velocity profile f' . It is observed that by increasing Prandtl number Pr the velocity profile decreases. *Fig.*5.2 indicates the influence of natural convection parameter λ over the velocity profile f' . When natural convection parameter λ increases the velocity profile also increases, that is, the natural convection parameter λ is directly proportionally to the velocity profile f' . Similarly by increasing the value of Weissenberg number We and Reynold number Re the velocity profile decreases (see *Figs.*5.3 and 5.4). Response of temperature profile due to variation in Prandtl number, natural convection parameter, Renold number and Weissenberg number can be seen in the *Figs.*(5.5 – 5.8). *Fig.*5.5 shows that after increasing the value of Prandtl number Pr , temperature profile decreases. *Fig.*5.6 depicts similar behaviour of temperature profile by increasing λ , that is, the temperature profile also decreases. In *Fig.*5.7 by increasing the value

of Reynold number Re , the temperature profile decreases. In *Fig.5.8* there is slight effect of Weissenberg number We on temperature profile.

Table 5.1 shows the boundary derivatives for the velocity profile at the surface of cylinder that corresponds to the skin friction coefficient at the surface tabulated for different values of We and Re . From table 5.1 it is observed that the magnitude of boundary derivative increases with the increase in both We and Re . Table 5.2 shows the values for local Nusselt numbers when different values of We and Pr are used. Table 5.2 witnesses that with increase in We (for fixed Pr), local Nusselt number increases whereas with increase in Pr (for fixed We), Nu_z decreases.

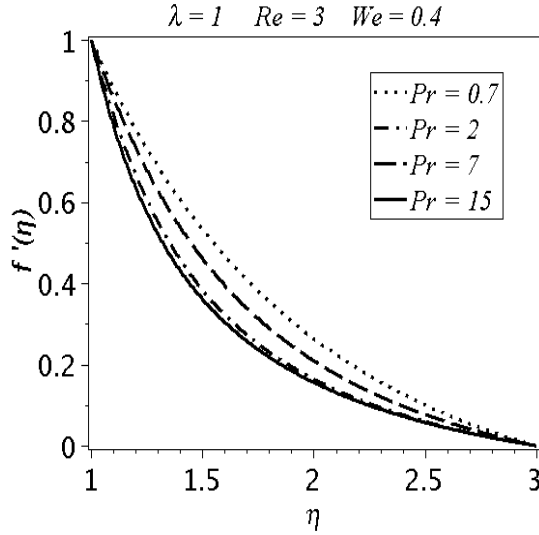


Fig.5.1 Influence of Prandtl number on velocity profile

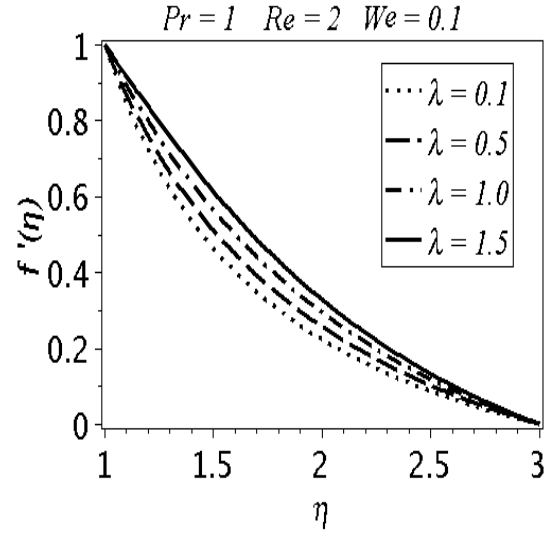


Fig.5.2 Influence of natural convection parameter on velocity profile

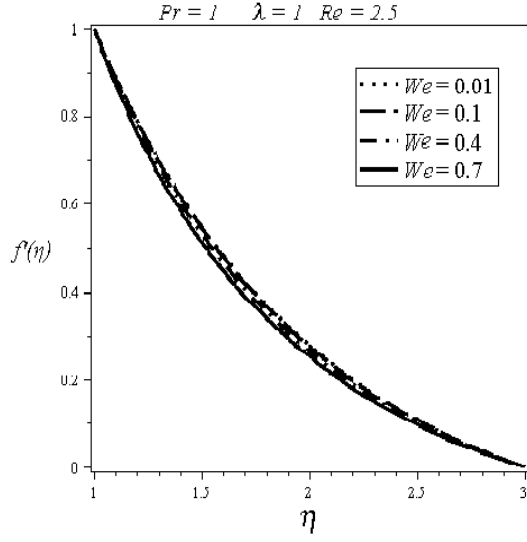


Fig.5.3 Influence of Weissenberg number on velocity profile

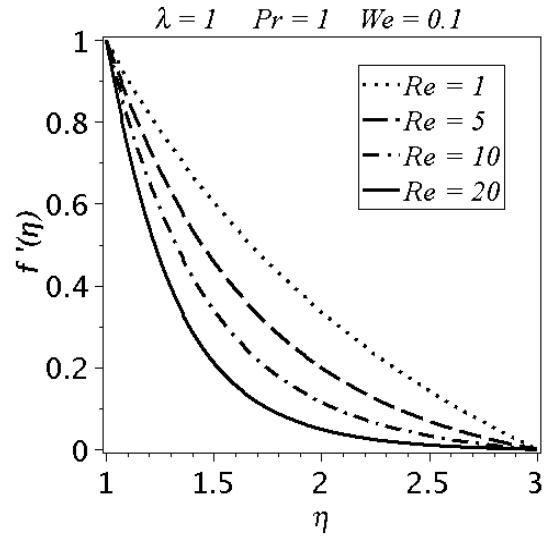


Fig.5.4 Influence of Reynold number on velocity profile

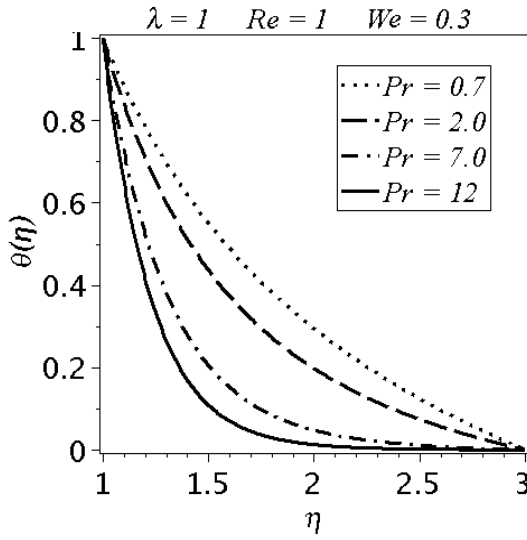


Fig.5.5 Influence of Prantdl number on temperature profile

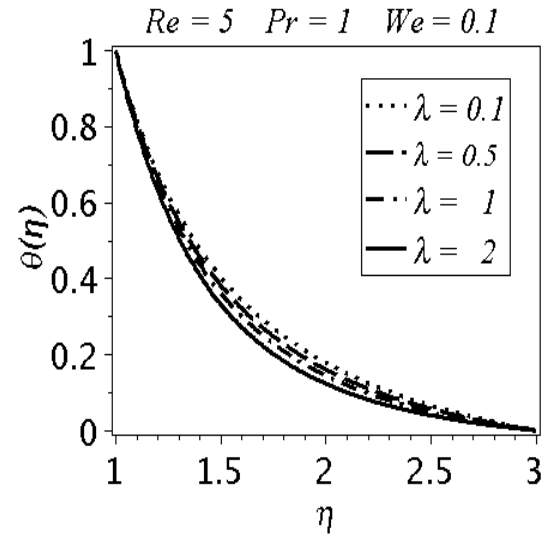


Fig.5.6 Influence of natural convection parameter on temperature profile

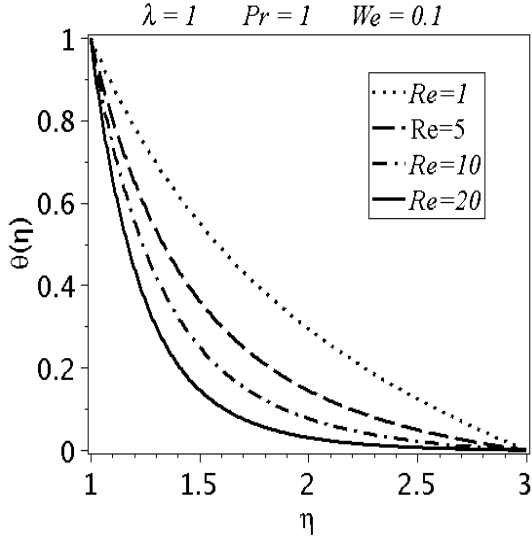


Fig.5.7 Influence of Reynold number on temperature profile

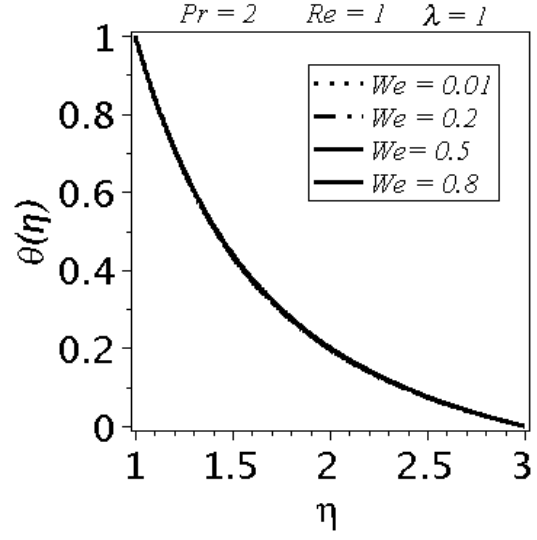


Fig.5.8 Influence of Weissenberg number on temperature profile

Table 5.1 Skin friction at the surface of the cylinder

Re \ We	0	0.1	0.2	0.3	0.4
1	0.9859	0.9903	0.9953	1.0011	1.0078
3	1.2212	1.2366	1.2544	1.2754	1.3012
5	1.4494	1.4755	1.5065	1.5452	1.5972
10	1.9274	1.9809	2.0499	2.1505	2.3941
15	2.3145	2.3968	2.5121	2.7246	2.9537

Table 5.2 Local Nusselt number

Pr \ We	0.0	0.1	0.2	0.3	0.4
0.2	1.1971	1.1967	1.1962	1.1957	1.1952
0.7	1.7912	1.7890	1.7866	1.7838	1.7808
3.0	3.5901	3.5808	3.5699	3.5566	3.5396
7.0	5.5503	5.5360	5.5182	5.4944	5.4580
10.0	6.6652	6.6491	6.6285	6.5999	6.5508

5.5 Conclusions

The following are the main findings of this chapter:

- Velocity decays upon increasing the Weissenberg, Prandtl and Reynold numbers.
- Larger convection parameter enhances the velocity.
- The temperature profile decreases by increasing Prandtl, Reynold, natural, Weissenberg numbers and convection parameter.
- The skin friction decreases by increasing Weissenberg and Renold numbers.
- The local Nusselt number increases when Prandtl number (fixed Weissenberg number) enhances or it decreases on increasing Weissenberg number (fixed Prandtl number).

Chapter 6

Boundary layer flow of Williamson nanofluid past a vertical exponentially stretching cylinder

6.1 Introduction

The boundary layer flow of Williamson nanofluid past an exponentially stretching surface is explored. The governing partial differential equations and the associated boundary conditions are reduced to nonlinear ordinary differential equations after using the boundary layer approximation and similarity transformation. The obtained system of nonlinear ordinary differential equations subject to the boundary conditions are solved numerically by employing Keller box method. The effects of different physical parameters (e.g. Reynold number Re , Schmidt number Sc , Prandtl number Pr , the natural convection parameter λ and Weissenberg number We , the buoyancy ratio N_r , the Brownian motion parameter N_b , the thermophoresis parameter N_t) on velocity, temperature and nano concentration profiles are presented through graphs. The skin friction coefficient and Nusselt number are also computed for different parameters.

6.2 Formulation

Consider the problem of natural convection and heat transfer of a Williamson nanofluid flowing past a vertical circular cylinder of radius a . Brownian motion thermophoresis are considered. The cylinder is stretched exponentially with velocity U_w . The temperature at the surface of the cylinder is assumed T_w and the uniform ambient temperature is taken as T_∞ . The flow under consideration is governed by

$$u_r + \frac{u}{r} + w_z = 0, \quad (6.1)$$

$$\begin{aligned} uw_r + ww_z &= \frac{\nu}{r}(\Gamma w_r^2 + w_r) + \nu[w_{rr} + 2\Gamma w_{rr}w_r] + g\beta(T - T_\infty)(1 - \phi_\infty) \\ &\quad + \frac{1}{\rho}(\rho^* - \rho)(\phi - \phi_\infty), \end{aligned} \quad (6.2)$$

$$uT_r + wT_z = \alpha(T_{rr} + \frac{1}{r}T_r) + \frac{\rho^*c_p^*}{\rho c_p}(D_T T_r \phi_r + \frac{D_T}{T_\infty} T_r^2), \quad (6.3)$$

$$u\phi_r + w\phi_z = D_B(\phi_{rr} + \frac{1}{r}\phi_r) + \frac{D_T}{T_\infty}(T_{rr} + \frac{1}{r}T_r). \quad (6.4)$$

In above expression, the velocity components along the (r, z) axes are (u, w) , ρ and ρ^* are the densities of the base fluid and the nanoparticle material respectively, k is the consistency coefficient, $\rho^*c_p^*$ is the effective heat capacity of the nanoparticle material and ρc_p is the effective heat capacity of the base fluid, g is the gravitational acceleration along the z - direction, D_B is Brownian diffusion coefficient, D_T is thermophoretic diffusion coefficient, β is the coefficient of thermal expansion, T is the temperature and α is the thermal diffusibility of base fluid. The corresponding boundary conditions can be written as

$$u(a, z) = 0, \quad w(a, z) = U_w \quad w(r, z) \longrightarrow 0 \text{ as } r \longrightarrow \infty, \quad (6.5)$$

$$T(a, z) = T_w(z), \quad T(r, z) \longrightarrow T_\infty \text{ as } r \longrightarrow \infty, \quad (6.6)$$

$$\phi(a, z) = \phi_w(z), \quad \phi(r, z) \longrightarrow \phi_\infty \text{ as } r \longrightarrow \infty, \quad (6.7)$$

in which $U_w = 2ake^{z/a}$ represents the fluid velocity at the surface of the cylinder.

6.3 Solution of the problem

Writing

$$u = -\frac{1}{2}U_w \frac{f(\eta)}{\sqrt{\eta}}, \quad w = U_w f'(\eta), \quad (6.8)$$

$$\theta = \frac{T - T_\infty}{T_w - T_\infty}, \quad \eta = \frac{r^2}{a^2}, \quad h = \frac{\phi - \phi_\infty}{\phi_w - \phi_\infty} \quad (6.9)$$

we have from *Eqs.* (6.1) to (6.4) as follows:

$$\eta f'''(4We\sqrt{\eta}f'' + 1) + f''(5We\sqrt{\eta}f'' + 1) + \text{Re}(ff'' - f'^2) + \text{Re}\lambda(1 - \phi_\infty)(\theta + N_r h) = 0, \quad (6.10)$$

$$\eta\theta'' + \theta' + \text{Re Pr}(f\theta' - f'\theta) + \eta\theta'(N_b h' + N_t \theta') = 0, \quad (6.11)$$

$$\eta h'' + h' + \frac{N_t}{N_b}(\eta\theta'' + \theta') + \text{Re Sc}(fh' - f'h) = 0. \quad (6.12)$$

in which $\lambda = g\beta a(T_w - T_\infty)/U_w^2$ is the natural convection parameter, $\text{Pr} = \nu/\alpha$ is the Prandtl number, $\text{Sc} = \nu/D_B$ is the Schmidt number, $We = 4\Gamma U_w/a$ is the local Weissenberg number, $N_r = (\rho^* - \rho)(\phi_w - \phi_\infty)/\rho\beta(T_w - T_\infty)(1 - \phi_\infty)$ is the buoyancy ratio, $N_b = \rho^*C_p^*D_B(\phi_w - \phi_\infty)/\rho C_p\alpha$ is the Brownian motion parameter, $N_t = \rho^*C_p^*D_T(\phi_w - \phi_\infty)/\rho C_p\alpha T_\infty$ is the thermophoresis parameter and $\text{Re} = aU_w/4\nu$ is the local Reynolds number. The boundary conditions can be expressed as

$$f(1) = 0, \quad f'(1) = 1, \quad \theta(1) = 1, \quad h(1) = 1, \quad (6.13)$$

$$f' \longrightarrow 0, \quad \theta \longrightarrow 0, \quad h \longrightarrow 0, \quad \text{as } \eta \longrightarrow \infty. \quad (6.14)$$

Flow quantities of interests are

$$\tau_w = \tau_{rz}|_{r=a}, \quad q_w = -k \tau_r|_{r=a}, \quad (6.15)$$

$$cf = \frac{\tau_w}{\rho U_w^2}, \quad Nu_z = \frac{ae^{z/a}q_w}{k(T_w - T_\infty)} \quad (6.16)$$

The solutions of the resulting problems are obtained by using Keller box method.

6.4 Results and discussion

The problem of natural convection boundary layer flow of Williamson nanofluid past an exponentially stretched cylinder is studied. The solution of the problem is obtained numerically with the help of Keller box method. Effect of the various parameters such as the Reynolds number Re , the Weissenberg number We , the Schmidt number Sc , the Brownian motion parameter N_b , the thermophoresis parameter N_t , the buoyancy ratio parameter N_r , the Prandtl number Pr and the natural convection parameter λ on the nondimensional velocity, temperature and concentration profiles are presented graphically in *Figs.6.1 – 6.10* and in *Tables 6.1 – 6.4*. From *Figs.6.1* to *6.4* the velocity profiles are presented for different physical parameters. *Fig.6.1* shows the effect of the buoyancy ratio parameter N_r on the velocity profile. It is observed that larger buoyancy ratio parameter N_r increases the velocity profile. *Fig.6.2* reflects the influence of natural convection parameter λ on the velocity profile. It is noticed that when natural convection parameter λ increases then velocity profile rapidly increases. That is the natural convection parameter λ is directly proportional to the velocity. In *Fig.6.3* the effects of the Weissenberg number We on the velocity profile are presented. Slight decrease in velocity profile is seen by increasing the values of Weissenberg number We . In *Fig.6.4*, with the increase of Reynold number Re , the velocity profile decreases. *Figs.6.5* to *6.8* reflect the behavior of temperature profiles for different physical parameters. *Fig.6.5* shows the influence of Prandtl number Pr on the temperature profile. By increasing the values of Prandtl number Pr , the temperature profile decreases. *Fig.6.6* describes the influence of Brownian motion parameter N_b on the temperature profile. The temperature profile increases by increasing the values of Brownian motion parameter N_b . *Fig.6.7* shows the effects of the Reynold number Re on the temperature profile. The temperature profile rapidly decreases by increasing the values of Reynold number Re . *Fig.6.8* shows the influence of the thermophoresis parameter N_t over the temperature profile. By increasing the values of the thermophoresis parameter N_t , the temperature profile increases. *Figs.6.9* and *6.10* highlight the nano concentration profile. In *Fig.6.9*, it is clear that by increasing the value of Schmidt number Sc the nano concentration profile decreases instantly.

In Fig.6.10, rising effect of Reynold number Re can be seen on nano concentration profile. By increasing the value of Reynolds number Re the nano concentration profile increases. Table 6.1 shows the boundary derivatives for the velocity profile at the surface of the cylinder that corresponds to the skin friction coefficient at the surface tabulated for different values of Re and λ . From table 6.1 it is observed that the magnitude of the boundary derivative increases with the increase in Re and it decreases by increasing the values of λ . Table 6.2 shows the boundary derivatives for the velocity profile at the surface of cylinder which corresponds to the skin friction coefficient at the surface tabulated for different values of N_r and λ . From table 6.2 it is observed that the magnitude of boundary derivative decreases by increasing both N_r and λ . Table 6.3 shows the values for local Nusselt numbers calculated for different values of N_b and Pr . From entries in the table it is noticed that with the increase in Pr , the local Nusselt number increases and it decreases by increasing N_b . Table 6.4 shows the values for local Nusselt numbers calculated for different values of N_t and Re . Tabulated values indicate that with the increase in Re the local Nusselt number increases and it decreases by increasing N_t .

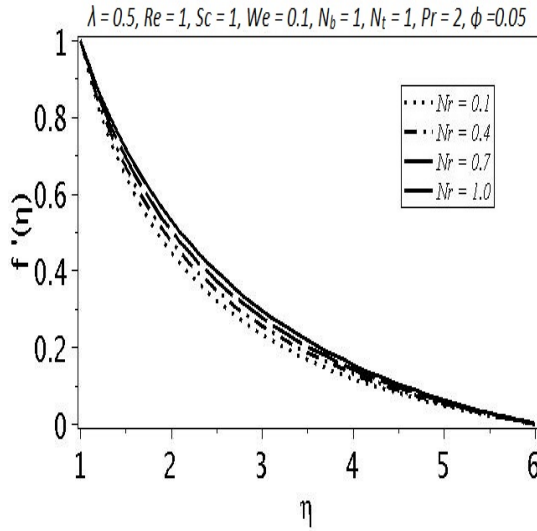


Fig.6.1 Influence of buoyancy ratio on velocity profile

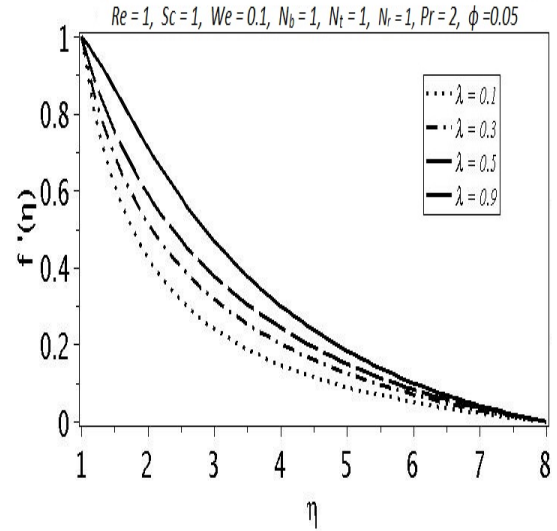


Fig.6.2 Influence of natural convection parameter on velocity profile

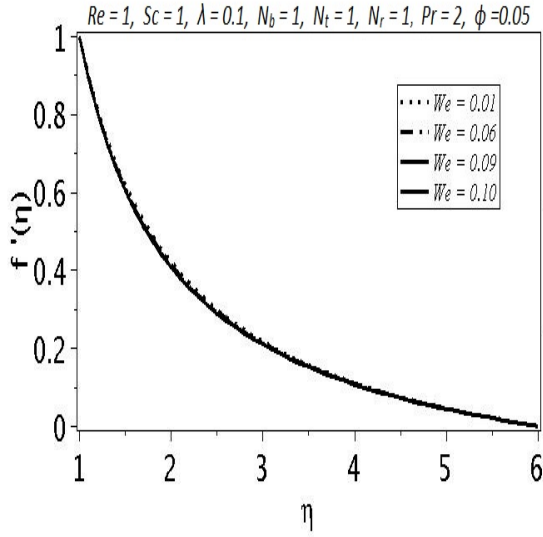


Fig.6.3 Influence of Weissenberg number on velocity profile

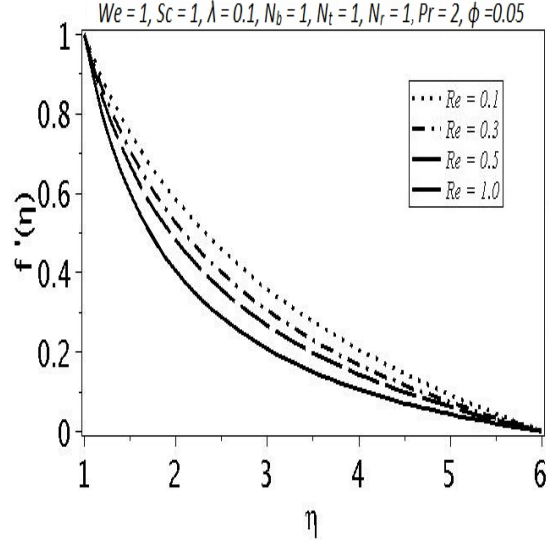


Fig.6.4 Influence of Reynolds number on velocity profile

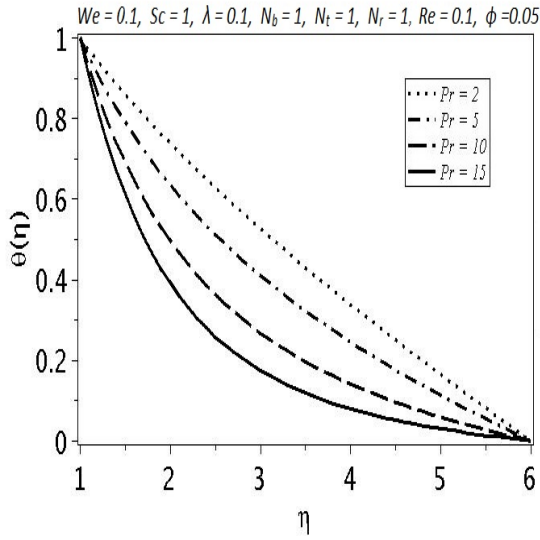


Fig.6.5 Influence of Prantdl number on temperature profile

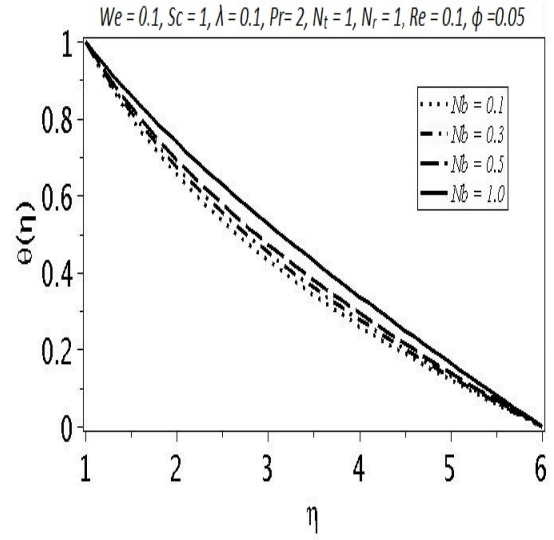


Fig 6.6 Influence of Brownian motion parameter on temperature profile

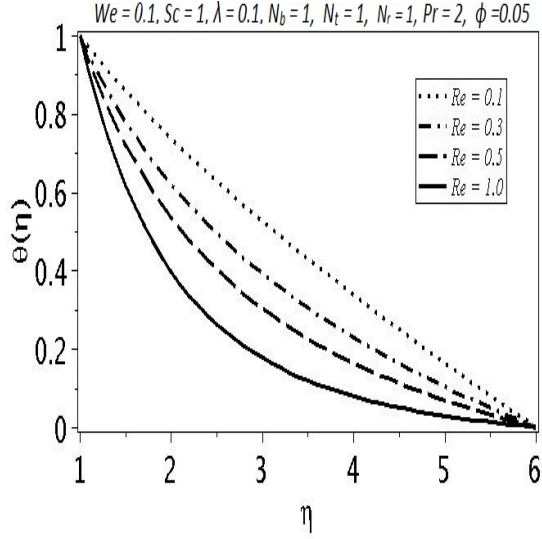


Fig.6.7 Influence of Reynold number on temperature profile

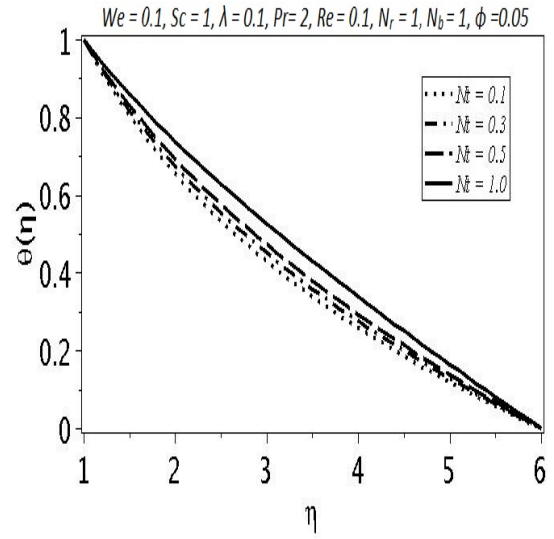


Fig.6.8 Influence of thermophoresis parameter on temperature profile

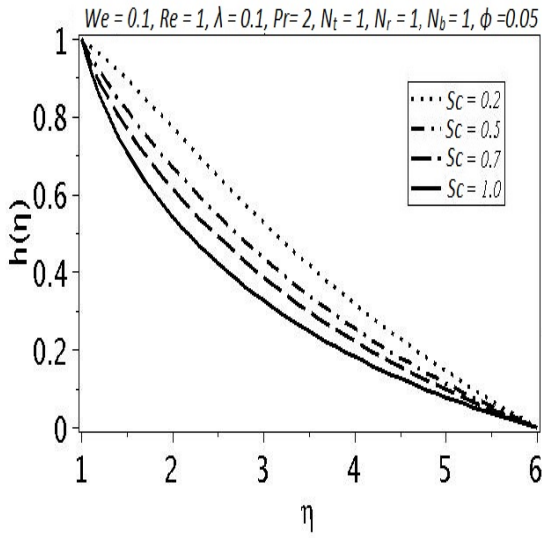


Fig.6.9 Influence of Schmidt number on concentration profile

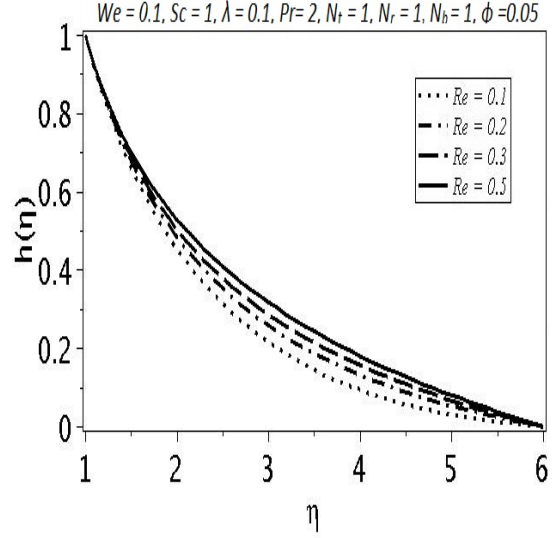


Fig.6.10 Influence of Reynold number on concentration profile

Table 6.1 : Skin friction coefficient at surface of the cylinder for $\lambda \backslash \text{Re}$.

$\lambda \backslash \text{Re}$	0.1	0.2	0.3	0.4	0.5	1.0
0.1	0.5417665	0.6472440	0.7405385	0.8256308	0.9048707	1.1877323
0.3	0.5047508	0.5878888	0.6638048	0.7338210	0.7991701	1.0823029
0.5	0.4685034	0.5308771	0.5911608	0.6478879	0.7011902	0.9304973
0.7	0.4329826	0.4759543	0.5220001	0.5667934	0.6093992	0.7926674
1.0	0.3809803	0.3970323	0.4237953	0.4526199	0.4810536	0.6052925

Table 6.2 : Skin friction coefficient at surface of the cylinder for $\lambda \backslash N_r$.

$\lambda \backslash N_r$	0.1	0.2	0.3	0.4	0.5	1.0
0.1	0.9225412	0.9170612	0.9115928	0.9061359	0.9006905	0.8736364
0.3	0.8274242	0.8119717	0.7966064	0.7813283	0.7661372	0.6914783
0.5	0.7389129	0.7145075	0.6903109	0.6663227	0.6425421	0.5267080
0.7	0.6557539	0.6231766	0.5909584	0.5590979	0.5275932	0.3752816
1.0	0.5391606	0.4954539	0.4523649	0.4098899	0.3680230	0.1674808

Table 6.3 : Local Nusselt numbers for different values of $\text{Pr} \backslash N_b$.

$\text{Pr} \backslash N_b$	0.1	0.2	0.3	0.4	0.5	1.0
1	0.3670232	0.3512651	0.3351202	0.3194159	0.3042953	0.2379131
3	0.5673555	0.5428482	0.5222006	0.5029387	0.4845972	0.4032442
5	0.7501875	0.7145851	0.6891727	0.6666279	0.6455541	0.5525502
10	1.1218606	1.0693323	1.0361168	1.0082439	0.9828072	0.8714786
15	1.4103439	1.3511575	1.3143805	1.2839238	1.2563011	1.1353196

Table 6.4 : Local Nusselt numbers for different values of $N_t \backslash \text{Re}$.

$N_t \backslash \text{Re}$	0.1	0.2	0.3	0.4	0.7	1.0
0.1	0.4577478	0.5829143	0.6903830	0.7851347	1.0196609	1.2079586
0.3	0.4197439	0.5424134	0.6478759	0.7408885	0.9709497	1.1553141
0.5	0.3846766	0.5047382	0.6081510	0.6994234	0.9251340	1.1057320
0.7	0.3524091	0.4697585	0.5710763	0.6606027	0.8820635	1.0590535
1.0	0.3089417	0.4220501	0.5201416	0.6070311	0.8222791	0.9941360

6.5 Conclusions

Keller box method is employed to find the numerical solution for flow of Williamson nanofluid past a vertical exponentially stretching cylinder. The main findings of the study are summarized below:

- The velocity profile increases upon increasing buoyancy ratio parameter and natural convection parameter but it decreases by increasing Weissenberg and Reynold numbers.
- The temperature profile increases for larger Brownian motion parameter N_b and thermophoresis parameter N_t .
- The nano concentration profile decreases upon increasing Schmidt number Sc and it increases by increasing Reynold number Re .
- Skin friction coefficient decreases upon increasing natural convection parameter λ and buoyancy ratio parameter N_r but it increases for increasing Reynold number Re .
- Local Nusselt number increases for larger Reynold and Prandtl numbers but it decreases when Brownian motion and thermophoresis parameters are increased.

Chapter 7

Dual stratified mixed convection flow of Eyring-Powell fluid past an inclined stretching cylinder with heat generation/absorption effect

7.1 Introduction

This chapter is proposed to study the effects of double stratified medium in the mixed convection boundary layer flow of Eyring-Powell fluid flow induced by an inclined stretching cylinder. Flow analysis is studied in the presence of heat generation/absorption. Temperature and concentration are assumed higher than ambient fluid across the surface of cylinder. The arising flow system of partial differential equations is primarily transformed into coupled non-linear ordinary differential equations with the aid of suitable transformations. Numerical solutions of resulting non-linear boundary value problem are computed successfully by utilizing fifth order Runge-Kutta algorithm with shooting technique. The velocity, temperature and concentration profiles are examined graphically. Further, the numerical findings are obtained for two distinct cases namely, zero (plate) and non-zero (cylinder) values of curvature parameter and the behaviour are presented through graphs for skin-friction coefficient, Nusselt number and Sherwood

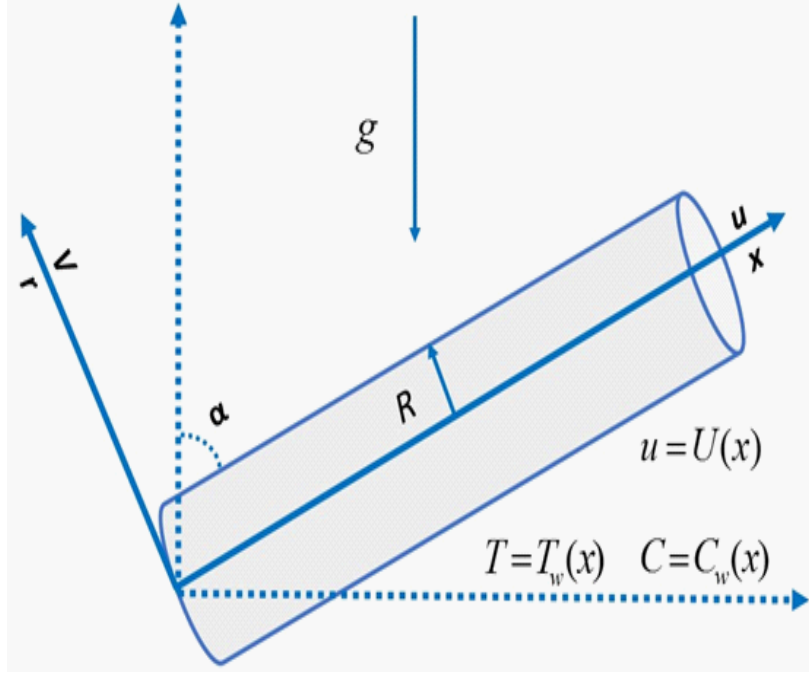


Figure 7-1: Fig. 7.1. Physical configuration and coordinate system.

number. The current analysis is validated by comparative analysis with previously published work.

7.2 Formulation

7.2.1 Flow analysis

Consider two dimensional and steady incompressible boundary layer flow of Eyring-Powell fluid by an inclined stretching cylinder. Flow analysis is taken with double stratification in the presence of mixed convection and heat generation/absorption. Temperature and concentration at the surface of cylinder are assumed at higher than the ambient fluid. The boundary layer approximation give rise to following expression:

$$\frac{\partial (ru)}{\partial x} + \frac{\partial (rv)}{\partial r} = 0, \quad (7.1)$$

$$u \frac{\partial u}{\partial x} + v \frac{\partial u}{\partial r} = \left(\nu + \frac{1}{\beta \rho c} \right) \frac{\partial^2 u}{\partial r^2} - \frac{1}{2\beta c^3 \rho} \left(\frac{\partial u}{\partial r} \right)^2 \frac{\partial^2 u}{\partial r^2} + \frac{1}{r} \left(\nu + \frac{1}{\beta \rho c} \right) \frac{\partial u}{\partial r} - \frac{1}{6\beta r \rho c^3} \left(\frac{\partial u}{\partial r} \right)^3 + g\beta_T (T - T_\infty) + g\beta_c (C - C_\infty) \cos \alpha. \quad (7.2)$$

The axial direction of cylinder is supposed as x - *axis* and r - *axis* is perpendicular to it. In the above expressions, the velocity components u and v are in the x and r direction respectively. Here ρ is the fluid density, ν is the kinematic viscosity, β_T is the coefficient of thermal expansion, β_c is the coefficient of concentration expansion and α is the inclination of cylinder with x - *axis* respectively. Note that β and c are the Eyring-Powell fluid parameters. The corresponding boundary conditions are

$$u(x, r) = U(x) = \frac{U_o}{L} x, v(x, r) = 0, \text{ at } r = R, \text{ and } u(x, r) \rightarrow 0, \text{ as } r \rightarrow \infty, \quad (7.3)$$

Stream function satisfying continuity Eq. (7.1) is defined by the equations:

$$u = \frac{1}{r} \left(\frac{\partial \psi}{\partial r} \right), \quad v = \frac{-1}{r} \left(\frac{\partial \psi}{\partial x} \right). \quad (7.4)$$

To trace out the solution of Eq. (7.2) under boundary conditions Eq. (7.3), we used following transformations:

$$\eta = \frac{r^2 - R^2}{2R} \left(\frac{U}{\nu L} \right)^{\frac{1}{2}}, \quad \psi = \left(\frac{U_0 \nu}{L} x^2 \right)^{\frac{1}{2}} R f(\eta), \quad u = \frac{U_0 x f'(\eta)}{L}, \quad v = -\frac{R}{r} \sqrt{\frac{U_0 \nu}{L}} f(\eta), \quad (7.5)$$

where U_0 is the free stream velocity, L is the reference length, $f'(\eta)$ represents dimensionless variable and prime denotes differentiation with respect to η (similarity variable) that is the velocity of fluid past an inclined stretching cylinder having radius R . Incorporating Eqs. (7.4) – (7.5) into Eq. (7.2), we get

$$(1 + 2K\eta)(1 + M)f''' + ff'' - (f')^2 + 2K(1 + M)f'' - \frac{4}{3}\lambda MK(1 + 2K\eta)(f'')^3$$

$$-M\lambda(1+2K\eta)^2(f'')^2 f''' + \lambda_m(\theta + N\phi)\cos\alpha = 0, \quad (7.6)$$

with

$$f'(0) = 1 \quad , \quad f(0) = 0 \quad , \quad f'(\infty) \rightarrow 0 \quad (7.7)$$

Here, K , M , λ , λ_m , and N denote curvature parameter, fluid parameters, mixed convection parameter and ratio of thermal to concentration buoyancy forces respectively. These definitions are

$$K = \frac{1}{R}\sqrt{\frac{\nu}{a}} \quad , \quad M = \frac{1}{\mu\beta c} \quad , \quad \lambda = \frac{ax^3}{2c^2\nu} \quad , \quad \lambda_m = \frac{Gr}{\text{Re}_x^2} \quad , \quad N = \frac{Gr}{Gr^*} \quad \text{and} \quad a = \frac{U_0}{L} \quad (7.8)$$

where Gr and Gr^* denotes Grashof number due to temperature and concentration respectively as

$$Gr^* = \frac{g\beta_T(T_w - T_0)x^3}{\nu^2} \quad , \quad Gr = \frac{g\beta_C(C_w - C_0)x^3}{\nu^2} \quad (7.9)$$

The skin friction coefficient at the surface of cylinder is considered as

$$C_f = \frac{\tau_w}{\rho \frac{U^2}{2}}, \quad (7.10)$$

$$\tau_w = \left[\mu \left(\frac{\partial u}{\partial r} \right) + \frac{1}{\beta c} \frac{\partial u}{\partial r} - \frac{1}{6\beta c^3} \left(\frac{\partial u}{\partial r} \right)^3 \right]_{r=R}, \quad (7.11)$$

where μ denotes dynamic viscosity of fluid and τ is the shear stress. The dimensionless form of skin friction coefficient is given by

$$C_f \text{Re}_x^{1/2} = 2(1+M)f''(0) - \frac{2M\lambda}{3}[f''(0)]^3, \quad (7.12)$$

with $\text{Re}_x = U_0^2 x / \nu L$ is local Reynolds number.

7.2.2 Heat and mass transfer analysis

Heat transfer analysis is carried out in the presence of heat generation/absorption. The destruction of fluctuation velocity gradients by action of viscous stresses in a laminar boundary layer flow of Eyring-Powell fluid is assumed small so the viscous dissipation is neglected. Thun under boundary layer approximation, the energy and concentration equations take the forms

$$u \frac{\partial T}{\partial x} + v \frac{\partial T}{\partial r} = \frac{K}{\rho C_P} \frac{\partial}{\partial r} \left(r \frac{\partial T}{\partial r} \right) + \frac{Q_0(T - T_\infty)}{\rho C_P}, \quad (7.13)$$

$$u \frac{\partial C}{\partial x} + v \frac{\partial C}{\partial r} = \frac{D}{r} \frac{\partial}{\partial r} \left(r \frac{\partial C}{\partial r} \right), \quad (7.14)$$

where K denotes thermal conductivity, C_P is specific heat at constant pressure, D the mass diffusivity and Q_0 the heat generation and absorption coefficient. Temperature and concentration boundary conditions for the fluid flow problem are

$$\begin{aligned} T(x, r) &= T_w(x) = T_0 + \frac{b x}{L}, \quad C(x, r) = C_w(x) = C_0 + d \frac{x}{L} \quad \text{at } r = R, \\ T(x, r) &\rightarrow T_\infty(x) = T_0 + \frac{c x}{L}, \quad C(x, r) \rightarrow C_\infty(x) = C_0 + e \frac{x}{L}, \quad \text{as } r \rightarrow \infty, \end{aligned} \quad (7.15)$$

where $T_w(x)$, $C_w(x)$, $T_\infty(x)$, $C_\infty(x)$, T_0 , C_0 denotes prescribed surface temperature, surface concentration, variable ambient temperature, variable ambient concentration, reference temperature and reference concentration respectively. Here b , c , d and e are positive constants. To find out the dimensionless forms of Eqs. (7.13) and Eq. (7.14) under boundary conditions, *i.e* Eq. (7.15), we define

$$\eta = \frac{r^2 - R^2}{2R} \left(\frac{U_0}{\nu L} \right)^{\frac{1}{2}}, \quad \theta(\eta) = \frac{T - T_\infty}{T_w - T_0}, \quad \phi(\eta) = \frac{C - C_\infty}{C_w - C_0}, \quad (7.16)$$

After substituting Eq. (7.16) in Eqs. (7.13) – (7.14), the dimensionless form of energy and concentration equations is given by

$$(1 + 2K\eta)\theta'' + 2K\theta' + \text{Pr} \left(f\theta' - f'\theta - f'\epsilon_1 + \delta_H\theta \right) = 0. \quad (7.17)$$

$$(1 + 2K\eta)\phi'' + 2K\phi' + Sc \left(f\phi' - f'\phi - f'\epsilon_2 \right) = 0, \quad (7.18)$$

subject to the transformed boundary conditions

$$\theta = 1 - \epsilon_1, \quad \phi = 1 - \epsilon_2 \quad \text{at} \quad \eta = 0, \quad \theta \rightarrow 0, \quad \phi \rightarrow 0, \quad \text{as} \quad \eta \rightarrow \infty, \quad (7.19)$$

where Pr , ϵ_1 , δ_H , Sc and ϵ_2 denote Prandtl number, thermal stratification parameter, heat generation/absorption parameter, Schmidt number and solutal stratification parameter respectively. These have definitions

$$\text{Pr} = \frac{\rho C_P}{K}, \quad \epsilon_1 = \frac{c}{b}, \quad \delta_H = \frac{LQ_0}{U_0 \rho C_P}, \quad Sc = \frac{\nu}{D}, \quad \epsilon_2 = \frac{e}{d} \quad (7.20)$$

The local Nusselt and Sherwood numbers are defined as

$$Nu_x = \frac{xq_w}{k(T_w - T_\infty)}, \quad q_w = -k \left(\frac{\partial T}{\partial r} \right)_{r=R} \quad (7.21)$$

$$Sh = \frac{-xj_w}{D(C_w - C_0)}, \quad j_w = -D \left(\frac{\partial C}{\partial r} \right)_{r=R} \quad (7.22)$$

in dimensionless form, these quantities are

$$Nu_x \text{Re}_x^{-1/2} = -\theta'(0), \quad Sh \text{Re}_x^{-1/2} = -\phi'(0), \quad (7.23)$$

7.3 Results and discussion

7.3.1 Numerical solution

The systems of governing coupled non-linear ordinary differential equations, *i.e* Eqs. (7.6), (7.17) and (7.18) subject to boundary conditions (7.7) and (7.19) are solved by employing shooting method with the aid of fifth order Runge-Kutta scheme. Firstly, reduction has been done in a

system of seven first order simultaneous equations by letting

$$\begin{aligned} Z_2 &= f', \\ Z_3 &= Z_2' = f'', \\ Z_5 &= \theta', \\ Z_6 &= \phi'. \end{aligned}$$

Then, the equivalent form of Eqs. (7.6), (7.17) and (7.18) under new variables is given by:

$$\begin{aligned} Z_1' &= Z_2, \\ Z_2' &= Z_3, \\ Z_3' &= \frac{(Z_2)^2 - Z_1 Z_3 - 2K(1+M)Z_3 + \frac{4}{3}\lambda MK(1+2K\eta)Z_3^3 - \lambda_m(Z_4 + NZ_6)\cos\alpha}{(1+2K\eta)(1+M) - M\lambda(1+2K\eta)^2 Z_3^2}, \\ Z_4' &= Z_5, \\ Z_5' &= \frac{\text{Pr}(Z_2 Z_4 + \epsilon_1 Z_2 - Z_1 Z_5 - \delta_H Z_4) - 2K Z_5}{1+2K\eta}, \\ Z_6' &= Z_7, \\ Z_7' &= \frac{Sc(Z_2 Z_6 + \epsilon_2 Z_1 - Z_1 Z_7) - 2K Z_7}{1+2K\eta}. \end{aligned} \tag{7.24}$$

The corresponding boundary conditions in new variables are given as follows:

$$\begin{aligned} Z_1(0) &= 0, \\ Z_2(0) &= 1, \\ Z_3(0) &= \text{unknown}, \\ Z_4(0) &= 1 - \epsilon_1, \\ Z_5(0) &= \text{unknown}, \\ Z_6(0) &= 1 - \epsilon_2, \\ Z_7(0) &= \text{unknown}. \end{aligned} \tag{7.25}$$

In order to integrate Eq. (7.25) as an initial value problem, we required values for $Z_3(0)$ i.e. $f''(0)$, $Z_5(0)$ i.e. $\theta'(0)$ and $Z_7(0)$ implies $\phi'(0)$. The initial conditions $Z_3(0)$, $Z_5(0)$, $Z_7(0)$ are not given but we have additional boundary conditions

$$\begin{aligned} Z_2(\infty) &= 0, \\ Z_4(\infty) &= 0, \\ Z_6(\infty) &= 0. \end{aligned} \tag{7.26}$$

<i>Table – 7.1 : Numerical values of skin friction coefficient for K, Pr and M.</i>			
K	Pr	M	$\frac{1}{2}C_f Re_x^{1/2} = (1 + M)f''(0) - \frac{M\lambda}{3}[f''(0)]^3$
0.1	1.1	0.1	-0.9809
0.2	-	-	-1.0254
0.3	-	-	-1.0694
0.1	1.1	0.1	-0.9809
-	1.2	-	-0.9825
-	1.3	-	-0.9839
0.1	1.1	0.1	-0.9809
-	-	0.2	-1.0268
-	-	0.3	-1.0779

By choosing favourable guessed values of $f''(0)$, $\theta'(0)$ and $\phi'(0)$, the integration of system of first order differential equations are carried out in such a way that the boundary conditions given in Eq. (7.27) holds absolutely. The step size $\Delta\eta = 0.05$ is used to obtain the numerical solution with four decimal accuracy as convergence criteria.

Tables 7.1 and 7.2 are constructed to indicate the influence of embedded physical parameters symbolically, K , Pr , M , λ , Sc , ϵ_1 , ϵ_2 on skin friction coefficient. Adopted parametric values are mixed convection parameter $\lambda_m = 0.1$, ratio of buoyancy forces $N = 0.1$, inclination angle $\alpha = 30^\circ$ and heat generation/absorption parameter $\delta_H = 0.1$. It is revealed that skin friction coefficient increases (in absolute sense) for higher values of curvature parameter K , thermal stratification parameter ϵ_1 , solutal stratification parameter ϵ_2 fluid parameter M , Prandtl

number Pr and Schmidt number Sc . Skin friction coefficient shows declined effect on fluid parameters λ .

<i>Table – 7.2 :</i> Numerical values of skin friction coefficient for λ , Sc , ϵ_1 and ϵ_2 .				
λ	Sc	ϵ_1	ϵ_2	$\frac{1}{2}C_f Re_x^{1/2} = (1 + M)f''(0) - \frac{M\lambda}{3}[f''(0)]^3$
0.1	1.1	0.1	0.1	-0.9809
0.2	-	-	-	-0.9760
0.3	-	-	-	-0.9738
0.1	1.1	0.1	0.1	-0.9809
-	1.2	-	-	-0.9850
-	1.3	-	-	-0.9893
0.1	1.1	0.1	0.1	-0.9809
-	-	0.2	-	-0.9868
-	-	0.3	-	-0.9937
0.1	0.2	0.1	0.1	-0.9809
-	-	-	0.2	-0.9887
-	-	-	0.3	-0.9995

Tables 7.3–7.4 show the influence of different physical parameters on heat and mass transfer rate for fluid parameters $\lambda = 0.1$ and $M = 0.1$, mixed convection parameter $\lambda_m = 0.1$, ratio of buoyancy forces $N = 0.1$, inclination angle $\alpha = 30^\circ$ and heat generation/absorption parameter $\delta_H = 0.1$. Particularly, Table 7.3 shows the variation of heat transfer rate against frequent values of curvature parameter K , Prandtl number Pr and thermal stratification parameter ϵ_1 . Table 7.4 shows the rate variation of mass transfer for different values of curvature parameter K , Schmidt number Sc and solutal stratification parameter ϵ_2 . It is examined that the heat and mass transfer rate increases for larger values of curvature parameter, Prandtl number Pr and Schmidt number Sc , respectively. Heat and mass transfer rates exhibit decreasing behavior towards thermal stratification parameter and solutal stratification parameter respectively. By having Eqs. (7.6) and (7.17) the flow problem can be identified by Ishak and Nazar [55]. Furthermore, in the absence of curvature parameter (i.e $K = 0$)

Table – 7.3 : Temperature gradient at the surface of cylinder
for various values of K , Pr and ϵ_1 .

K	Pr	ϵ_1	$-\theta'(0)$
0.1	1.1	0.1	1.0983
0.2	-	-	1.1306
0.3	-	-	1.1632
0.1	1.1	0.1	1.0983
-	1.2	-	1.1553
-	1.3	-	1.2101
0.1	1.1	0.1	1.0983
-	-	0.2	1.0567
-	-	0.3	1.0144

Table – 7.4 : Mass transfer rate at outer surface of cylinder
for different values of K , Sc and ϵ_2 .

K	Sc	ϵ_2	$-\phi'(0)$
0.1	0.2	0.1	0.4500
0.2	-	-	0.5020
0.3	-	-	0.5512
0.1	0.2	0.1	0.4500
-	0.3	-	0.5220
-	0.4	-	0.6068
0.1	0.2	0.1	0.4500
-	-	0.2	0.4013
-	-	0.3	0.3711

For $M = 0$, $\lambda = 0$, $\lambda_m = 0$, $\alpha = 0^\circ$, $\epsilon_1 = 0$, and $\delta_H = 0$, Eqs. (7.6) and (7.17) reduce to the flow problem given by Grubka and Bobba [56] . Table 7.5 is constructed to compare the heat transfer rate for various values of Prandtl number Pr in a limited sense. An excellent agreement has been found which leads to conformity of present work.

<i>Table – 7.5 : Comparision of heat transfer rate for different values of Prandtl number Pr</i>			
Pr	Grubka and Bobba [56]	Ishak and Nazar [55]	Present study
0.72	0.8086	0.8086313	0.8089
1.00	1.0000	1.0000000	1.0000
3.00	1.9237	1.9236825	1.9239
10.0	3.7207	3.7206739	3.7208

7.3.2 Velocity profiles

Figs. 7.2 – 7.8 illustrate the effects of flow controlling parameters on non-dimensional velocity profiles. Fig. 7.2 shows that an increase in thermal stratification parameter ϵ_1 leads to decrease in velocity profile. This effect is due to drop of convective potential between surface of cylinder and ambient temperature. Fig. 7.3 identifies that an increase in mixed convection parameter λ_m yields an increase in fluid velocity. Physically, this is due to enhancement of thermal buoyancy force. Higher values of mixed convection parameter λ_m lead to an increase in velocity within a boundary layer. The behaviour of an inclination α on velocity is depicted in Fig. 7.4. It is noticed that for higher values of an inclination α the velocity profile declines. Because by increasing an inclination α relative to x -axis the influence of gravity is reduced which results decline in velocity within a boundary layer. Fig. 7.5 illustrates that for larger values of curvature parameter K the radius of cylinder decreases and fluids motion accelerates. This is due to reduction of contact surface area of cylinder with fluid which offers less resistance to fluid flow. So increase in curvature parameter K causes increase in velocity profile within the boundary layer. The effect of solutal stratification parameter ϵ_2 on velocity is displayed in Fig. 7.6. It is observed that the fluid velocity decreases within boundary layer for the increasing values of solutal stratification parameter ϵ_2 . Fig. 7.7 evidents that the velocity profile increases against increasing value of fluid parameter M . Because fluid parameter M has inverse relation with viscosity so higher values of fluid parameter M brings fluid to be less viscous which results increase in rate of deformation. Fig. 7.8 is sketched to examine the effects of ratio of buoyancy forces N on velocity profile. As N is the ratio of concentration to the thermal buoyancy forces, so larger values of buoyancy forces N reflects dominance in concentration buoyancy force which yield an increase in velocity distribution within a boundary layer.

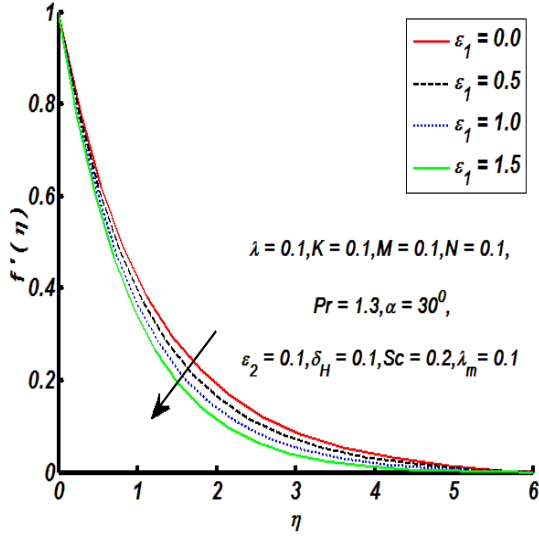


Fig. 7.2. Effect of thermal stratification parameter ϵ_1 on velocity profile.

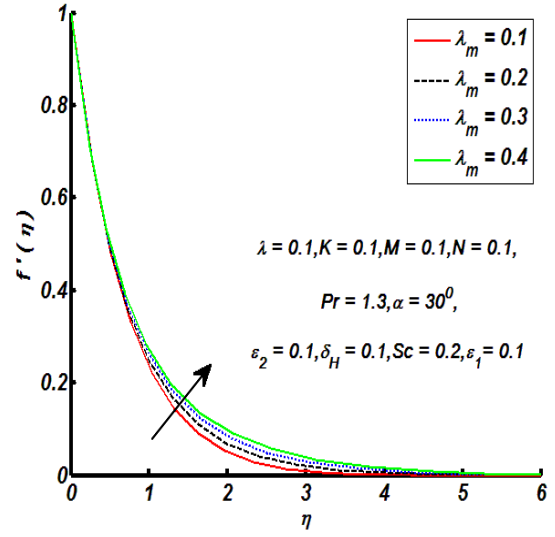


Fig. 7.3. Effect of mixed convection parameter on velocity profile.

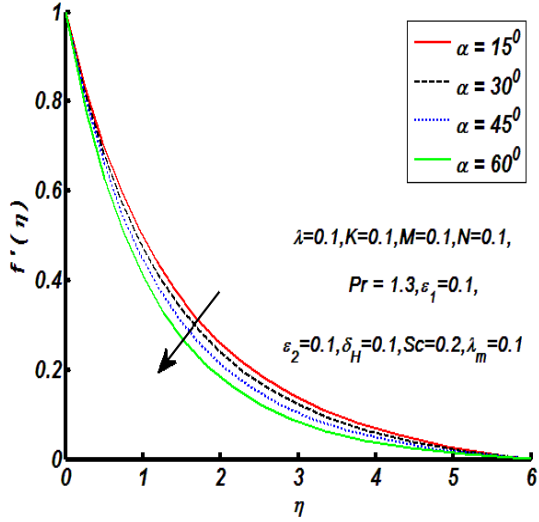


Fig. 7.4. Effect of an inclination on velocity profile.

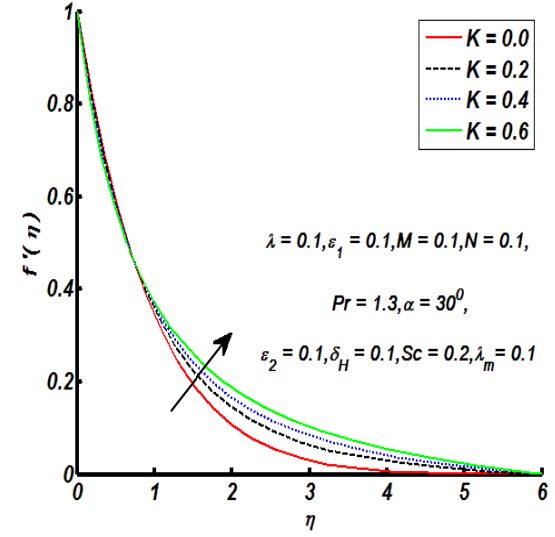


Fig. 7.5. Effect of curvature parameter K on velocity profile.

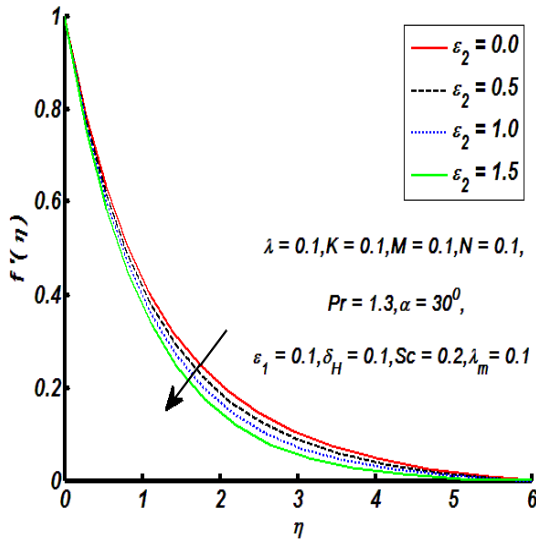


Fig. 7.6. Effect of solutal stratification parameter on velocity profile.

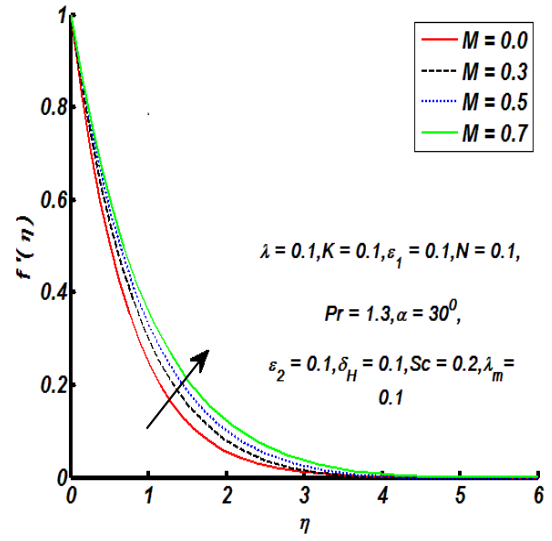


Fig. 7.7. Effect of fluid parameter M on velocity profile.

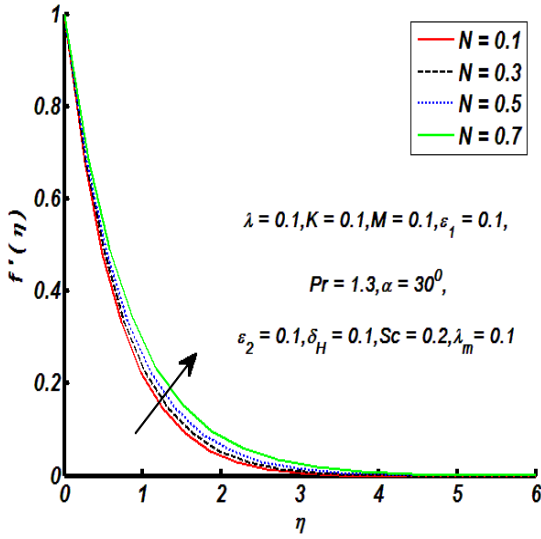


Fig. 7.8. Effect of ratio of buoyancy forces N on velocity profile.

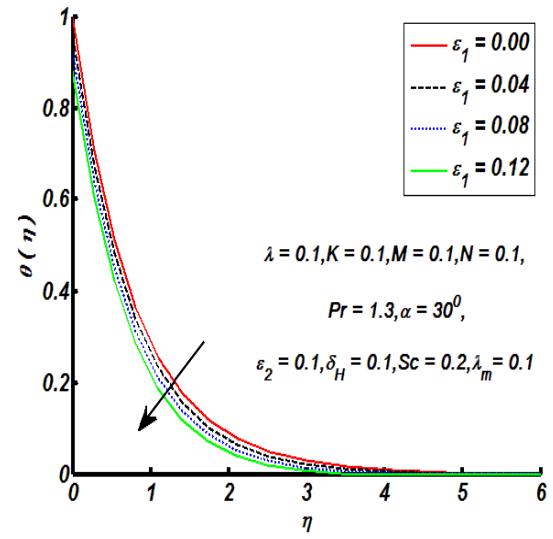


Fig. 7.9. Effect of thermal stratification parameter on temperature profile.

7.3.3 Temperature profile

Figs. 7.9–7.14 reflect the impacts of different physical flow parameters on temperature profiles. Influence of thermal stratification parameter ϵ_1 on temperature profile is given by Fig. 7.9. It is prominent from figure that the temperature distribution decreases for increasing values of thermal stratification parameter ϵ_1 . This outcome is due to declined in temperature difference between surface of cylinder and ambient fluid. Hence temperature profile decreases within thermal boundary layer. Fig. 7.10 provides the influence of an inclination α against temperature distribution. It is noticed that an increase in inclination α shows enhancement in temperature within a boundary layer. This fact is due to gravity effect. For larger values of an inclination α the gravity effect reduces. It shows decrease in rate of heat transfer. Therefore temperature distribution increases. Fig. 7.11 elaborates the influence of heat generation/heat absorption parameter δ_H on temperature distribution. It is explored that increase in heat generation/heat absorption parameter δ_H causes increase in temperature of fluid. Here significant heat is produced during heat generation phenomena which results an increase in temperature distribution. Fig. 7.12 illustrates that the temperature distribution increases due to larger curvature parameter K . Temperature is stated as an average kinetic energy so, when we increase curvature parameter K of cylinder, velocity of the fluid increases which results increase in kinetic energy and due to which temperature increases. Note that temperature profile decreases adjacent to the surface of cylinder and it increases away from it. It is clearly seen that an increase in intensity of buoyancy forces shows an increase in temperature of fluid. Fig. 7.13 indicates that the temperature distribution increases for higher values of solutal stratification parameter ϵ_2 . Fig. 7.14 presents the influence of Prandtl number Pr on temperature profile. Prandtl number Pr has inverse relation towards thermal conductivity, fluid with higher Prandtl number Pr . Hence an increase in Prandtl number Pr causes a strong reduction in temperature of the fluid which results thinner thermal boundary layer. Sometimes we may have overshoot in the thermal boundary layer due to higher thermal conductivity. That effect can be controlled by introducing heat sink which helps to moderate the temperature.

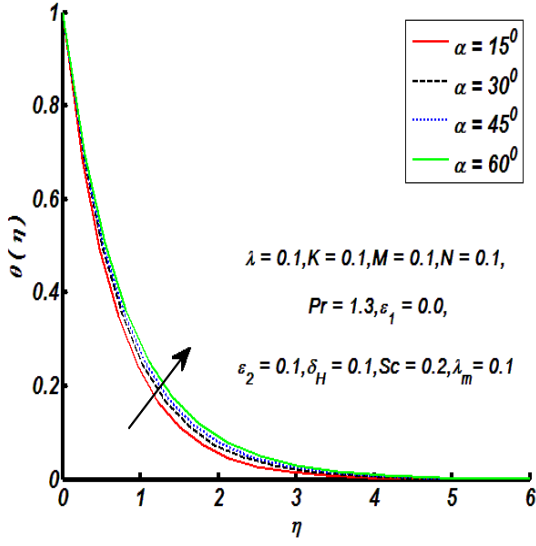


Fig. 7.10. Effect of an inclination on temperature profile.

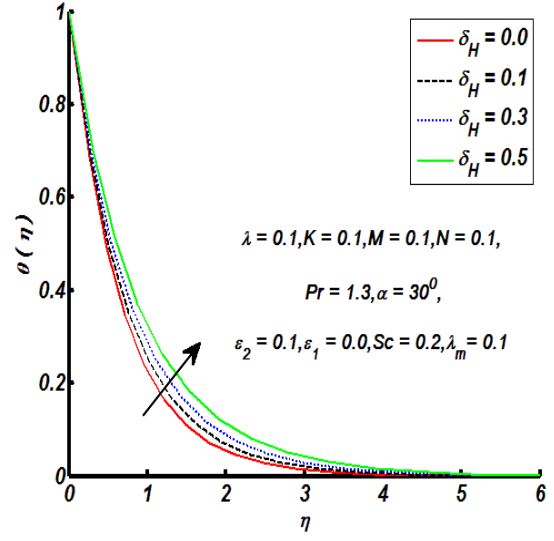


Fig. 7.11. Effect of heat generation/absorption parameter on temperature profile

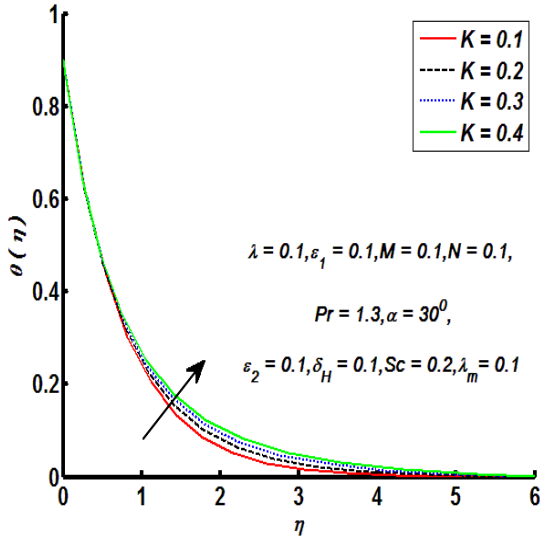


Fig. 7.12. Effect of curvature parameter K on temperature profile.

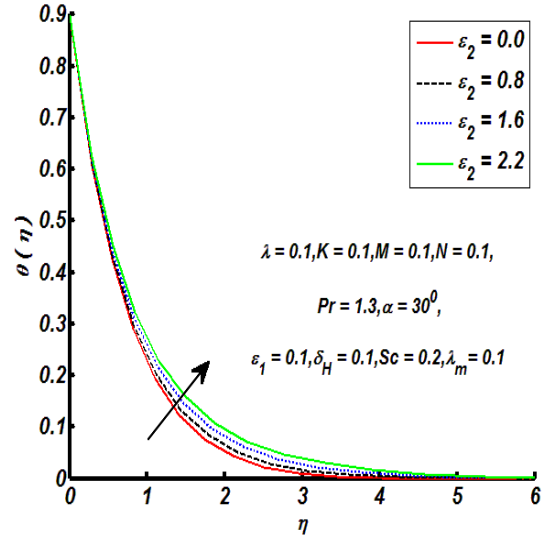


Fig. 7.13. Effect of solutal stratification parameter on temperature profile.

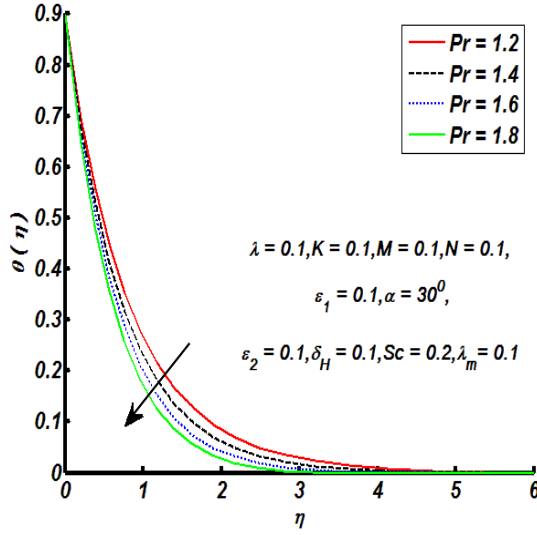


Fig. 7.14. Effect of Prandtl number Pr on temperature profile.

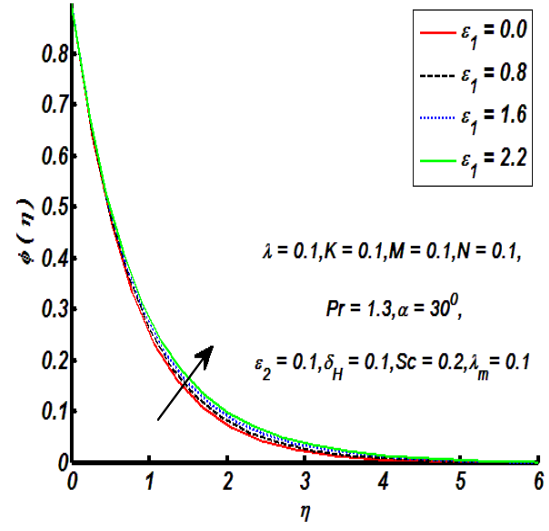


Fig. 7.15. Effect of thermal stratification parameter on concentration profile.

7.3.4 Concentration profile

Figs. 7.15 – 7.20 include the effects of several involved parameters over concentration profile. Fig. 7.15 demonstrates the impact of thermal stratification parameter ϵ_1 on concentration profile. An increase in thermal parameter ϵ_1 brings inciting in fluid concentration across the surface of cylinder. From Fig. 7.16, it is witnessed that the concentration boundary layer decreases by increasing Schmidt number Sc . Since this effect is similar to Pr verses thermal boundary layer. As Sc has inverse proportional behavior towards mass diffusivity. Thus higher values of Schmidt number Sc bring thinning in the concentration boundary layer. As a result concentration distribution decreases. Influence of solutal stratification parameter ϵ_2 is described through Fig. 7.17 over concentration profile. It is clear that concentration, the boundary layer thickness decreases for higher values of solutal stratification coefficient ϵ_2 . Influence of an inclination α and mixed convection parameter λ_m on skin friction coefficient for both plate and cylinder is sketched in Fig. 7.18. It is acknowledged that for increasing values of an inclination α the skin friction coefficient increases whereas it shows opposite effect for mixed convection parameter λ_m . Further, the magnitude of skin friction coefficient is higher for cylinder when compared with plate. Fig. 7.19 witnesses that mass transfer rate decreases for larger values

of an inclination α and heat generation/absorption parameter δ_H . It is also noticed that the strength of mass transfer rate is slightly larger for cylinder than plate. Fig. 7.20 is constructed to examine the behaviour of mixed convection λ_m and ratio of thermal to concentration buoyancy forces N on mass transfer rate. It is analyzed that for larger values of both mixed convection parameter λ_m and ratio of buoyancy forces N , the mass transfer rate increases. The magnitude of mass transfer rate for cylinder is more when compared to plate.

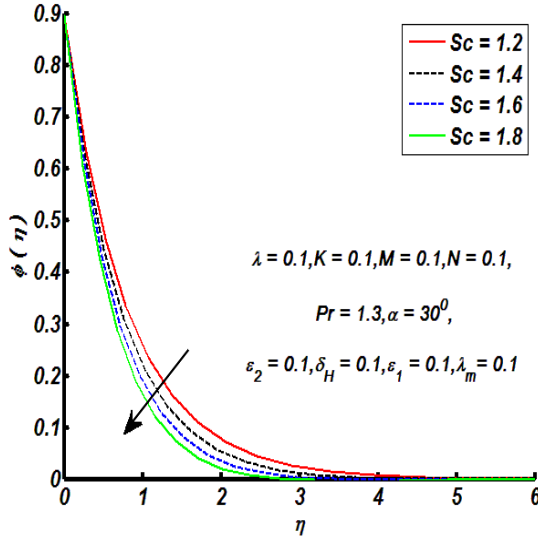


Fig. 7.16. Effect of Schmidt number Sc on concentration profile.

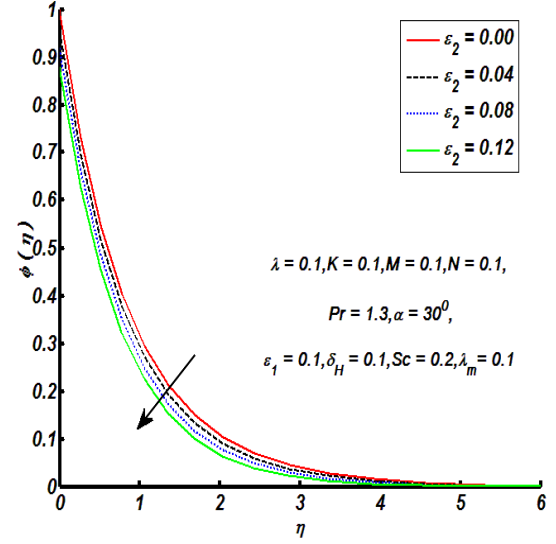


Fig. 7.17. Effect of solutal stratification parameter on concentration profile.

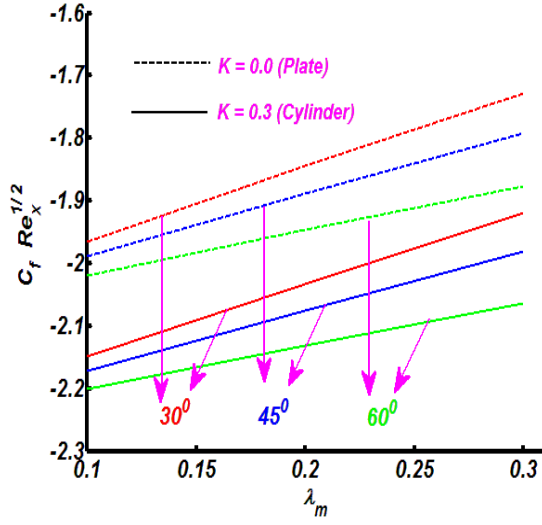


Fig. 7.18. Effect of an inclination and mixed convection on skin friction.

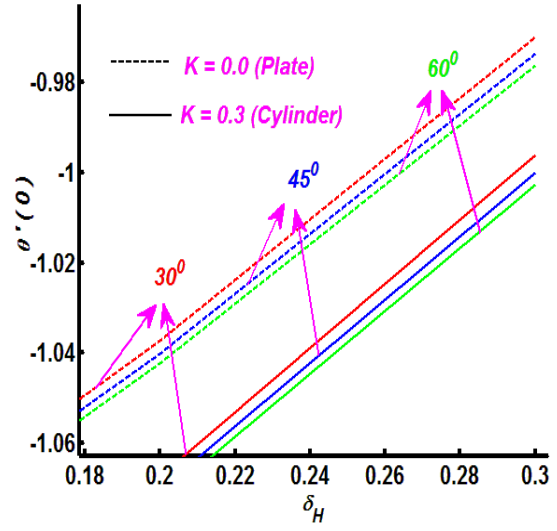


Fig. 7.19. Effect of an inclination and heat generation parameter on local Nusselt number.

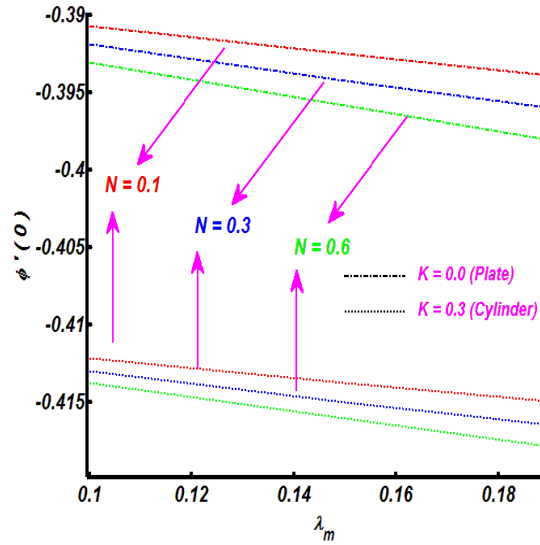


Fig. 7.20. Effect of mixed convection and ratio of buoyancy forces N on local Sherwood number.

7.4 Conclusions

Double stratified mixed convection boundary layer flow of Eyring-Powell fluid induced by an inclined stretching cylinder is reported. Flow analysis is carried out with heat generation process. The findings of present study are listed as follows:

- The fluid velocity increases significantly for larger values of curvature parameter K , fluid parameter M , mixed convection parameter λ_m and ratio of buoyancy forces N . However velocity profile shows opposite variation for thermal stratification parameter ϵ_1 , solutal stratification parameter ϵ_2 and an inclination α .
- The fluid temperature is increasing function of solutal stratification parameter ϵ_2 , curvature parameter K , an inclination α and heat generation/absorption parameter δ_H . Temperature decays for thermal stratification parameter ϵ_1 and Prandtl number Pr .
- The concentration profile increases for increasing values of thermal stratification parameter ϵ_1 while it decreases for solutal stratification parameter ϵ_2 and Schmidt number Sc .
- Skin friction coefficient expressively enriches for cylinder in comparison to plate regarding an inclination α and it reduces for mixed convection parameter λ_m .
- Higher values of an inclination α and heat generation/absorption parameter δ_H shows reduction in heat transfer rate.
- Mass transfer rate considerably increases for both mixed convection parameter λ_m and ratio of buoyancy forces N .

Chapter 8

Boundary layer flow of second grade fluid past a vertical exponentially stretching cylinder

8.1 Introduction

In this chapter, we obtained the similarity solution for the boundary layer flow of a second grade fluid past a vertical cylinder stretching exponentially along its radial direction. Heat transfer is also analyzed. The resulting boundary layer problems are solved. The obtained system of equations subject to the boundary conditions are solved with the help of homotopy analysis method (HAM). The effects of the different parameters including Reynolds numbers, Prandtl numbers and the natural convection parameter are presented through graphs. The skin friction coefficient and Nusselt numbers are studied for different parameters.

8.2 Mathematical formulation

Consider the problem of natural convection boundary layer flow of a second grade fluid flowing over a vertical circular cylinder of radius a . The cylinder is assumed to be stretched exponentially with velocity U_w . The temperature at the surface of the cylinder is T_w and the uniform ambient temperature is taken as T_∞ such that $T_w - T_\infty > 0$ in case of the assisting flow, while

$T_w - T_\infty < 0$ for opposing flow, respectively. Under these assumptions the boundary layer equations of motion and heat transfer are

$$u_r + \frac{u}{r} + w_z = 0, \quad (8.1)$$

$$\begin{aligned} uw_r + ww_z &= \nu(w_{rr} + \frac{1}{r}w_r) + \frac{\alpha_1}{\rho}[uw_{rrr} + ww_{rrz} + w_{rr}w_z - w_ru_{rr} \\ &\quad + \frac{1}{r}(uw_{rr} + ww_{rz} + w_rw_z - w_ru_z)] + g\beta(T - T_\infty), \end{aligned} \quad (8.2)$$

$$uT_r + wT_z = \alpha(T_{rr} + \frac{1}{r}T_r), \quad (8.3)$$

where the velocity components along the (r, z) axes are (u, w) , ρ is density, ν is the kinematic viscosity, p is pressure, g is the gravitational acceleration along the z - direction, β is the coefficient of thermal expansion, T is the temperature and α is the thermal diffusivity. The corresponding boundary conditions for the problem are

$$u(a, z) = 0, \quad w(a, z) = U_w \quad w(r, z) \longrightarrow 0 \text{ as } r \longrightarrow \infty, \quad (8.4)$$

$$T(a, z) = T_w(z), \quad T(r, z) \longrightarrow T_\infty \text{ as } r \longrightarrow \infty, \quad (8.5)$$

where $U_w = 2ake^{z/a}$ is the fluid velocity at the surface of the cylinder.

8.3 Solution of the problem

By considering the following similarity transformations:

$$u = -\frac{1}{2}U_w \frac{f(\eta)}{\sqrt{\eta}}, \quad w = U_w f'(\eta), \quad (8.6)$$

$$\theta = \frac{T - T_\infty}{T_w - T_\infty}, \quad \eta = \frac{r^2}{a^2}, \quad (8.7)$$

The *Eqs.* (8.1) to (8.3) take the form

$$\begin{aligned} \eta f''' + f'' + \text{Re}(ff'' - f'^2) - 2A(\eta f f^{iv} + 2f f''') \\ - 2\eta f' f''' - \eta f''^2 - 2f' f'' + \text{Re} \lambda \theta = 0, \end{aligned} \quad (8.8)$$

$$\eta\theta'' + \theta' + \frac{1}{2} \text{Re Pr}(f\theta' - f'\theta) = 0, \quad (8.9)$$

in which $\lambda = g\beta a(T_w - T_\infty)/U_w^2$ is the natural convection parameter, $\text{Pr} = \nu/\alpha$ is the Prandtl number, $A = \alpha_1 U_w/2a\nu\rho$ is second grade fluid parameter and $\text{Re} = aU_w/4\nu$ is the local Reynolds number. The boundary conditions in nondimensional form become

$$f(1) = 0, \quad f'(1) = 1, \quad \theta(1) = 1, \quad (8.10)$$

$$f' \longrightarrow 0, \quad \theta \longrightarrow 0, \quad \text{as } \eta \longrightarrow \infty. \quad (8.11)$$

The important physical quantities such as the shear stress at the surface τ_w , the skin friction coefficient c_f , the heat flux at the surface of the cylinder q_w and the local Nusselt number Nu_z are

$$\tau_w = \tau_{rz} \big|_{r=a}, \quad q_w = -k\tau_r \big|_{r=a}, \quad (8.12)$$

$$c_f = \frac{\tau_w}{\rho U_w^2}, \quad Nu_z = \frac{ae^{z/a}q_w}{k(T_w - T_\infty)} \quad (8.13)$$

8.4 Homotopy solution

In order to develop solutions, we employ the homotopic technique suggested by Liao [58]. The HAM is preferred due to the following facts. (i) The HAM does not require any small/large parameters in the problem. (ii) It gives us a way to verify the convergence of the developed series solutions. (iii) It is useful in providing incredible flexibility in the developing equation type of linear functions of solutions.

The initial guesses and linear operator are:

$$f_0(\eta) = (1 - e^{1-\eta}), \quad \theta_0(\eta) = \exp(1 - \eta), \quad (8.14)$$

and linear operators satisfying the properties

$$\mathcal{L}_f = \frac{d^3}{d\eta^3} - \frac{d}{d\eta}, \quad \mathcal{L}_\theta = \frac{d^2}{d\eta^2} + \frac{d}{d\eta}, \quad (8.15)$$

$$\mathcal{L}_f(C_1 + C_2 e^\eta + C_3 e^{-\eta}) = 0, \quad \mathcal{L}_g(C_4 + C_5 e^{-\eta}) = 0, \quad (8.16)$$

where C_i ($i = 1 - 5$) indicate the arbitrary constants.

8.4.1 Zeroth-order deformation problems

The corresponding problems at the zeroth order are presented in the following forms:

$$(1 - q) \mathcal{L}_f [\hat{f}(\eta; q) - f_0(\eta)] = q \hbar_f \mathcal{N}_f [\hat{f}(\eta; q)], \quad (8.17)$$

$$(1 - q) \mathcal{L}_\theta [\hat{\theta}(\eta; q) - \theta_0(\eta)] = q \hbar_\theta \mathcal{N}_\theta [\hat{f}(\eta; q), \hat{\theta}(\eta; q)], \quad (8.18)$$

$$\hat{f}(1; q) = 0, \quad \hat{f}'(1; q) = 1, \quad \hat{\theta}(0, q) = 1,$$

$$\hat{\theta}(\infty, q) = 0, \quad \hat{f}'(\infty; q) = 0. \quad (8.19)$$

$$\begin{aligned} \mathcal{N}_f[\hat{f}(\eta, q), \hat{\theta}(\eta, q)] = & \eta \frac{\partial^3 \hat{f}(\eta, q)}{\partial \eta^3} + \frac{\partial^2 \hat{f}(\eta, q)}{\partial \eta^2} + \text{Re} \left(\frac{\hat{f}(\eta, q) \frac{\partial^2 \hat{f}(\eta, q)}{\partial \eta^2}}{\left(\frac{\partial \hat{f}(\eta, q)}{\partial \eta} \right)^2} \right) - 2A \left(\frac{\eta \hat{f}(\eta, q) \frac{\partial^4 \hat{f}(\eta, q)}{\partial \eta^4}}{+ 2 \hat{f}(\eta, q) \frac{\partial^3 \hat{f}(\eta, q)}{\partial \eta^3}} \right), \\ & - 2\eta \frac{\partial \hat{f}(\eta, q)}{\partial \eta} \frac{\partial^3 \hat{f}(\eta, q)}{\partial \eta^3} - \eta \left(\frac{\partial^2 \hat{f}(\eta, q)}{\partial \eta^2} \right)^2 - 2 \frac{\partial \hat{f}(\eta, q)}{\partial \eta} \frac{\partial^2 \hat{f}(\eta, q)}{\partial \eta^2} + \text{Re} \lambda \hat{\theta}(\eta, q) \end{aligned} \quad (8.20)$$

$$\mathcal{N}_\theta[\hat{f}(\eta, q), \hat{\theta}(\eta, q)] = \eta \frac{\partial^2 \hat{\theta}(\eta, q)}{\partial \eta^2} + \frac{\partial \hat{\theta}(\eta, q)}{\partial \eta} + \frac{1}{2} \text{Re Pr} \left(\hat{f}(\eta, q) \frac{\partial \hat{\theta}(\eta, q)}{\partial \eta} - \frac{\partial \hat{f}(\eta, q)}{\partial \eta} \hat{\theta}(\eta, q) \right). \quad (8.21)$$

Here q is an embedding parameter, \hbar_f and \hbar_θ the non-zero auxiliary parameters and \mathcal{N}_f and \mathcal{N}_θ indicate the nonlinear operators.

8.4.2 mth-order deformation problems

$$\mathcal{L}_f [f_m(\eta) - \chi_m f_{m-1}(\eta)] = \hbar_f R_m^f(\eta), \quad (8.22)$$

$$\mathcal{L}_\theta [\theta_m(\eta) - \chi_m \theta_{m-1}(\eta)] = \hbar_\theta R_m^\theta(\eta), \quad (8.23)$$

$$f'_m(1) = 0, \quad f_m(1) = 0, \quad \theta_m(1) = 0,$$

$$f'_m(\infty) = 0, \quad \theta_m(\infty) = 0, \quad (8.24)$$

$$\begin{aligned}
R_m^f(\eta) = & \eta f_{m-1}''' + f_{m-1}'' + \text{Re} \sum_{k=0}^{m-1} (f_{m-1-k} f_k'' - f_{m-1-k}' f_k') - 2A \sum_{k=0}^{m-1} (\eta f_{m-1-k} f_k'''' + 2f_{m-1-k} f_k''') \\
& - 2\eta \sum_{k=0}^{m-1} (f_{m-1-k}' f_k''') - \eta \sum_{k=0}^{m-1} (f_{m-1-k}'' f_k'') - 2 \sum_{k=0}^{m-1} (f_{m-1-k}' f_k'') + \text{Re} \lambda \theta_{m-1}', \quad (8.25)
\end{aligned}$$

$$R_j^\theta(\eta) = \eta \theta_{j-1}'' + \theta_{j-1}' + \frac{1}{2} \text{Re Pr} \sum_{k=0}^{m-1} (f_{m-1-k} \theta_k' - f_{m-1-k}' \theta_k). \quad (8.26)$$

$$\chi_m = \begin{cases} 0, & m \leq 1, \\ 1, & m > 1. \end{cases} \quad (8.27)$$

The general solutions (f_m, θ_m) consisting of special solutions (f_m^*, θ_m^*) are

$$f_m(\eta) = f_m^*(\eta) + C_1 + C_2 e^\eta + C_3 e^{-\eta}, \quad (8.28)$$

$$\theta_m(\eta) = \theta_m^*(\eta) + C_4 + C_5 e^{-\eta}, \quad (8.29)$$

in which the values of $C_i (i = 1 - 5)$ are

$$\begin{aligned}
C_1 &= \left(-\frac{\partial f_m^*(\eta)}{\partial \eta} - f_m^*(\eta) \right)_{\eta=0}, \quad C_2 = 0, \quad C_3 = \frac{\partial f_m^*(\eta)}{\partial \eta}, \quad C_4 = -\theta_m^*(\eta), \\
C_5 &= 0. \quad (8.30)
\end{aligned}$$

8.5 Discussion

In this section, the homotopic solutions are analyzed for the effect of various parameters such as the Reynolds number Re , the second grade parameter A , the Prandtl number Pr and the natural convection parameter λ on the nondimensional velocity and temperature. Here *Fig.8.1* shows the effect of Prandtl number Pr on the velocity profile f' . From *Fig.8.1* it is observed that by increasing Prandtl number Pr the velocity profile decreases. *Fig.8.2* shows the influence of the natural convection parameter λ on the velocity profile f' . Clearly when natural convection parameter λ increases then velocity profile also increases. That is, the natural convection parameter λ is directly proportional to the velocity profile f' . Similar characteristics are observed for second grade fluid parameter A in the *Figs. 8.3* and *8.4*. By increasing the value of Reynold number Re the velocity profile decreases. In *Fig.8.5* the h-curves of velocity profile for different

values of Reynold number are displayed when $Pr = 10, \lambda = 1, A = 0.5$. *Fig.8.6* shows that after increasing Prandtl number Pr the temperature profile decreases. *Fig.8.7* shows opposite behaviour of temperature profile upon increasing natural convection parameter λ . The temperature profile rapidly decreases by increasing the value of second grade parameter A (see *Fig.8.8*) and similar behaviour of temperature profile is examined by increasing the values of Reynold number Re (see *Fig.8.9*). *Fig.8.10* shows the convergence region for temperature profile through h-curves for different values of Prandtl number Pr when $\lambda = 1, Re = 2, A = 0.5$.

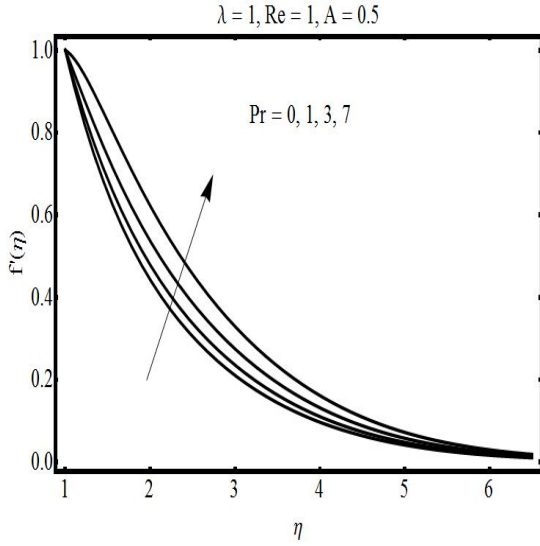


Fig.8.1 Influence of Prandtl number on velocity profile

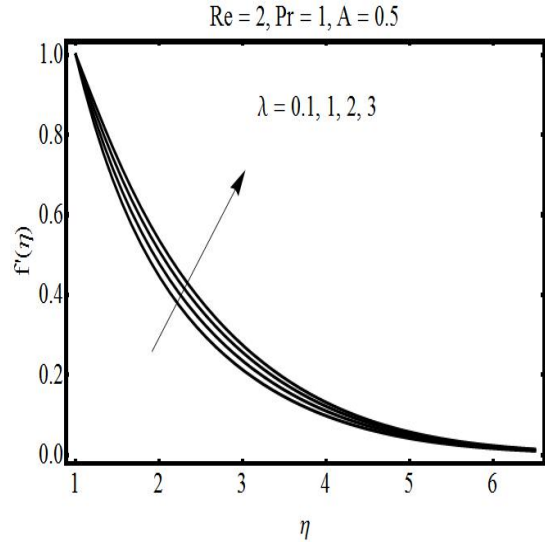


Fig.8.2 Influence of natural convection parameter on velocity profile

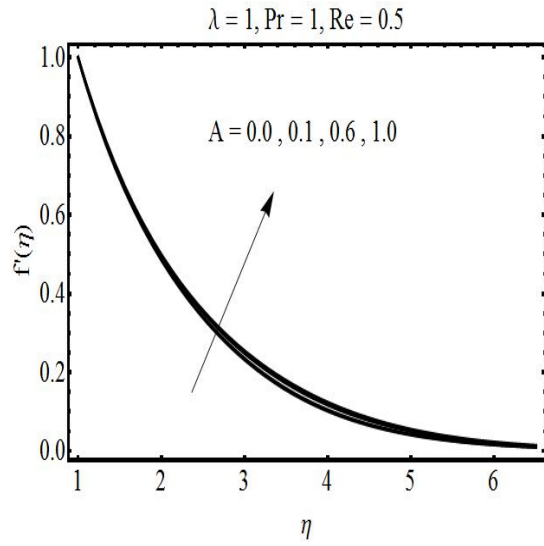


Fig.8.3 Influence of second grade parameter on velocity profile

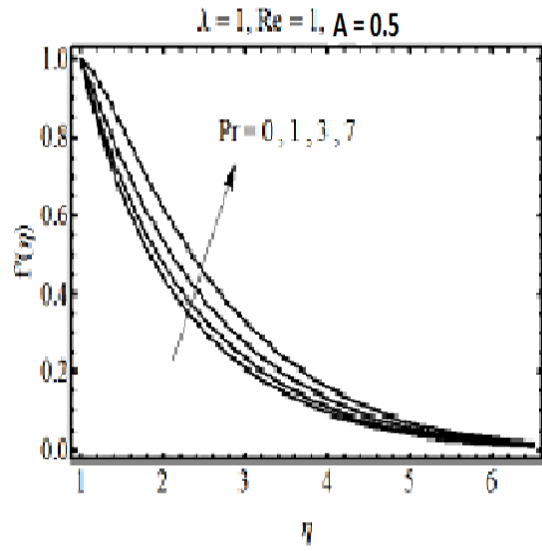


Fig.8.4 Influence of Reynolds number on velocity profile

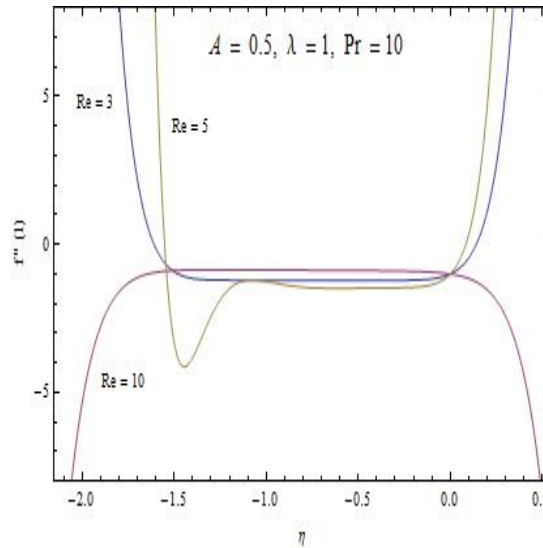


Fig.8.5 h-curve for velocity profile

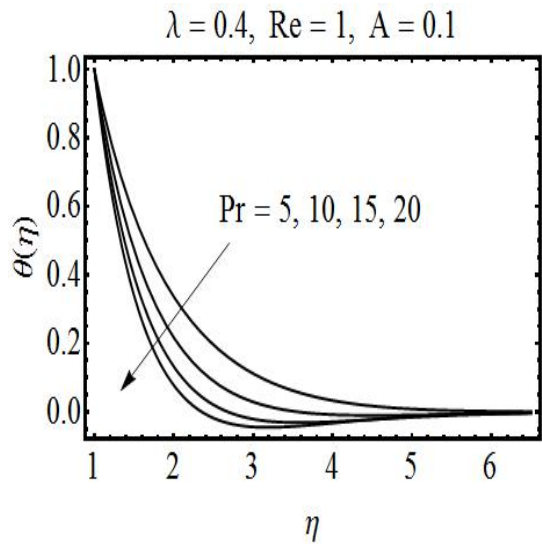


Fig.8.6 Influence of Prandtl number on
temperature profile

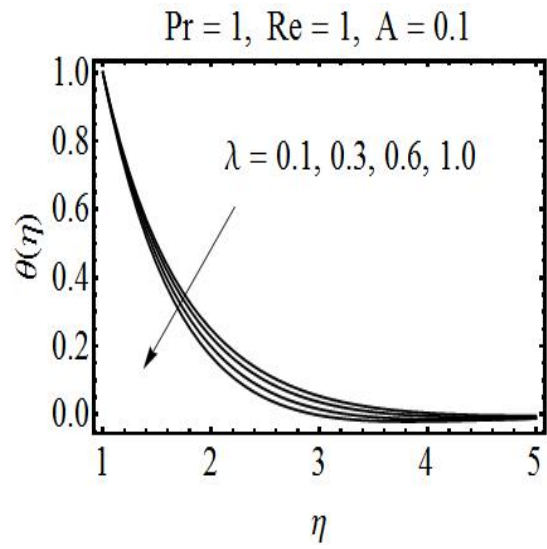


Fig.8.7 Influence of natural convection on
temperature profile

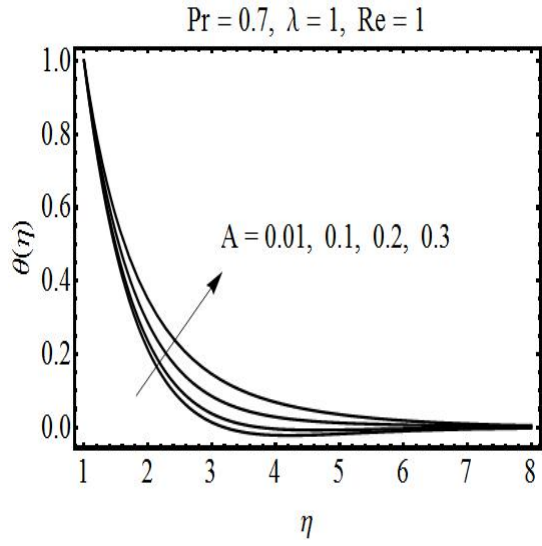


Fig.8.8 Influence of second grade parameter on temperature profile

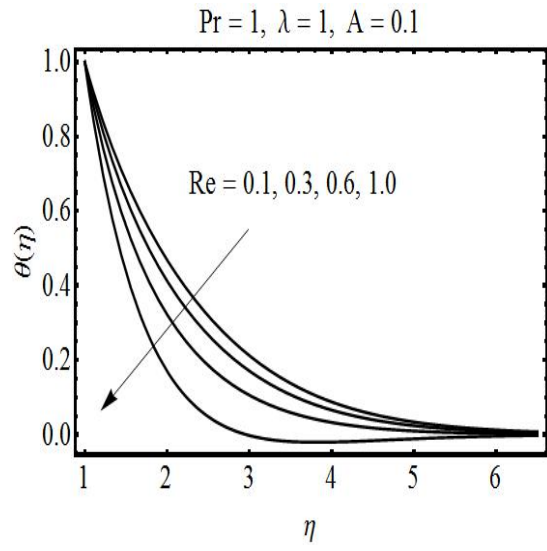


Fig.8.9 Influence of Reynolds number on temperature profile

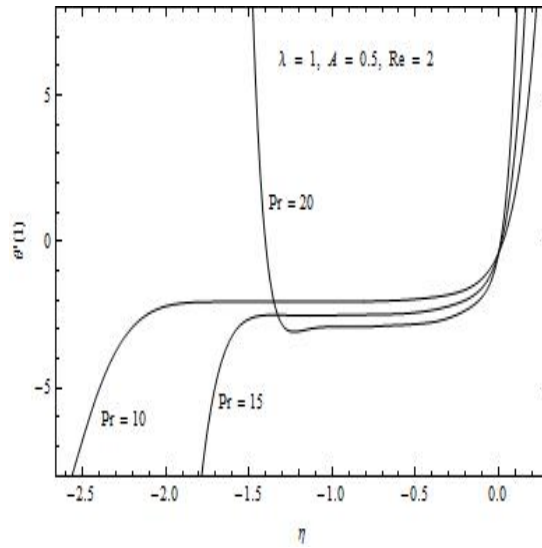


Fig.8.10 h-curve for temperature profile

Table 8.1 : Skin friction coefficient at the surface of the cylinder.

Re\Pr	0.7	1.0	7.0	10.0	15.0
0.5	0.331799	0.362456	0.843729	1.01324	1.1986
1.0	0.398152	0.457414	1.20143	1.4362	1.76274
1.5	0.459415	0.537164	1.4491	1.73577	2.13661
2.0	0.516379	0.612262	1.67114	2.0068	2.46585
2.5	0.568956	0.679781	1.86795	2.243470	2.689060

Table 8.2 : Local Nusselt numbers.

Re\λ	0.0	0.5	1.0	1.5	2.0
0.5	0.853004	0.823586	0.794351	0.765297	0.736421
1.0	1.00715	0.95683	0.907285	0.858489	0.810423
3.0	1.47889	1.38199	1.28968	1.20125	1.11607
5.0	1.83133	1.70796	1.59150	1.48009	1.37257
10.0	2.47349	2.32467	2.16570	2.01174	1.86475

8.6 Conclusions

The homotopy analysis method is employed to study the natural convection boundary layer flow of second grade fluid past an exponentially stretched cylinder. The main findings of the study are summarized as below:

- The velocity profile increases for larger Prandtl number, natural convection parameter and second grade parameter but it decreases by increasing Reynold number.
- The temperature profile increases on increasing Reynold number, natural convection parameter and Prandtl number but it decreases by increasing second grade parameter.
- Skin friction coefficient is an increasing function of Reynold and Prandtl numbers.
- Local Nusselt number enhances upon increasing natural convection parameter but it decreases by increasing Reynold number.

Bibliography

- [1] L. Prandtl, Uber Flussigkeitsbewegungen bei sehr kleiner Reibung, Verhandlg. III Intern. Math. Kongr. Heidelberg, (1904) 484-491.
- [2] H. Blasius, Grenzsichten in Flussigkeiten mit kleiner Reibung, Z. Math. Phys. 56(1) (1908) 1-37.
- [3] M. S. Abel, M. M. Nandeppanavar, S. B. Malipatil, Heat transfer in a second grade fluid through a porous medium from a permeable stretching sheet with non-uniform heat source/sink, Int. J. Heat Mass Tran. 53 (2010) 1788-1795.
- [4] B. Sahoo, Y. Do, Effects of slip on sheet-driven flow and heat transfer of a third grade fluid past a stretching sheet, Int. Comm. Heat Mass Tran. 37 (2010) 1064-1071.
- [5] B. Sahoo , S. Poncet , Blasius flow and heat transfer of fourth-grade fluid with slip, App. Math. Mech. 34(12) (2013) 1465-1480.
- [6] S. Nadeem , R. Haq , N. S. Akbar , Z. H. Khan , MHD three-dimensional Casson fluid flow past a porous linearly stretching sheet, Alexandria Eng. J. 52(4) (2013) 577-582.
- [7] N. A. Khan, H. Khan, A boundary layer flows of non-Newtonian Williamson fluid, Non-linear Eng. 3(2) (2014) 107-115.
- [8] S. A. M. Tonekaboni , R. Abkar , R. Khoeilar , On the Study of Viscoelastic Walters' B Fluid in Boundary layer flows, Math. Prob. Eng. (2012), Article ID 861508.
- [9] T. Hayat, Z. Iqbal, M. Qasim, S. Obaidat, Steady flow of an Eyring Powell fluid over a moving surface with convective boundary conditions, Int. J. Heat Mass Tran. 55 (2012) 1817-1822.

- [10] Abdul Rehman, S. Nadeem, Mixed convection heat transfer in micropolar nanofluid over a vertical slender cylinder, *Chin. Phys. Lett.* 29(12) (2012) 124701.
- [11] C. Wang, C. Chen, Mixed convection boundary layer flow of non-Newtonian fluids along vertical wavy plates, *Int. J. Heat Fluid Flow*, 23 (2002) 831-839.
- [12] N. A. Khan, F. Riaz, F. Sultan, Effects of chemical reaction and magnetic field on a couple stress fluid over a non-linearly stretching sheet, *Eur. Phys. J. Plus* 129(18) (2014) 1-12.
- [13] S. Nadeem, R. Haq, Z. H. Khan, Numerical study of MHD boundary layer flow of a Maxwell fluid past a stretching sheet in the presence of nanoparticles, *J. Taiwan Ins. Che. Eng.* 45 (2014) 121-126.
- [14] N. S. Akbar, S. Nadeem, R. Haq. Z. H. Khan, Numerical solutions of Magnetohydrodynamic boundary layer flow of tangent hyperbolic fluid towards a stretching sheet, *Indian J. Phys.* 87(11) (2013) 1121-1124.
- [15] R. Malik, M. Khan, A. Munir, W. A. Khan, Flow and heat transfer in Sisko fluid with convective boundary condition, *Plos One*, 9(10) (2014) e107989.
- [16] T. Hayat, S. Asad, M. Mustafa, A. Alsaedi, Boundary layer flow of Carreau fluid over a convectively heated stretching sheet, *App. Math. Comp.* 246 (2014) 12-22.
- [17] M. A. A. Hamad, S. M. AbdEl-Gaied, W. A. Khan, Thermal jump effects on boundary layer flow of a Jeffrey fluid near the stagnation point on a stretching/shrinking sheet with variable thermal conductivity, *J. Fluids*, (2013) Article ID 749271.
- [18] T. Hayat, S. Mumtaz, Resonant oscillations of plate in an electrically conducting rotating Johnson-Segalman fluid, *Comp. Math. App.* 50 (2005) 1669-1676.
- [19] N. Phan-Thien, Stagnation flows for the Oldroyd-B fluid, *Rheologica Acta* , 23(2) (1984) 172-176.
- [20] P. Ravindran, J. M. Krishnan, K. R. Rajagopal , A note on the flow of a Burgers' fluid in an orthogonal rheometer, *Int. J. Eng. Sci.* 42(20) (2004) 1973-1985.

- [21] R. G. Pai, A. Kandasamy, Entrance region flow of Herschel-Bulkley fluid in an annular cylinder, *App. Math.* 5 (2014) 1964-1976.
- [22] N. Nirmalkar, R. P. Chhabra, R. J. Poole, On creeping flow of a Bingham plastic fluid past a square cylinder, *J. Non-Newtonian Fluid Mech.* 171 (2012) 17-30.
- [23] L. J. Crane, Flow past a stretching plate. *J. Appl. Math. Phys. (ZAMP)*. 21 (1970) 645-647.
- [24] D. Pal, Mixed convection heat transfer in the boundary layers on an exponentially stretching surface with magnetic field. *Appl. Math. Comp.* 217 (2010) 2356-2369.
- [25] T. R. Mahapatra, A. S. Gupta, Heat transfer in stagnation-point flow towards a stretching sheet, *Heat Mass Transfer* 38 (2002) 517-521.
- [26] N. Bachok, A. Ishak, I. Pop, Stagnation-point flow over a stretching/shrinking sheet in a nanofluid, *Nanoscale Res. Lett.* 6 (2011) 623.
- [27] T. C. Chiam, Magnetohydrodynamic heat transfer over a non-isothermal stretching sheet, *Acta Mech.* 122 (1997) 169-179.
- [28] M. Z. Salleh, R. Nazar, I. Pop, Boundary layer flow and heat transfer over a stretching sheet with Newtonian heating, *J. Taiwan Ins. Che.Eng.* 41 (2010) 651-655.
- [29] S. Mukhopadhyay, Slip effects on MHD boundary layer flow over an exponentially stretching sheet with suction/blowing and thermal radiation, *Ain Shams Eng. J.* 4 (2013) 485-491.
- [30] S. Mukhopadhyay, MHD boundary layer flow and heat transfer over an exponentially stretching sheet embedded in a thermally stratified medium, *Alexandria Eng. J.* 52 (2013) 259-265.
- [31] T. Fang, Y. Zhong, Viscous flow over a shrinking sheet with an arbitrary surface velocity, *Commun Nonlinear Sci Numer Simulat* 15 (2010) 3768-3776.
- [32] R. Bhargava, S. Sharma, H. S. Takhar, O. A. Beg, P. Bhargava, Numerical Solutions for Micropolar Transport Phenomena over a Nonlinear Stretching Sheet, *Nonlinear Analysis: Modelling and Control*, 12(1) (2007) 45-63.

- [33] T. Fang, S. Yao, J. Zhang, Abdul Aziz, Viscous flow over a shrinking sheet with a second order slip flow model, *Commun Nonlinear Sci Numer Simulat* 15 (2010) 1831-1842.
- [34] J. H. Merkin, V. Kumaran, The unsteady MHD boundary-layer flow on a shrinking sheet, *European Journal of Mechanics B/Fluids* 29 (2010) 357-363.
- [35] N. A. Yacob, A. Ishak, I. Pop, Melting heat transfer in boundary layer stagnation-point flow towards a stretching/shrinking sheet in a micropolar fluid, *Computers & Fluids* 47 (2011) 16-21.
- [36] L. Zheng, J. Niu, X. Zhang, L. Ma, Dual solutions for flow and radiative heat transfer of a micropolar fluid over stretching/shrinking sheet, *International Journal of Heat and Mass Transfer* 55 (2012) 7577–7586.
- [37] A. Ishak, R. Nazar, I. Pop, Uniform suction/blowing effect on flow and heat transfer due to a stretching cylinder, *Applied Mathematical Modelling* 32 (2008) 2059-2066.
- [38] A. Ishak, MHD boundary layer flow due to an exponentially stretching sheet with radiation effect, *Sains Malaysiana* 40(4) (2011) 391–395.
- [39] K. Govardhan, N. Kishan, Unsteady MHD boundary layer flow of an incompressible micropolar fluid over a stretching sheet, *Journal of Applied Fluid Mechanics*, 5(3) (2012) 23-28.
- [40] A. Ahmad, S. Asghar, Flow of a second grade fluid over a sheet stretching with arbitrary velocities subject to a transverse magnetic field, *Applied Mathematics Letters* 24 (2011) 1905–1909.
- [41] P. D. Weidman, E. Magyari, Generalized Crane flow induced by continuous surfaces stretching with arbitrary velocities, *Acta Mech* 209 (2010) 353–362.
- [42] J. Phakirappa, P. H. Veena, V. K. Pravin, Boundary layer flow and heat transfer flow past stretching sheet with temperature gradient dependent heat sink and internal heat eneration, *Int. J. of Mod. Eng. Res. (IJMER)*, 2(5) (2012) 3298-3305.

- [43] M. A. A. Mahmoud, M. Abd-Elaty Mahmoud, S. E. Waheed, Hydromagnetic boundary layer micropolar fluid flow over a stretching surface embedded in a non-Darcian porous medium with radiation, *Math. Prob. in Eng.*, Article ID 39392 (2006) 1–10.
- [44] F. T. Gang, Z. Ji, Z. Y. Fang, T. Hua, Unsteady viscous flow over an expanding stretching cylinder, *Chin. Phys. Lett.* 28(12) (2011) 124707.
- [45] H. A. Attia, Heat transfer in a stagnation point flow of a micropolar fluid over a stretching surface with heat generation/absorption, *Tamk. J. of Sci. and Eng.*, 9(4) (2006) 299-305.
- [46] B. Bidin, R. Nazar, Numerical solution of the boundary layer flow over an exponentially stretching sheet with thermal radiation, *Eur. J. of Sci. Res.* 33(4) (2009) 710-717.
- [47] H. Rosali, A. Ishak, I. Pop, Micropolar fluid flow towards a stretching/shrinking sheet in a porous medium with suction, *Int. Comm. in Heat and Mass Tran.* 39 (2012) 826–829.
- [48] M. Turkyilmazoglu, MHD fluid flow and heat transfer due to a stretching rotating disk, *Int. J. of Ther. Sci.* 51 (2012) 195-201.
- [49] M. A. Seddeek, Effects of Hall and ion-slip currents on magneto-micropolar fluid and heat transfer over a non-isothermal stretching sheet with suction and blowing, *Proc. R. Soc. Lond. A* (2001) 457, 3039-3050.
- [50] P.K. Kameswaran, S. Shaw, P. Sibanda, P.V.S.N. Murthy, Homogeneous–heterogeneous reactions in a nanofluid flow due to a porous stretching sheet, *Int. J. of Heat and Mass Trans.* 57 (2013) 465-472.
- [51] W. Ibrahim, B. Shankar, MHD boundary layer flow and heat transfer of a nanofluid past a permeable stretching sheet with velocity, thermal and solutal slip boundary conditions, *Comp. & Fluids* 75 (2013) 1-10.
- [52] N. Bachok, A. Ishak, Flow and heat transfer over a stretching cylinder with prescribed surface heat flux, *Malaysian Journal of Mathematical Sciences* 4(2) (2010) 159-169.
- [53] O.D. Makinde, W.A. Khan, Z.H. Khan, Buoyancy effects on MHD stagnation point flow and heat transfer of a nanofluid past a convectively heated stretching/shrinking sheet, *International Journal of Heat and Mass Transfer* 62 (2013) 526-533.

- [54] W. Ibrahim, B. Shankar, M. M. Nandeppanavar, MHD stagnation point flow and heat transfer due to nanofluid towards a stretching sheet, *International Journal of Heat and Mass Transfer* 56 (2013) 1-9.
- [55] A. Ishak and R. Nazar, Laminar boundary flow along a stretching cylinder, *European Journal of Scientific Research* 36 (2009) 22-29.
- [56] L.G. Grubka and K.M. Bobba, Heat transfer characteristics of a continuous stretching surface with variable temperature, *Journal of Heat Transfer* 107 (1985) 248-250.
- [57] S. Nadeem, S. Akram, Peristaltic transport of a hyperbolic tangent fluid model in an asymmetric channel, *Z. Naturforsch.* 64a (2009) 559-567.
- [58] S. J. Liao, *Beyond Perturbation: Introduction to Homotopy Analysis Method*, Chapman and Hall, CRC Press, Boca Raton, 2003.

Numerical study of non-Newtonian fluids past a stretching cylinder

by Muhammad Naseer

FILE	A_THESIS.PDF (1.76M)		
TIME SUBMITTED	22-NOV-2016 07:30PM	WORD COUNT	18414
SUBMISSION ID	741493456	CHARACTER COUNT	85240

Chapter 1

Introduction

Chapter 2

3

Boundary layer flow of a casson nano fluid over a vertically exponential cylinder

Introduction Mathematical model

Mathematical formulation

Solution of the problem

Results and discussion

Conclusions

Chapter 3

Numerical study of convective heat transfer on the Power law fluid over a vertical exponentially stretching cylinder

Introduction

Mathematical model

Mathematical formulation

Solution of the problem

Results and discussion

Conclusions

Chapter 4

13

The boundary layer flow of hyperbolic tangent fluid over a vertical exponentially stretching cylinder

Introduction

Mathematical model

Mathematical formulation

Solution of the problem

Results and discussion

Conclusions

Chapter 5

The boundary layer flow of Williamson fluid over a vertical exponentially stretching cylinder

Introduction

Mathematical model

Mathematical formulation

Solution of the problem

Results and discussion

Conclusions

Chapter 6

The boundary layer flow of Williamson nano fluid over a vertical exponentially stretching cylinder

Introduction

Mathematical model

Mathematical formulation

Solution of the problem

Results and discussion

Conclusions

Chapter 7

Convective boundary layer flow of Eyring-Powell fluid over a vertical exponentially stretching cylinder

Introduction

Mathematical model

Mathematical formulation

Solution of the problem

Results and discussion

Conclusions

Chapter 8

The boundary layer flow of Second grade fluid over a vertical exponentially stretching cylinder

Introduction

Mathematical model

Mathematical formulation

Solution of the problem

Results and discussion

Conclusions

Chapter 1

Introduction

The unavailability of a solitary stress tensor that can be used to model all the non-Newtonian fluids diversifies the field of fluid mechanics from other disciplines. For flow problems allied with diverse fluid models the attained mathematical formulism consists of a set of coupled highly non-linear partial differential equations. In numerous situations, the exact solution for such system, for a wide range of the involved physical parameters is yet a dream for the researchers even after putting enormous labor. The concept of boundary layers has overcome this exertion in various circumstances. The idea was first socialized by Ludwig Prandtl when he presented his paper at the 3rd International Congress of Mathematicians in Heidelberg, Germany in 1904 [1]. Since then the theory is applied to virtually all the available non-Newtonian fluid models for diverse problems of fluid flowing under different physical constraints and the highly nonlinear coupled system of partial differential equations is abridged into a much simple one by systematically negating the less contributing slice. Mathematically, the role of the boundary layer is often to reduce the original elliptic nature scheme of partial differential equations into a more simple parabolic nature. The sensitivity of boundary layer theory is exceedingly enhanced by Blasius by adding the essence of transformed domain similarity solutions for the problem of viscous fluid flow over a flat plate [2]. Together, the boundary layer approximations and the similarity transformations have become a strong tool for the researchers and have been successfully applied on almost every available fluid model. Abel et al. [3] inspected the impact of viscous dissipation and non-uniform heat source/sink on the boundary layer flow and heat transfer of a second grade fluid flowing through a porous medium. Sahoo and Do [4] have probed into the effects of

magnetic field and the partial slip on the flow and heat transfer of an electrically conducting third grade fluid flow due to a linearly stretched surface. In another work, Sahoo and Poncet [5] have inspected the effects of slip and magnetic field on the flow and heat transfer of an incompressible, electrically conducting fourth grade fluid flowing past an infinite porous plate. Nadeem et al. [6] have studied the magnetohydrodynamic effects over the boundary layer flow of a Casson fluid, for the case when the fluid is flowing in two lateral directions past a porous linearly stretched surface. Khan and Khan [7] have presented the solutions of the steady boundary layer flow of Williamson fluid flowing under four different situations, namely the Blasius flow, the Sakiadis flow, the stretching and the stagnation point flows. Tonekaboni et al. [8] have presented the similarity solutions for three different cases of the boundary layer flow of non-Newtonian viscoelastic Walters' B fluid flow, namely stagnation-point flow problem, the Blasius flow problem and the Sakiadis flow problem. Hayat et al. [9] have presented the solutions for the problem of boundary layer flow and heat transfer for the Eyring Powell fluid flowing over a moving surface with convective boundary conditions by means of homotopy analysis method. Rehman and Nadeem [10] have discussed the problem of nanoparticles effects over the boundary layer flow of a micropolar fluid flowing over a vertical slender cylinder. Wang and Chen [11] have discussed the problem of steady laminar boundary layer flow of a non-Newtonian power-law fluid flowing past a semi-infinite symmetric structure with a wavy surface and a uniform wall temperature such that the axis of symmetry is aligned with the oncoming uniform stream. Khan et al. [12] have examine the influence of magnetic field and chemical reaction over the boundary layer flow of an electrically conducting non-Newtonian couple stress fluid flowing over sheet that is stretched along its surface with a non-linear surface stretching velocity. Nadeem et al. [13] have discussed the effects of magnetohydrodynamics and nanoparticles for the boundary layer flow of non-Newtonian Maxwell fluid flowing past a stretching sheet. Akber et al. [14] have analyzed the problem of boundary layer flow of tangent hyperbolic fluid towards a stretching sheet. Malik et al. [15] have studied the boundary layer flow and heat transfer in Sisko fluid flowing over a nonisothermal nonlinearly stretching surface with convective boundary condition under the influence of a uniform transverse magnetic field. Hayat et al. [16] have presented the analysis for momentum and thermal boundary layers arising from the motion of Carreau fluid flowing above a stretching sheet with convective boundary conditions. Hamad et al. [17]

have studied the dynamics of the thermal boundary layer flow of a steady, incompressible non-Newtonian Jeffrey fluid near the stagnation point on a stretching sheet taking into account the thermal jump condition at the surface of the sheet. Hayat and Mumtaz [18] have presented an analysis for the hydromagnetic boundary layer flow of a non-Newtonian Johnson-Segalman fluid flowing over a semi-infinite expanse of electrically conducting rotating plate in the presence of a transverse magnetic field. Phan-Thien [19] has obtained the solutions for the boundary layer stagnation point flows of an Oldroyd-B fluid flow for the case of plane stagnation point and axi-symmetric stagnation flows. Ravindran et al. [20] analyzed the occurrence of boundary layers due to the flow of a Burgers' fluid flow in an orthogonal rheometer. Pai and Kandasamy [21] have studied the momentum boundary layer profile due to the entrance region flow of a Herschel-Bulkley fluid flowing through an annular cylinder. Nirmalkar et al. [22] have studied the boundary layer creeping flow of a Bingham plastic fluid flowing past a two dimensional cylinder of square cross-section.

The study of stretching sheet was initiated by Crane [23]. Since then, the study of fluid flow over a stretching sheet has become a problem of concentration for researchers due to its inclusive applications in collective engineering processes such as wire drawing, polymer processing, paper production, glass blowing, metal spinning, manufacturing, cooling of metallic plates, extrusion of polymers, aerodynamic extrusion of plastic sheets, purification of liquefied metal from non-metallic inclusion, manufacturing process of artificial films and fibers, polymeric sheets, crystal growing and hot rolling. It is also used to assemble car body works in automobiles and to manufacture aircraft fuselages in aeronautics. It is experimentally validated that at high temperature; material passes through extrusion in liquefied state. This elongation of material is approximately proportional to the distance from the stagnation point. Particularly, for the flow problem over an exponentially stretching surface, the annealing and thinning of copper wires the final product depends on the heat transfer rate at the surface of the stretching continuous object with exponential variations of stretching velocity and temperature distribution. During such practices, the kinematics of stretching and the heating/cooling have a crucial impact on the quality of the final products [24]. Mahapatra and Gupta [25] have debated the stagnation point flow of viscous fluid over a flat deformable sheet. They perceived a boundary layer immediate to the stretching surface and also observed that the configuration of this boundary layer rest

on the ratio of the velocity of the stretching surface to that of the frictionless potential flow in the neighborhood of the stagnation point. Bachok et al. [26] explained the problem of stagnation point flow over a stretching/shrinking sheet which is placed inside a nanofluid. The solution was carried for three specific water-based nano particles that are copper, alumina and titania. According to their results skin-friction coefficient has the largest magnitude for copper while the least for alumina while the local Nusselt numbers have the largest values for copper while the least for titania. Chiam [27] studied the problem of boundary layer flow and heat transfer of an electrically conducting fluid over a non-isothermal stretching sheet under the influence of a transverse magnetic field. Salleh et al. [28] have provided numerical solutions using Keller-box technique for the problem of boundary layer flow and heat transfer over a stretching sheet with Newtonian heating. They examined the influence of Prandtl number over the temperature profiles and the heat transfer coefficient. They were of the view that the thermal boundary layer thickness has a strong dependence upon the Prandtl number and that the temperature profile decreases with an increase in the Prandtl number. Mukhopadhyay [29] has numerically analyzed the problem of boundary layer flow and heat transfer towards a porous exponentially stretched sheet in presence of a magnetic field with partial slip conditions for the velocity and temperature functions at the surface of the sheet. She concluded that the surface shear stress is an increasing function of the magnetic field parameter and that the thermal boundary layer thickness is an increasing function of both the magnetic field parameter and the non-dimensional radiation parameter. In another effort, Mukhopadhyay [30] has presented the numerical results for the problem of steady, incompressible magnetohydrodynamic boundary layer flow and heat transfer of a viscous fluid flowing over a porous surface that is stretched with some exponential velocity along the surface of the object and is embedded in a thermally stratified medium. She obtained the result that the velocity field is suppressed by both the magnetic field parameter and the suction parameter. She also commented that the rate of heat transfer is a decreasing function of the non-dimensional stratification parameter. Fang and Zhong [31] have presented closed form analytic solutions for the boundary layer flow over a stretching/shrinking sheet with different stretching/shrinking velocity distributions assumed at the surface of the cylinder. They considered the surface stretching velocities to be linear, bilinear, nonlinear exponential, quadratic, power-law and periodic functions of the distance over

the points⁹⁶ on the surface of the cylinder from that of the stagnation point.

They commented that solution for such a problem is important for the case when¹⁵¹ mass transfer at the wall is a function of the surface stretching velocity of the wall. Bhargava et al. [32]² have studied the problem of steady incompressible boundary layer flow of the non-Newtonian micropolar fluid flow, heat and mass transfer over a nonlinear stretching Sheet.¹¹¹ The problem was⁴³ solved numerically with the help of Finite difference and the finite element methods. Their work showed that the solutions obtained with both the methods were in contract. They concluded that the convective parameter can adeptly be used for stability of the temperature distribution. In another work, Fang et al. [33]¹⁴ analyzed the slip flow of viscous fluid flowing over a stretching/shrinking surface. They solved the problem for Wu's second order slip flow model. Merkin and Kumaran in their work [34]¹² have examined the problem of unsteady, 2D laminar, incompressible, boundary layer flow of a viscous fluid flowing over an impulsively stretching/shrinking sheet.⁷ The fluid was assumed to be under the influence of a constant transverse magnetic field.¹⁴² Different solutions were obtained depending upon distinct values of the magnetic parameter that is the strength of the imposed magnetic field relative to the stretching velocity of the surface. In [35], Yacob et al. have commented over the melting effects over the boundary layer flow and heat transfer of a non-Newtonian micropolar fluid flowing over a stretching/shrinking sheet.¹² They observed that the presence of melting route has decreases the friction and the heat transfer rate at the solid-liquid interface.¹⁴¹ Zheng et al [36]³⁷ have analyzed the problem of boundary layer analysis is presented for the flow and radiative heat transfer of an incompressible non-Newtonian micropolar fluid flowing over a stretching/shrinking sheet with nonlinear power-law surface stretching velocity and temperature functions.¹⁴⁰ They applied the homotopy analysis method to obtain the dual solutions associated with the problem and included a detailed analysis of the effects of power-law index on the velocity and radiative temperature fields.¹¹⁰ Ishak et al. [37] have obtained numerical solutions through the Keller-box technique for the problem of flow and heat transfer of steady, incompressible boundary layer viscous fluid flowing outside a stretching permeable hollow cylinder with suction/injection. Their important observation was that the skin friction coefficient remains unchanged with varying Prandtl numbers and that skin friction reduces when the fluid flow is influenced by injection. They also predicted that in case of feeble injection water is a healthier cooling

mediator than air.

Ishak [38] has also numerically analyzed the effects of thermal radiation and magnetohydrodynamic on the two dimensional boundary layer flow and heat transfer of a steady, incompressible viscous fluid flowing over an exponentially stretching sheet. His conclusion was that both the magnetic and the radiation parameters have an inverse behavior on the temperature function. Govardhan and Kishan [39] have investigated the magnetohydrodynamic effects on the problem of boundary layer flow and heat transfer of unsteady, incompressible non-Newtonian micropolar fluid flowing over a stretching surface, when the sheet is stretched in its own plane linearly with the distance along the surface of the sheet. The problem was solved numerically with the help of Adams-Predictor Corrector technique for both the transient and the steady state flow outlines. They commented that the microrotation influence is more evident for $n = 1/2$ as compared with $n = 0$. The microrotation function has a parabolic distribution for $n = 0$, while for $n = 1/2$ the distribution is always decreasing. Due to impulsive motion they found the skin friction coefficient having large magnitude values for small time at start of the motion. The skin friction coefficient magnitude values have a monotonic decrease till they reached the steady state values. Ahmad and Asghar [40] have obtained the exact analytic solutions for the flow and heat transfer of non-Newtonian second grade fluid flowing over a stretching surface with arbitrary velocity and appropriate wall transpiration. They considered the surface stretching velocities at the surface of the sheet to be linear, quadratic and polynomial functions of the length of the surface from the stagnation point. Weidman and Magyari [41] have obtained an exact solution of the Crane-type boundary layer partial differential equations arising from the problem of steady, incompressible viscous fluid flow encouraged by a planar stretching surface having an appropriate distribution of wall transpiration. They concluded that for any type of surface stretching velocity, the Crane-type boundary layer equations can be generated if the stretching sheet is permeable and an appropriate dissection of the wall transpiration subsists. Phakirappa et al. [42] have debated on the flow pattern of boundary layer viscous fluid and heat transfer in presence of a porous medium when the flow happens due to a non-isothermal stretching sheet with free convection and a temperature gradient reliant heat sink along with internal heat generation and suction/injection beneath the influence of a transvers magnetic field. Their attained exact solutions for the velocity and temperature

profiles were in terms of the Kummer's function. Mahmoud et al. [43] have studied the impact of radiation and a uniform magnetic field on the hydromagnetic boundary layer flow and heat transfer of an electrically conducting non-Newtonian micropolar fluid flows over a continuously moving stretching surface embedded in a non-Darcian porous medium. On the basis of the numerical solutions that were obtained, they were of the view that both the linear and angular velocity functions were in inverse proportion to the magnetic parameter and the Darcy number and that the radiation parameter increases the rate of heat transfer at the surface of the sheet. Gang et al. [44] have presented the exact solutions of the Navier-Stokes equations appearing from the boundary layer flow of a viscous fluid on an expending cylinder. Where the surface stretching velocity of the cylinder was assumed to be proportional to the axial distance from the origin and a decreasing function of time. The radius of the cylinder was taken as a time dependent entity that fetched the impact of unsteady expansion of the cylinder in the analysis. Attia [45] has discussed the steady, laminar incompressible fluid flow problem of stagnation point boundary layer flow of micropolar fluid flowing over a permeable stretching surface with heat generation/absorption with constant wall and steam temperatures. His numerical solution based on the finite difference approximation indicated that the velocity boundary layer thickness is a decreasing function of the stretching velocity of the surface of the sheet. Bidin and Nazar [46] have carried an analysis for the problem of steady laminar incompressible two dimensional boundary layer flow and heat transfer of a viscous fluid flow over a stretching sheet with thermal radiation. The surface stretching velocity is assumed to be an exponential function of the distance on the surface from the stagnation point. Their analysis was based on the implicit finite difference scheme, the Keller-box technique. Rosali et al. [47] have numerically analyzed the boundary layer flow of non-Newtonian micropolar fluid flow towards a permeable stretching/shrinking sheet in a porous medium with suction/injection. They showed that by increasing the permeability parameter the skin friction coefficient enhances. Turkyilmazoglu [48] has studied the magnetohydrodynamic, steady laminar boundary layer flow of a viscous fluid flowing through a radially stretchable rotating disk in presence of a uniform vertical magnetic field with viscous dissipation and Joule heating. The problem is a generalization of the classical von Karman pump problem. Their analysis showed a strong dependence of the viscous and thermal boundary layer thicknesses over the rotation strength of the disk and the magnetic

field strength. They concluded that the role of Joule heating is that to enhance the temperature distribution near the wall. Seddeek [49] has studied the magnetohydrodynamic hall and ion-slip current effects over the steady boundary layer flow of a non-Newtonian fluid flow and heat transfer of a stretching sheet with suction and blowing. They included an interesting comment in their conclusion that unclean fluids may be preferable over the clean fluids in industrial applications where control of convective heat transfer is important. Kameswaran et al. [50] have analyzed the homogeneous-heterogeneous effects over the flow of boundary layer viscous nanofluid flowing over a stretching or shrinking sheet in a porous medium. The analysis was carried for the copper-water and the silver-water nanofluids such that the diffusion coefficients of the reactant and the auto catalyst are equal. They concluded that the nanoparticle volume fraction decreases the velocity profile and that the nanoparticle concentration at the surface is a decreasing function of the strength of the heterogeneous reaction for both copper-water and silver-water nanofluids. It was also mentioned that for the shrinking sheet problem the velocity profile is a decreasing function of the increasing values of the nanoparticle volume fraction for both the copper-water and silver-water nanofluids. Ibrahim and Shankar [51] have investigated the problem of boundary layer flow and heat transfer of a viscous nanofluid flowing over a permeable stretching sheet with slip boundary condition and thermal radiation. The flow was also assumed to be under the influence of a uniform magnetic field. They included a detailed analysis for the effects of radiation, Brownian motion, thermophoresis parameter and nanoparticle fraction on the boundary layer flow and heat transfer due to nanofluids. They concluded that the boundary layer thickness is a decreasing function of the magnetic field strength, the thermal boundary layer thickness is a decreasing function of the slip parameter while an increasing function of the radiation parameter, the magnetic field parameter and the thermophoresis parameter. Bachok and Ishak [52] have analyzed the problem of boundary layer flow and heat transfer of steady, laminar incompressible viscous fluid flow due to a stretching cylinder with prescribed surface heat flux. They commented that both the shear stress at the surface and the heat transfer rate at the surface are increasing functions of the curvature parameter. Makinde et al. [53] analyzed the combined effects of the buoyancy force, convective heating, Brownian motion, thermophoresis and magnetic field over the stagnation point boundary layer flow and heat transfer due to nanofluid flowing towards a stretching sheet. Ibrahim et al. [54] have dis-

1 cussed the effect of magnetic field on stagnation point flow and heat transfer of nanofluid flowing towards a stretching sheet. Two important works about fluid flow over stretching surfaces are cited in [55-58].

19 The present dissertation is centered mainly for the boundary layer flow of non-Newtonian fluid and heat transfer analysis by a stretching cylinder. Flow caused is by an exponentially stretching cylinder. The structure of thesis is arranged in eight chapters. The chapter wise arrangement is given below.

Literature review is presented in chapter 1. Chapter 2 studies flow Casson fluid past an exponentially stretching cylinder. Nanofluid is considered. Numerical solution by Runge-Kutta Fehlberg technique is developed. Contents of this chapter are published in “Applied NanoScience”

71 Chapter 3 contains a study of heat transfer in boundary layer flow power law fluid past a vertical stretching cylinder. Further the solution of the problem is obtained using the Runge-Kutta Fehlberg technique. Contents of this chapter are published in “Applied and Computational Mathematics”

4 Chapter 4 presents an analysis for boundary layer flow and heat transfer for hyperbolic tangent fluid. Stretching cylinder is examined. This problem is solved with the help of Runge-Kutta-Fehlberg method. Contents of the chapter are published in “Alexandria Engineering Journal”

2 The steady boundary layer flow of Williamson fluid past a stretching cylinder is examined. in chapter 5. The obtained modeled equations are solved numerically with the help of Keller box method. Chapter 6 addresses Williamson material with Brownian motion and thermophoresis.

Chapter 7 is developed to study the effects of double stratification effect in mixed convection boundary layer flow of Eyring-Powell fluid by an inclined stretching cylinder. Numerical solutions of resulting intricate non-linear boundary value problem are computed successfully by utilizing fifth order Runge-Kutta algorithm with shooting technique. Contents of this chapter are published in “AIP Advances”.

1 Finally chapter 8 gives the solution for steady boundary layer flow of a second grade fluid past a vertical stretching cylinder. Heat transfer is discussed. The obtained system of equations subject to the boundary conditions are solved with the help homotopy analysis method

(HAM). The effects of different parameters like Reynolds numbers, Prandtl numbers and the natural convection parameter are studied. The skin friction coefficient and Nusselt numbers are presented for different parameters.

Chapter 2

³Boundary layer flow of a Casson nanofluid over a vertically exponential cylinder

2.1 Introduction

The effects of Casson nanofluid due to a vertically exponential cylinder are studied in this chapter. ²⁸ Similarity solution of the boundary layer flow is computed by choosing suitable transformation. The governing partial differential equations and boundary conditions ⁵ are reduced to a system of nonlinear ordinary differential equations. The solutions of the problems are obtained by using the numerical technique known as Runge Kutta Fehlberg method. Velocity and temperature profiles are presented through graphs. ⁵ The important physical quantities such as the skin friction coefficient and the local Nusselt number are computed to examine the behavior of different parameters. ²⁰ ⁵⁰

2.2 Mathematical formulation

² Consider the problem of natural convection boundary layer flow of Casson nanofluid induced by a vertical circular cylinder of radius a . The cylinder is assumed to be stretched exponentially along the axial direction with velocity U_w . The temperature at the surface of cylinder is assumed

T_w and the uniform ambient temperature is taken as T_∞ such that the quantity $T_w - T_\infty > 0$ in case of the assisting flow while $T_w - T_\infty < 0$ in case of the opposing flow, respectively. Under these assumptions the boundary layer equations of motion, heat transfer and nanoparticle concentration are

$$u_r + \frac{u}{r} + w_z = 0, \quad (2.1)$$

$$uw_r + ww_z = \nu(1 + \frac{1}{\beta})(w_{rr} + \frac{1}{r}w_r) + g\beta(T - T_\infty)(1 - \phi_\infty) + \frac{1}{\rho}(\rho^* - \rho)(\phi - \phi_\infty), \quad (2.2)$$

$$uT_r + wT_z = \alpha(T_{rr} + \frac{1}{r}T_r) + \frac{\rho^*c_p^*}{\rho c_p}(D_T T_r \phi_r + \frac{D_T}{T_\infty} T_r^2), \quad (2.3)$$

$$w\phi_\infty + u\phi_r = D_B(\phi_{rr} + \frac{1}{r}\phi_r) + \frac{D_T}{T_\infty}(T_{rr} + \frac{1}{r}T_r), \quad (2.4) \quad 134$$

where the velocity components along r and z directions are u and w respectively. ρ is the density, ν is the kinematic viscosity, p is the pressure, g is the gravitational acceleration along z -axis, β is the coefficient of thermal expansion, T is the temperature and α is the thermal diffusivity. The corresponding boundary conditions for the problem are

$$u(a, z) = 0, \quad w(a, z) = U_w \quad w(r, z) \longrightarrow 0 \text{ as } r \longrightarrow \infty, \quad (2.5)$$

$$T(a, z) = T_w(z), \quad T(r, z) \longrightarrow T_\infty \text{ as } r \longrightarrow \infty, \quad (2.6)$$

$$\phi(a, z) = \phi_w(z), \quad \phi(r, z) \longrightarrow \phi_\infty \text{ as } r \longrightarrow \infty, \quad (2.7)$$

where $U_w = 2ake^{z/a}$ is the fluid velocity at the surface of the cylinder.

2.3 Solution of the problem

We have the following similarity transformations:

$$u = -\frac{1}{2}U_w \frac{f(\eta)}{\sqrt{\eta}}, \quad w = U_w f'(\eta), \quad (2.8)$$

$$\theta = \frac{T - T_\infty}{T_w - T_\infty}, \quad \eta = \frac{r^2}{a^2}, \quad h = \frac{\phi - \phi_\infty}{\phi_w - \phi_\infty} \quad (2.9)$$

where the characteristic temperature and nanoparticles concentration difference is calculated from the relations $T_w - T_\infty = ce^{z/a}$ and $\phi_w - \phi_\infty = e^{z/a}$. With the help of transformations (2.8) and (2.9), Eqs. (2.1) to (2.4) take the form

$$(1 + \frac{1}{\beta})(\eta f''' + f'') + \text{Re}(f f'' - f'^2) + \text{Re} \lambda(1 - \phi_\infty)(\theta + N_r h) = 0 \quad (2.10)$$

$$\eta \theta'' + \theta' + \text{Re} \text{Pr}(f \theta' - f' \theta) + \eta \theta'(N_b h' + N_t \theta') = 0 \quad (2.11)$$

$$\eta h'' + h' + \frac{N_t}{N_b}(\eta \theta'' + \theta') + \text{Re} Le(fh' - f'h) = 0 \quad (2.12)$$

in which $\lambda = g\beta a(T_w - T_\infty)/U_w^2$ is the natural convection ¹ parameter, $\text{Pr} = \nu/\alpha$ is the Prandtl number, $Le = \nu/D_B$ is the Lewis number, $N_r = (\rho^* - \rho)(\phi_w - \phi_\infty)/\rho\beta(T_w - T_\infty)(1 - \phi_\infty)$ is the buoyancy ratio, $N_b = \rho^* C_p^* D_B(\phi_w - \phi_\infty)/\rho C_p \alpha$ is the Brownian motion parameter, $N_t = \rho^* C_p^* D_T(\phi_w - \phi_\infty)/\rho C_p \alpha T_\infty$ is the thermophoresis parameter and $\text{Re} = aU_w/4\nu$ is the Reynolds number. The boundary conditions in nondimensional form become

$$\begin{aligned} f(1) &= 0, \quad f'(1) = 1, \quad \theta(1) = 1, \quad h(1) = 1, \end{aligned} \quad (2.13)$$

$$f' \longrightarrow 0, \quad \theta \longrightarrow 0, \quad h \longrightarrow 0, \quad \text{as } \eta \longrightarrow \infty. \quad (2.14)$$

The important physical quantities such as the shear stress at the surface τ_w , the skinfriction coefficient c_f , the heat flux at the surface of the cylinder q_w and the local Nusselt number Nu are

$$\tau_w = \tau_{rz}|_{r=a}, \quad q_w = -k\tau_r|_{r=a}, \quad (2.15)$$

$$c_f = \frac{\tau_w}{\rho U_w^2}, \quad Nu_z = \frac{ae^{z/a} q_w}{k(T_w - T_\infty)} \quad (2.16)$$

The numerical solution of the present problem is computed by using Runge-Kutta-Fehlberg method.

2.4 ³ Results and discussion

Here ¹⁰⁸ the effect of the various parameters such as the Reynolds number Re , the Casson fluid parameter β , the Brownian motion parameter N_b , the thermophoresis parameter N_t , the buoy-

buoyancy ratio parameter N_r , the Prandtl number Pr and the natural convection parameter λ on the nondimensional velocity, temperature and concentration profiles are presented graphically and through tabular values. Fig.2.1 shows the effect of Casson fluid parameter β on the velocity profile f' . From Fig.2.1 it is observed that for increasing the value of β the velocity profile decreases. Fig.2.2 shows the influence of mixed convection parameter λ on the velocity profile f' . It is noticed that the velocity increases for large mixed convection parameter. That is the mixed convection parameter λ is directly proportionally to the velocity profile f' for constant values of other parameters. Similar pattern is observed for the buoyancy ratio N_r in Fig.2.3. In Fig.2.4 by increasing the value of Reynolds number Re the velocity profile decreases. Figs.2.5 and 2.6 show a very slow increase in temperature profile by increasing the values of Brownian motion parameter N_b and the thermophoresis parameter N_t . Figs.2.7 and 2.8 reflect similar behaviour of temperature profile, i.e. by increasing the value of Reynolds number Re and the Prandtl number Pr , the temperature profile decreases rapidly. In Fig. 2.9 it is clear that by increasing the value of Lewis number Le the nano concentration profile decreases instantly. Fig.2.10 shows slow effect of Reynolds number Re on nano concentration profile by increasing Reynolds number Re . Table 2.1 shows the boundary derivatives for the velocity profile at the surface of the cylinder that corresponds to the skin friction coefficient for different values of β and λ . Tabulated values indicate that the magnitude of the boundary derivative increases with the increase in β and it decreases by increasing the values of λ . Table 2.2 illustrates the values for local Nusselt numbers for different values of Re and Pr . It is noticed that local Nusselt number increases when Re and Pr are increased.

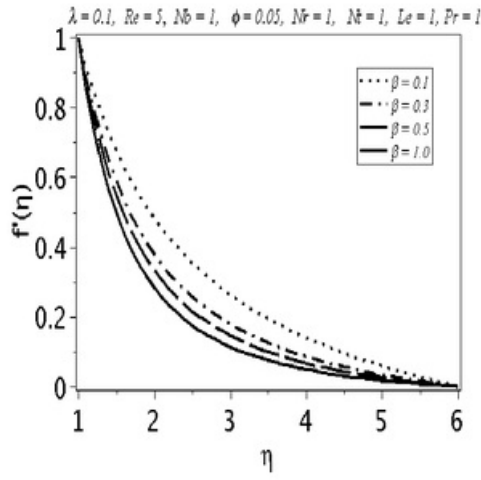


Fig.2.1 Influence of Casson fluid parameter on velocity profile

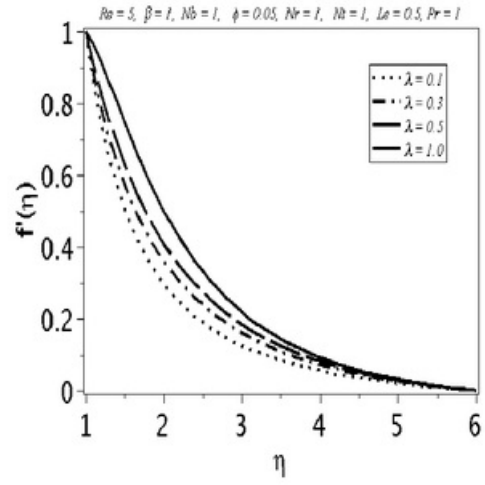


Fig. 2.2 Influence of natural convection parameter on velocity profile

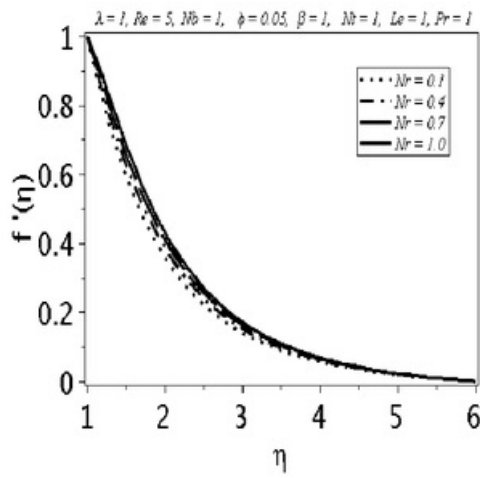


Fig.2.3 Influence of buoyancy ratio parameter on velocity profile

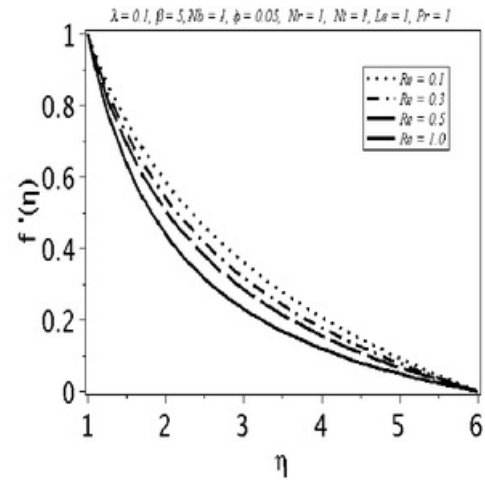


Fig.2.4 Influence of Reynolds numbers on velocity profile

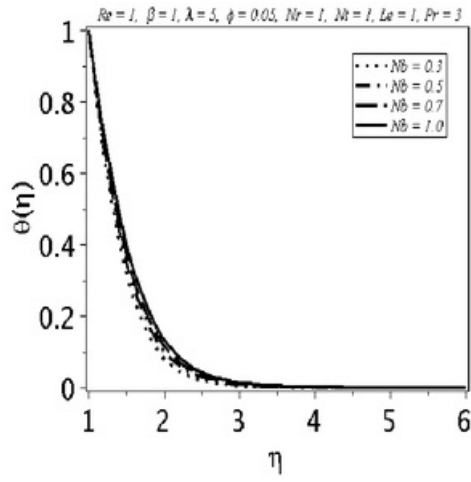


Fig.2.5 Influence of Brownian motion parameter on temperature profile

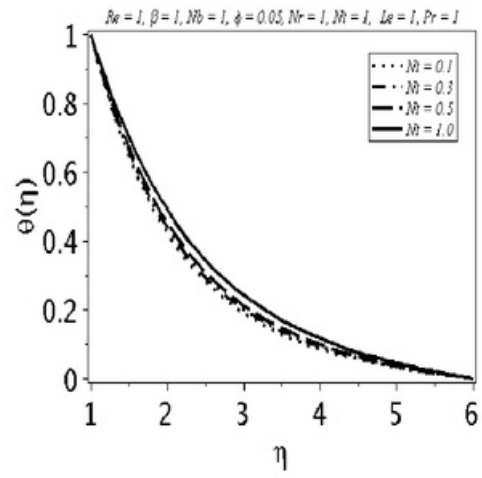


Fig.2.6 Thermophoresis parameter on temperature profile

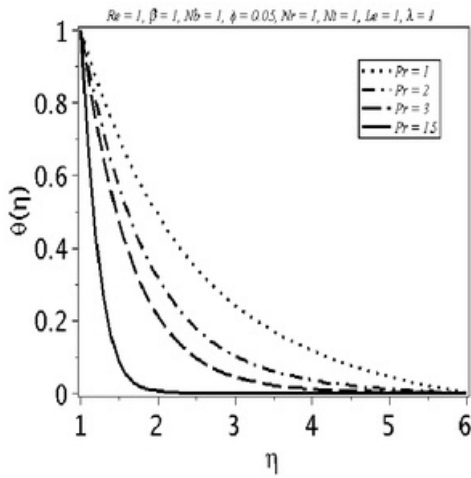


Fig.2.7 Influence of Prantle numbers on temperature profile

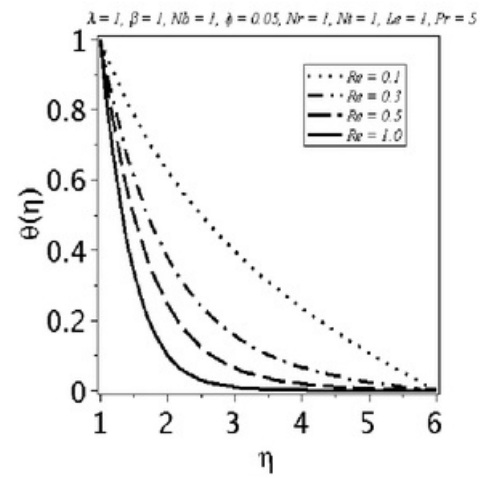


Fig.2.8 Influence of Reynold numbers on temperature profile

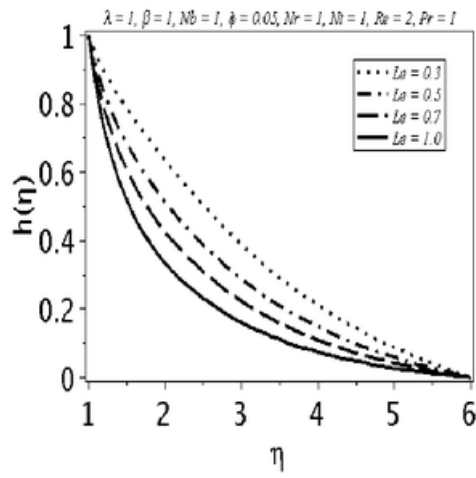


Fig.2.9 Influence of Lewis number on concentration profile

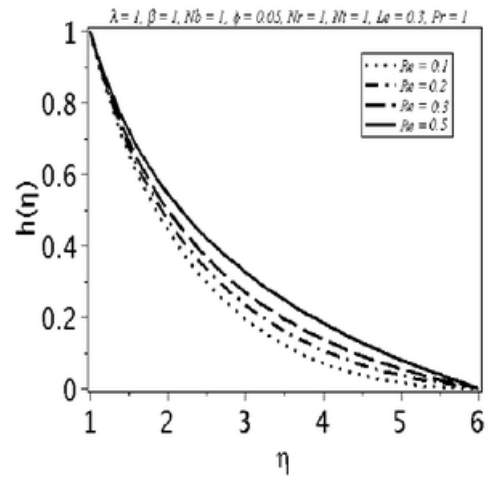


Fig.2.10 Effect of variation of Reynolds number on concentration profile.

Table 2.1 Skin friction coefficient at the surface of the cylinder for $\lambda \backslash \beta$

$\lambda \backslash \beta$	0.1	0.3	0.5	0.7	1.0
0.2	0.5333	0.6479	0.7154	0.7608	0.8071
0.4	0.5141	0.6021	0.6516	0.6840	0.7161
0.6	0.4950	0.5572	0.5895	0.6095	0.6283
0.8	0.4761	0.5130	0.5288	0.5369	0.5431

Table 2.2 Local Nusselt number.

Pr \ Re	0.1	0.2	0.3	0.4	0.5
1	0.2442	0.3094	0.3700	0.4260	0.4776
3	0.3826	0.5627	0.7173	0.8505	0.9668
5	0.5118	0.7844	1.0058	1.1904	1.3489
7	0.6327	0.9814	1.2546	1.4790	1.6714
15	1.0499	1.6121	2.0318	2.3762	2.6739

2.5 Conclusions

This study was focused on natural convection boundary layer flow of a Casson nanofluid. Numerical ⁴ solution of the problem is obtained with the help of Runge-Kutta-Fehlberg method. Main findings of present analysis are listed below:

- Velocity profile increases by increasing buoyancy ratio parameter N_r and natural convection parameter λ but it decreases when Casson fluid parameter β and Reynold number Re are enhanced.
- Temperature profile increases for larger Brownian motion parameter N_b whereas thermophoresis parameter N_t decreases by increasing Reynold number Re and Prandtl number Pr .
- Nano concentration profile increases on increasing Reynold number Re and it decreases by increasing Lewis number Le .
- Skin friction coefficient decreases on increasing natural convection parameter λ and it increases for increasing Casson fluid parameter β .
- Local Nusselt number increases for larger Reynold number Re and Prandtl number Pr .

Chapter 3

Numerical study of convective heat transfer in flow of power law fluid by an exponentially stretching cylinder

3.1 Introduction

This chapter focuses on flow of power law fluid model due to vertical exponentially stretching cylinder with heat transfer. The governing partial differential equations are transformed to a system of ordinary differential equations. For numerical solution Runge-Kutta-Fehlberg method is used. The effects of variation in physical parameters on velocity and temperature are highlighted through graphs. The important physical quantities such as the skin friction coefficient and the local Nusselt number are computed.

3.2 Formulation

Here the problem of natural convective boundary layer flow of a power law fluid flowing by a vertical circular cylinder of radius a is under consideration. The cylinder is assumed by an exponentially stretching sheet. The sheet stretches with velocity U_w . The temperature at the surface of the cylinder is assumed to be T_w and the uniform ambient temperature is taken as T_∞ such that the quantity $T_w - T_\infty > 0$ for assisting flow whereas $T_w - T_\infty < 0$ for opposing

flow, respectively. Under these assumptions the boundary layer equations of motion and heat transfer are

$$u_r + \frac{u}{r} + w_z = 0, \quad (3.1)$$

$$uw_r + ww_z = \frac{k}{\rho} \left(\frac{w_r^n}{r} + nw_r^{n-1} w_{rr} \right) + g\beta(T - T_\infty), \quad (3.2)$$

$$uT_r + wT_z = \alpha \left(T_{rr} + \frac{1}{r} T_r \right), \quad (3.3)$$

In above equations the velocity components along the (r, z) axes are (u, w) , ρ is fluid density, k is the consistency coefficient, p is pressure, g is the gravitational acceleration along the z -direction, β is the coefficient of thermal expansion, T is the temperature and α is the thermal diffusivity. The corresponding boundary conditions are expressed as follows:

$$u(a, z) = 0, \quad w(a, z) = U_w \quad w(r, z) \longrightarrow 0 \text{ as } r \longrightarrow \infty, \quad (3.4)$$

$$T(a, z) = T_w(z), \quad T(r, z) \longrightarrow T_\infty \text{ as } r \longrightarrow \infty. \quad (3.5)$$

Here $U_w = 2ake^{z/a}$ denotes the fluid velocity at the surface of cylinder.

3.3 Solutions

We write

$$u = -\frac{1}{2} U_w \frac{f(\eta)}{\sqrt{\eta}}, \quad w = U_w f'(\eta), \quad (3.6)$$

$$\theta = \frac{T - T_\infty}{T_w - T_\infty}, \quad \eta = \frac{r^2}{a^2}, \quad (3.7)$$

where the characteristic temperature difference is calculated from the relations $T_w - T_\infty = ce^{z/a}$. With the help of transformations (3.6) and (3.7), Eqs. (3.1) to (3.3) become

$$\boxed{132} (n+1)\eta^{\frac{n-1}{2}} (f'')^n + 2n\eta^{\frac{n+1}{2}} f''' (f'')^{n-1} + \boxed{64} \text{Re}_a (f f'' - f'^2) + \text{Re}_a \lambda \theta = 0 \quad (3.8)$$

$$\eta \theta'' + \theta' + \frac{1}{2} \text{Re Pr} (f \theta' - f' \theta) = 0, \quad (3.9)$$

in which $\lambda = g\beta a(T_w - T_\infty)/U_w^2$ is the natural convection parameter, $Pr = k/\rho\alpha$ is the Prandtl number, $Re_a = \rho a^n U_w^{2-n}/k$ is the local Reynolds number and $Re = \rho U_w/4k$ is the Reynolds number. The boundary conditions are reduced to

$$f(1) = 0, \quad f'(1) = 1, \quad \theta(1) = 1, \quad (3.10)$$

$$f' \rightarrow 0, \quad \theta \rightarrow 0, \quad \text{as } \eta \rightarrow \infty. \quad (3.11)$$

The skin friction coefficient c_f and the local Nusselt number Nu_z are

$$\tau_w = \tau_{rz}|_{r=a}, \quad q_w = -k\tau_r|_{r=a}, \quad (3.12)$$

$$c_f = \frac{\tau_w}{\rho U_w^2}, \quad Nu_z = \frac{ae^{z/a}q_w}{k(T_w - T_\infty)} \quad (3.13)$$

3.4 Discussion

Our interest in this section is to investigate the effects of the Reynolds number Re , the local Reynolds number Re_a , the power law index n , the Prandtl number Pr and the natural convection parameter λ over the nondimensional velocity and temperature profiles. For this purpose, the graphs and tables will be prepared. *Fig. 3.1* shows the effects of natural convection parameter λ on the velocity profile f' when $n = 1$. From *Fig. 3.1* it is observed that by increasing the values of natural convection parameter λ the velocity profile increases. *Fig. 3.2* shows the influence of local Reynolds number Re_a over the velocity profile f' when $n = 1$. It is observed that for larger local Reynolds number Re_a the velocity profile f' decreases. *Figs. 3.3* and *3.4* show the effects of variation in Prandtl number Pr and Reynolds number Re on temperature profile when $n = 1$. Here the temperature profile decreases when Prandtl number Pr and Reynolds number Re are increased. The effects of natural convection parameter λ on the velocity profile f' are shown in *Fig. 3.5* when $n = 2$. The velocity profile f' decreases by increasing the values of natural convection parameter λ . *Fig. 3.6* shows opposite behavior of velocity profile f' when $n = 2$, that is, the velocity profile increases by increasing the local Reynolds number Re_a . The temperature profiles presented in *Figs. 3.7* and *3.8* have similar behavior both for $n = 1$ and $n = 2$. The values of skin friction coefficient and local Nusselt number at the surface of the

cylinder are presented in Tables 3.1 and 3.2. Table 3.1, indicates that skin friction coefficient increases upon increasing local Reynolds number Re_a but for fixed value of Prandtl number Pr , the local Nusselt number decreases for larger Reynolds number Re .

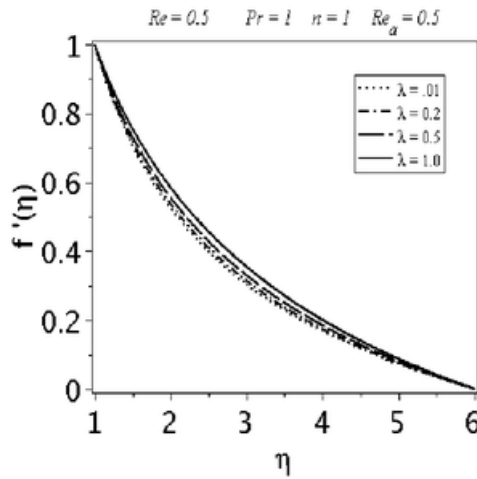


Fig.3.1 Influence of natural convection parameter on velocity profile

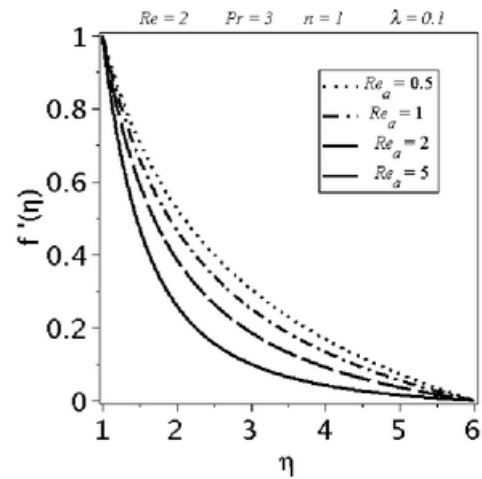


Fig.3.2 Influence of local Reynolds number on velocity profile

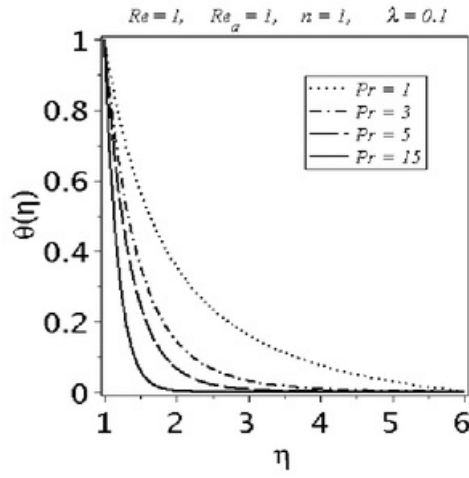


Fig.3.3 Influence of Prandtl number on temperature profile

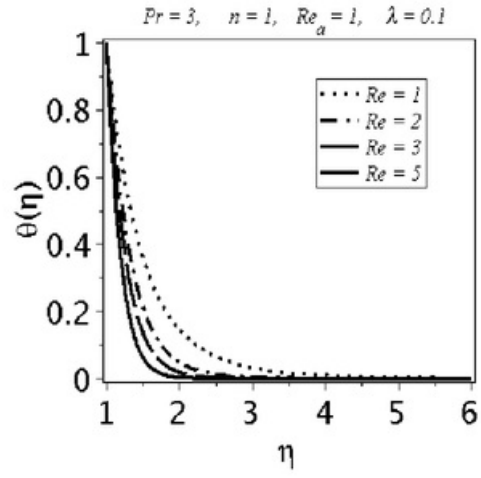


Fig.3.4 Influence of Reynolds number on temperature profile

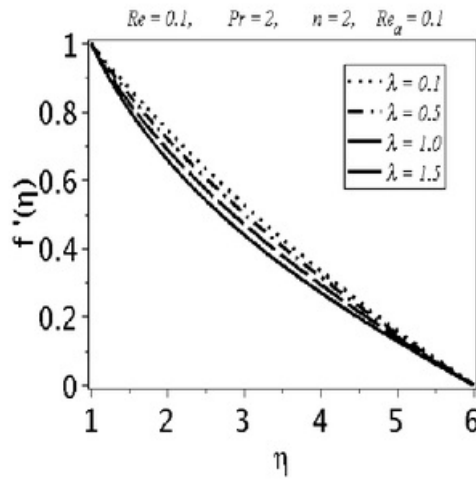


Fig.3.5 Influence of natural convection parameter on velocity profile

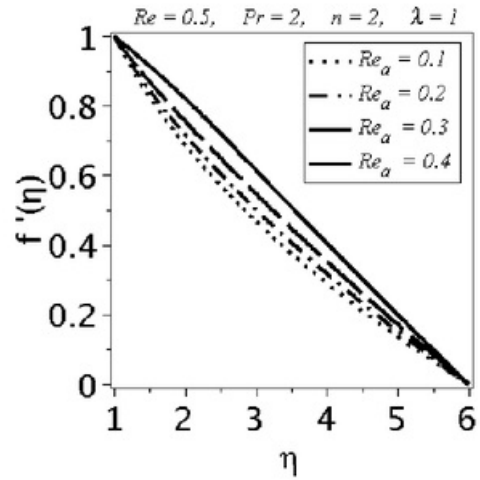


Fig.3.6 Influence of local Reynolds number on velocity profile

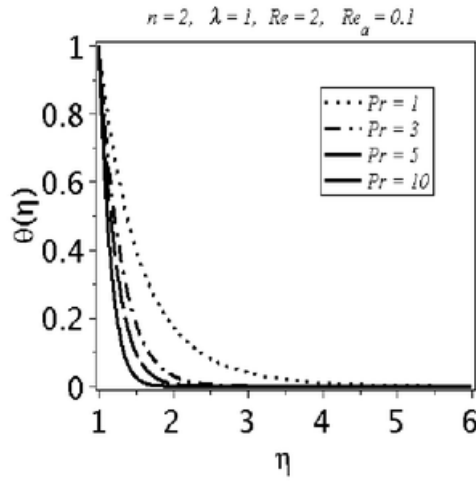


Fig.3.7 Influence of Prandtl number on temperature profile

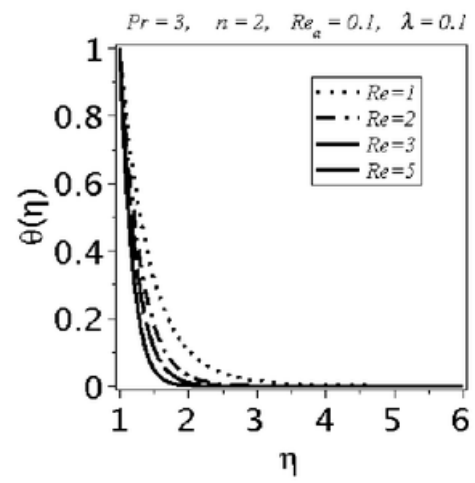


Fig.3.8 Influence of Reynolds number on temperature profile

Table 3.1 Skin friction coefficient at the surface.

$\lambda \backslash Re_a$	0	0.1	0.2	0.3	0.4
1	0.9859	0.9903	0.9953	1.0011	1.0078
3	1.2212	1.2366	1.2544	1.2754	1.3012
5	1.4494	1.4755	1.5065	1.5452	1.5972
10	1.9274	1.9809	2.0499	2.1505	2.3941
15	2.3145	2.3968	2.5121	2.7246	2.9537

Table 3.2 Local Nusselt number.

Pr \ Re	0.0	0.1	0.2	0.3	0.4
1	1.1971	1.1967	1.1962	1.1957	1.1952
7	1.7912	1.7890	1.7866	1.7838	1.7808
10	3.5901	3.5808	3.5699	3.5566	3.5396
15	5.5503	5.5360	5.5182	5.4944	5.4580
25	6.6652	6.6491	6.6285	6.5999	6.5508

3.5 Conclusion

This study is proposed just to address the flow of power law fluid model past a vertical exponentially stretching cylinder with heat transfer. Main results are mentioned below:

- The velocity profile gives opposite behavior for $n = 1$ and 2. That is, the fluid velocity increases for $n = 1$ and it decreases for $n = 2$ when natural convection parameter λ enhances.
- On increasing local Reynolds number Re_a the fluid velocity decreases for $n = 1$ but it increase when $n = 2$.
- The temperature profile decreases both for $n = 1$ and 2 when Reynold number Re and Prandtl number Pr are increased.
- Skin friction coefficient enhances on increasing natural convection parameter λ and local Reynold number Re_a .
- Local Nusselt number increases on increasing Prandtl number Pr but it decreases for larger Reynold number Re .

Chapter 4

²Boundary layer flow of an incompressible tangent hyperbolic fluid past stretching cylinder

4.1 Introduction

¹³The tangent hyperbolic fluid is a four constant pseudoplastic fluid model capable of relating the shear thinning phenomenon. It is a metrial which measures the fluid resistance when flow decreases with an increasing rate of shear stress. Modelled partial differential equations are transformed to system of ordinary differential equations by applying transformations. Numerical solution has been computed by using Runge-Kutta-Fehlberg method. The fluid ⁹²velocity and temperature profiles are presented for different values of physical parameters. Furthermore ²²the skin friction coefficient and Nusselt number described for the influential variables.

4.2 Fluid model

The continuity and momentum ¹equations are

$$\text{div } \mathbf{V} = 0,$$

$$\rho \frac{d\mathbf{V}}{dt} = \text{div } \boldsymbol{\tau} + \rho \mathbf{b},$$

where ρ is the density, \mathbf{V} is the velocity, $\boldsymbol{\tau}$ is the Cauchy stress tensor, \mathbf{b} represents the specific body force and d/dt represents the material time derivative. The constitutive equations of hyperbolic tangent fluid model [8] are given as

$$\boldsymbol{\tau} = -p\mathbf{I} + \mathbf{S},$$

$$\mathbf{S} = [\eta_\infty + (\eta_0 + \eta_\infty) \tanh(\Gamma \bar{\dot{\gamma}})^n] A$$

in which p is the pressure, \mathbf{I} is the identity tensor, $\boldsymbol{\tau}$ is the extra stress tensor, A is second invariant strain tensor, η_0 and η_∞ are the limiting viscosities at zero and at infinite shear rate, $\Gamma > 0$ is the time constant and $\bar{\dot{\gamma}}$ is defined as

$$\bar{\dot{\gamma}} = \sqrt{\frac{1}{2} \sum_i \sum_j \dot{\gamma}_{ij} \dot{\gamma}_{ji}} = \sqrt{\frac{1}{2} \Pi}$$

where

$$\begin{aligned} \Pi &= \sum_i \sum_j \dot{\gamma}_{ij} \dot{\gamma}_{ji} = \text{tr}[(\text{grad } V) + (\text{grad } V)^t]^2 \\ V &= [u(r, z), 0, w(r, z)] \end{aligned}$$

and

$$\bar{\dot{\gamma}} = \sqrt{(u_r^2 + w_z^2) + \frac{1}{2}(u_z + w_r)^2 + \frac{2u^2}{r^2}}$$

We consider the case for which $\eta_\infty = 0$ and $\Gamma \bar{\dot{\gamma}} < 1$. Therefore, the component of extra stress tensor can be written as

$$\mathbf{S} = \eta_0 (\Gamma \bar{\dot{\gamma}})^n A = \eta_0 [1 + n (\Gamma \bar{\dot{\gamma}} - 1)] A$$

4.3 Formulation

Consider the problem of natural convection ³ boundary layer flow of a hyperbolic tangent fluid flow is caused by a vertical circular cylinder of radius a . The cylinder is assumed exponentially stretching with velocity U_w . The temperature at the surface of the cylinder is assumed to be T_w and the uniform ambient temperature is taken as T_∞ such that the quantity $T_w - T_\infty > 0$ in case of the assisting flow while $T_w - T_\infty < 0$ for opposing flow respectively. Under these assumptions the boundary layer equations of motion and heat transfer are

$$u_r + \frac{u}{r} + w_z = 0, \quad (4.1)$$

$$uw_r + ww_z = g\beta(T - T_\infty) + \nu[(1 - n)(w_{rr} + \frac{1}{r}w_r) + \frac{n\Gamma}{2}w_r(2w_{rr} + \frac{1}{r}w_r)] \quad (4.2)$$

$$uT_r + wT_z = \alpha(T_{rr} + \frac{1}{r}T_r), \quad (4.3)$$

where the velocity components along the r -, z -axes are u and w , ρ is density, ν ¹⁰ is the kinematic viscosity, p is pressure, g is the gravitational acceleration along z - direction, β is the coefficient of thermal expansion, T is the temperature, η_∞ is the infinite shear rate viscosity, η_0 ¹⁰ is the viscosity at zero shear rate, Γ is the time constant, n is the power law index and α is the thermal diffusivity. The corresponding ²³ boundary conditions for the problem are

$$u(a, z) = 0, \quad w(a, z) = U_w \quad w(r, z) \longrightarrow 0 \text{ as } r \longrightarrow \infty, \quad (4.4)$$

$$T(a, z) = T_w(z), \quad T(r, z) \longrightarrow T_\infty \text{ when } r \longrightarrow \infty, \quad (4.5)$$

in which $U_w = 2ake^{z/a}$ (k is dimensional constant) is the fluid velocity at the surface of the cylinder.

4.4 Solution

We write

$$u = -\frac{1}{2}U_w \frac{f(\eta)}{\sqrt{\eta}}, \quad w = U_w f'(\eta), \quad (4.6)$$

$$\theta = \frac{T - T_\infty}{T_w - T_\infty}, \quad \eta = \frac{r^2}{a^2}, \quad (4.7)$$

where the characteristic temperature difference is calculated from the relations $T_w - T_\infty = T_0 e^{z/a}$. With the help of transformations (4.6) and (4.7), Eqs. (4.1) to (4.3) are reduced to

$$2(1-n)(\eta f''' + f'') + nWe\sqrt{\eta}f''(4\eta f''' + 3f'') + \text{Re}(ff'' - f'^2) + \text{Re}\lambda\theta = 0, \quad (4.8)$$

$$\eta\theta'' + \theta' + \text{RePr}(f\theta' - f'\theta) = 0, \quad (4.9)$$

in which $\lambda = g\beta a(T_w - T_\infty)/U_w^2$ is the natural convection parameter, $\text{Pr} = \nu/\alpha$ is the Prandtl number, $We = 4\Gamma U_w/a$ is the Weissenberg number and $\text{Re} = aU_w/4\nu$ is the Reynolds number.

The boundary conditions in nondimensional form become

$$f(1) = 0, \quad f'(1) = 1, \quad \theta(1) = 1, \quad (4.10)$$

$$f' \rightarrow 0, \quad \theta \rightarrow 0, \quad \text{as } \eta \rightarrow \infty. \quad (4.11)$$

The important physical quantities such as the shear stress at the surface τ_w , the skin friction coefficient c_f , the heat flux at the surface of the cylinder q_w and the local Nusselt number Nu_z are

$$\tau_w = \tau_{rz}|_{r=a}, \quad q_w = -k\tau_r|_{r=a}, \quad (4.12)$$

$$c_f = \frac{\tau_w}{\rho U_w^2}, \quad Nu_z = \frac{ae^{z/a}q_w}{k(T_w - T_\infty)} \quad (4.13)$$

The solution of the present problem is obtained numerically by using the Runge Kutta Fehlberg method.

4.5 Results and discussion

In this chapter an analysis is carried out for natural convection boundary layer flow of a hyperbolic tangent fluid due to an exponentially stretched cylinder. It is assumed that the cylinder is stretched exponentially along its radial direction. Here $U_w = 2ake^{z/a}$ is the assumed exponential stretching velocity at the surface of cylinder. For the solution of problem the Runge-Kutta-Fehlberg method is used. The impact of different parameters such as the Reynolds number Re , the Prandtl number Pr , the Weissenberg number We and the natural convection parameter λ on the non-dimensional velocity and temperature profiles are presented graphically (see Figs.4.1 – 4.5). Here Fig. 4.1 shows the influence of Weissenberg number We on the velocity function f' . From the graph it is clear that velocity profile decreases by increasing the values of Weissenberg number We . Fig. 4.2 shows the effects of Reynolds number Re on the velocity f' . The velocity profile increases by increasing the values of Re . Fig. 4.3 shows the influence of natural convection parameter λ on velocity profile when $n = 1$. From the graph it is clear that by increasing the values of λ the velocity profile decreases. Fig. 4.4 describes the impact of Prandtl number Pr on temperature profile. The temperature profile increases for larger values of Pr . Fig. 4.5 shows the influence of Reynolds number Re on the temperature profile. The temperature profile increases when Re is enhanced. Table. 4.1 shows the behavior of heat flux at the surface of the stretching cylinder for different values of Pr and Re when $n = 0.3$. Entries in Table. 4.1 show that increase in both Pr and Re increases the heat flux at the surface. Table. 4.2 shows magnitude of the velocity profile when $n = 0.3$. Entries in Table. 4.2 depict that the magnitude of boundary derivative increases by increasing both the Weissenberg and the Reynolds numbers.

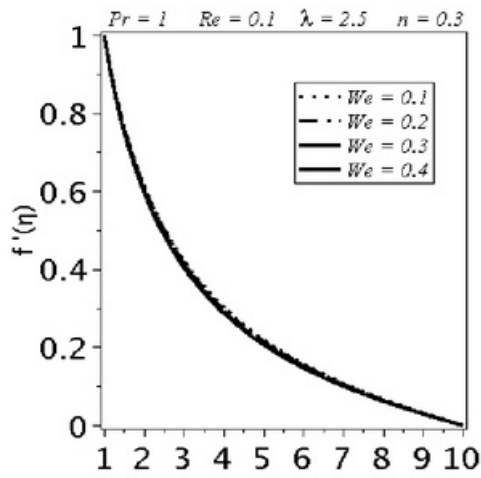


Fig.4.1 Influence of Wessonburg number
on velocity profile

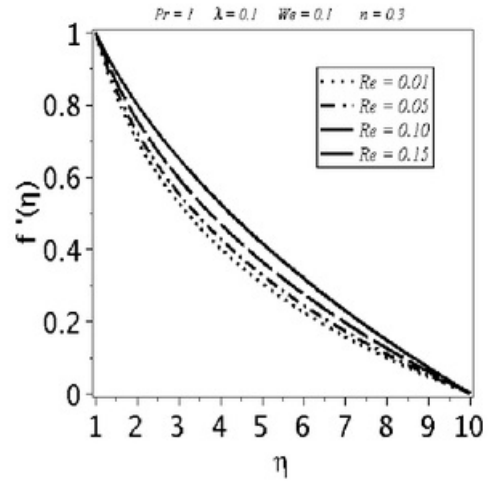


Fig.4.2 Influence of Reynolds number on
velocity profile

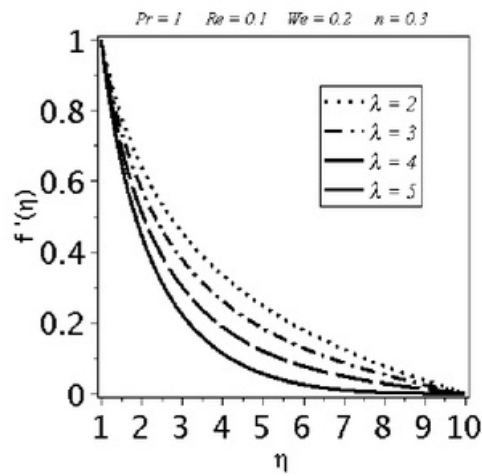


Fig.4.3 Influence of natural convection
parameter on velocity profile

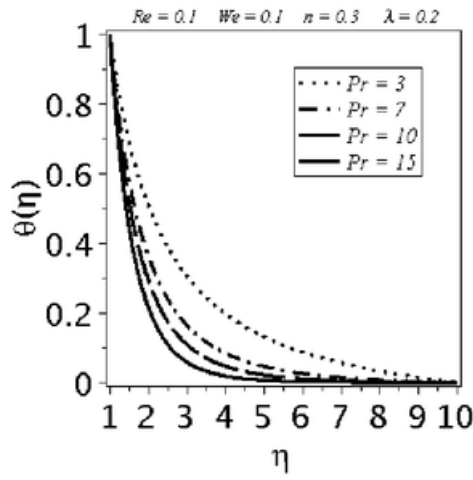


Fig.4.4 Influence of Prandtl number on temperature profile

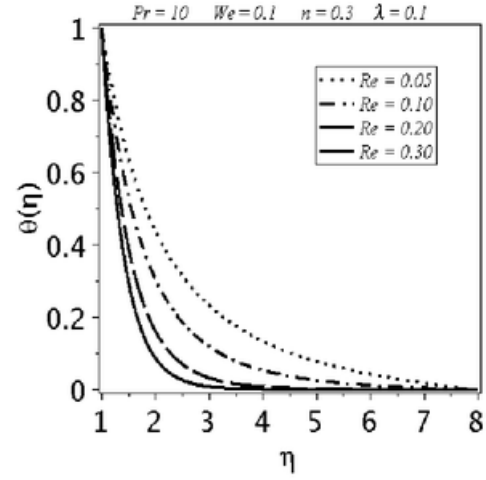


Fig.4.5 Influence of Reynolds number on temperature profile

Table 4.1 Local Nusselt number

Pr\Re	0.1	0.2	0.3	0.4	0.5	1.0
1	0.9613	0.9786	0.9963	1.0141	1.0323	1.1263
3	1.0610	1.0617	1.0624	1.0632	1.0639	1.0667
5	1.1578	1.1589	1.1601	1.1612	1.1624	1.1684
7	1.2517	1.2533	1.2548	1.2563	1.2579	1.2658
15	1.6018	1.6045	1.6071	1.6098	1.6125	1.6264

Table 4.2 Skin friction coefficient at the surface

We\Re	0.1	0.2	0.3	0.4	0.5	1.0
0.1	0.9621	1.0041	1.0450	1.0850	1.1240	1.3082
0.2	0.9767	1.0231	1.0687	1.1136	1.1580	1.3741
0.3	0.9943	1.0464	1.0982	1.1499	1.2017	1.4666
0.4	1.0163	1.0761	1.1366	1.1982	1.2612	1.6159

4.6 Conclusions

The following points are worth mentioning.

- Increase in natural convection parameter, Weissenberg number and Reynolds number reduces the fluid velocity.
- Increase in Prandtl and Reynolds numbers reduces the fluid temperature.
- Larger Prandtl and Reynolds numbers, give rise to heat flux at the surface.
- The magnitude of boundary derivative increases by increasing both the Weissenberg and the Reynolds numbers.

Chapter 5

Flow of Williamson fluid past a vertical exponentially stretching cylinder

5.1 Introduction

This chapter addresses the boundary layer flow of Williamson fluid, occurs in many industrial processes and natural phenomena. Most of the interest in this subject is due to its applications. Flow caused is because of an exponentially stretching cylinder. The governing partial differential equations systems are reduced to nonlinear ordinary differential equations systems. Keller box technique is implemented for the numerical solution. The effects of different physical parameters (e.g. Reynold number Re , Prandtl number Pr , the natural convection parameter λ and Weissenberg number We) are presented through graphs. The skin friction coefficient is computed to see the effects of different parameters.

5.2 Mathematical formulation

Consider the problem of natural convection boundary layer flow of Williamson fluid due to a vertical circular cylinder of radius a . The cylinder is assumed stretched exponentially along the axial direction with velocity U_w . The temperature at the surface of the cylinder is assumed T_w

and the uniform ambient temperature is taken as T_∞ such that the quantity $T_w - T_\infty > 0$ in case of the assisting flow, while $T_w - T_\infty < 0$ in case of the opposing flow, respectively. The boundary layer flow under consideration are governed by

$$u_r + \frac{u}{r} + w_z = 0, \quad (5.1)$$

$$uw_r + ww_z = \frac{\nu}{r}(\Gamma w_r^2 + w_r) + \nu[w_{rr} + 2\Gamma w_{rr}w_r] + g\beta(T - T_\infty), \quad (5.2)$$

$$uT_r + wT_z = \alpha(T_{rr} + \frac{1}{r}T_r), \quad (5.3)$$

where the velocity components along the (r, z) axes are (u, w) , ρ is density, ν is the kinematic viscosity, p is pressure, g is the gravitational acceleration along the z - direction, β is the coefficient of thermal expansion, T is the temperature and α is the thermal diffusibility. The corresponding boundary conditions for the problem are

$$u(a, z) = 0, \quad w(a, z) = U_w \quad w(r, z) \longrightarrow 0 \text{ as } r \longrightarrow \infty, \quad (5.4)$$

$$T(a, z) = T_w(z), \quad T(r, z) \longrightarrow T_\infty \text{ as } r \longrightarrow \infty, \quad (5.5)$$

where $U_w = 2ake^{z/a}$ is the fluid velocity at the surface of the cylinder.

5.3 Solution of the problem

We consider

$$u = -\frac{1}{2}U_w \frac{f(\eta)}{\sqrt{\eta}}, \quad w = U_w f'(\eta), \quad (5.6)$$

$$\theta = \frac{T - T_\infty}{T_w - T_\infty}, \quad \eta = \frac{r^2}{a^2}, \quad (5.7)$$

where the characteristic temperature difference is calculated from the relations $T_w - T_\infty = ce^{z/a}$. With the help of transformations (5.6) and (5.7), Eqs. (5.1) to (5.3) are reduced to

$$\eta f''' + f'' + \text{Re}(ff'' - f'^2) + We\sqrt{\eta}f''(\eta f''' + f'') + \text{Re}\lambda\theta = 0 \quad (5.8)$$

$$\eta\theta'' + \theta' + \frac{1}{2}\text{RePr}(f\theta' - f'\theta) = 0, \quad (5.9)$$

in which $\lambda = g\beta a(T_w - T_\infty)/U_w^2$ is the natural convection parameter, $Pr = \nu/\alpha$ is the Prandtl number, $We = 4\Gamma U_w/a$ Weissenberg number and $Re = aU_w/4\nu$ is the Reynolds number. The boundary conditions now reduce to

$$f(1) = 0, \quad f'(1) = 1, \quad \theta(1) = 1, \quad (5.10)$$

$$f' \rightarrow 0, \quad \theta \rightarrow 0, \quad \text{as } \eta \rightarrow \infty. \quad (5.11)$$

The important physical quantities such as the shear stress at the surface τ_w , the skin friction coefficient c_f , the heat flux at the surface of the cylinder q_w and the local Nusselt number Nu_z are

$$\tau_w = \tau_{rz}|_{r=a}, \quad q_w = -k \tau_r|_{r=a}, \quad (5.12)$$

$$c_f = \frac{\tau_w}{\rho U_w^2}, \quad Nu_z = \frac{ae^{z/a} q_w}{k(T_w - T_\infty)} \quad (5.13)$$

Keller box Method is employed for the numerical solution.

5.4 Outcomes

In this section, the results are analyzed for the Reynolds number Re , the Weissenberg number We , the Prandtl number Pr and the natural convection parameter λ for the nondimensional velocity and temperature profiles. This objective is achieved through Figs.(5.1 – 5.8) and Tables 5.1 and 5.2. Fig.5.1 shows the effect of Prandtl number Pr on the velocity profile f' . It is observed that by increasing Prandtl number Pr the velocity profile decreases. Fig.5.2 indicates the influence of natural convection parameter λ over the velocity profile f' . When natural convection parameter λ increases the velocity profile also increases, that is, the natural convection parameter λ is directly proportionally to the velocity profile f' . Similarly by increasing the value of Weissenberg number We and Reynold number Re the velocity profile decreases (see Figs.5.3 and 5.4). Response of temperature profile due to variation in Prandtl number, natural convection parameter, Renold number and Weissenberg number can be seen in the Figs.(5.5 – 5.8). Fig.5.5 shows that after increasing the value of Prandtl number Pr , temperature profile decreases. Fig.5.6 depicts similar behaviour of temperature profile by increasing λ , that is, the temperature profile also decreases. In Fig.5.7 by increasing the value

of Reynold number Re , the temperature profile decreases. In *Fig.5.8* there is slight effect of Weissenberg number We on temperature profile.

Table 5.1 shows the boundary derivatives for the velocity profile at the surface of cylinder that corresponds to the skin friction coefficient at the surface tabulated for different values of We and Re . From table 5.1 it is observed that the magnitude of boundary derivative increases with the increase in both We and Re . Table 5.2 shows the values for local Nusselt numbers when different values of We and Pr are used. Table 5.2 witnesses that with increase in We (for fixed Pr), local Nusselt number increases whereas with increase in Pr (for fixed We), Nu_z decreases.

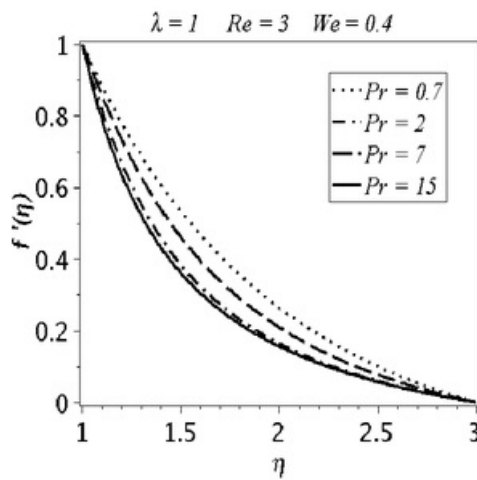


Fig.5.1 Influence of Prandtl number on velocity profile

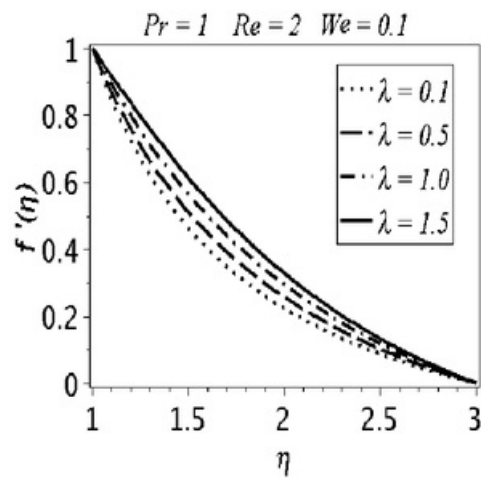


Fig.5.2 Influence of natural convection parameter on velocity profile

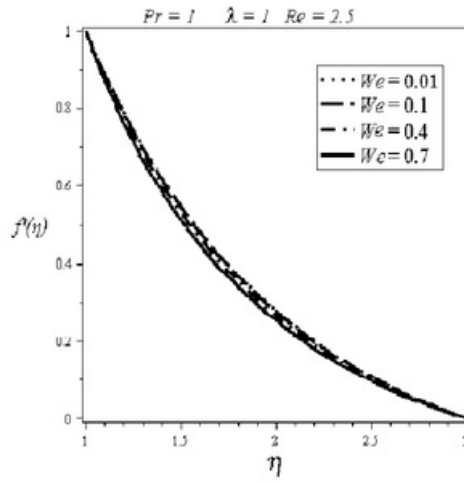


Fig.5.3 Influence of Weissenberg number on velocity profile

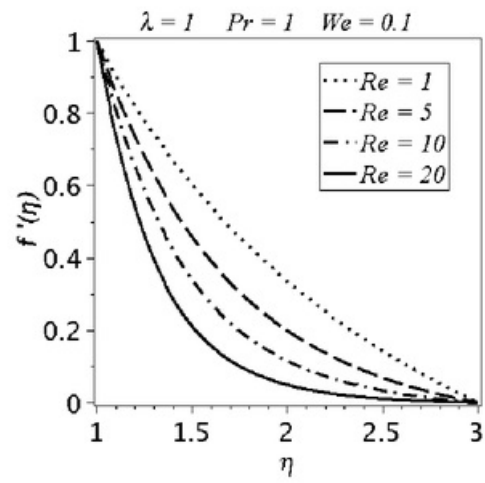


Fig.5.4 Influence of Reynold number on velocity profile

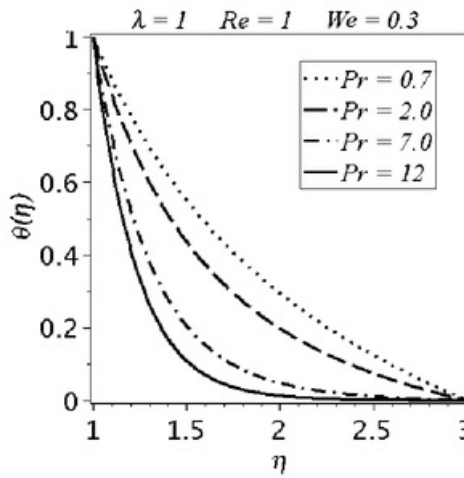


Fig.5.5 Influence of Prantdl number on temperature profile

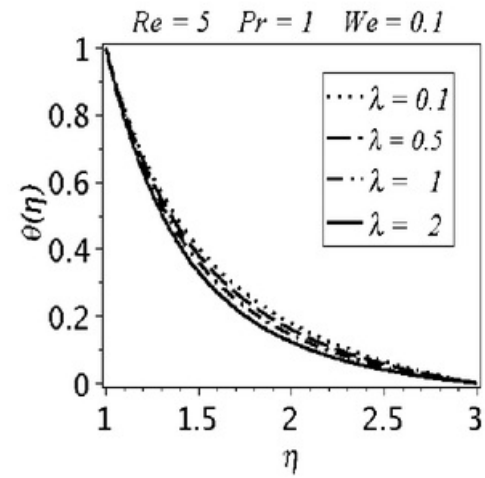


Fig.5.6 Influence of natural convection parameter on temperature profile

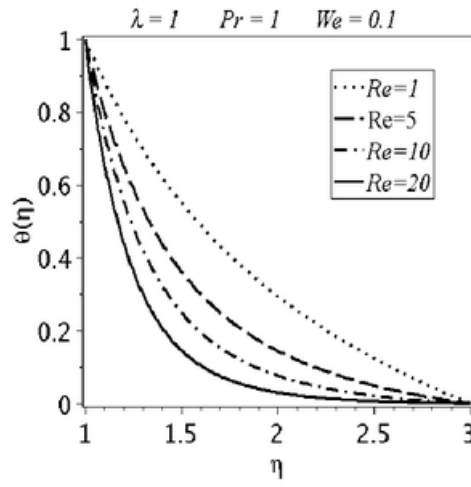


Fig.5.7 Influence of Reynold number on temperature profile

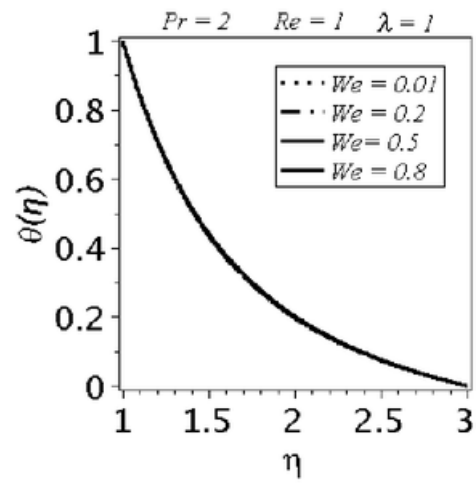


Fig.5.8 Influence of Weissenberg number on temperature profile

Table 5.1 Skin friction at the surface of the cylinder

Re \ We	0	0.1	0.2	0.3	0.4
1	0.9859	0.9903	0.9953	1.0011	1.0078
3	1.2212	1.2366	1.2544	1.2754	1.3012
5	1.4494	1.4755	1.5065	1.5452	1.5972
10	1.9274	1.9809	2.0499	2.1505	2.3941
15	2.3145	2.3968	2.5121	2.7246	2.9537

Table 5.2 Local Nusselt number

Pr \ We	0.0	0.1	0.2	0.3	0.4
0.2	1.1971	1.1967	1.1962	1.1957	1.1952
0.7	1.7912	1.7890	1.7866	1.7838	1.7808
3.0	3.5901	3.5808	3.5699	3.5566	3.5396
7.0	5.5503	5.5360	5.5182	5.4944	5.4580
10.0	6.6652	6.6491	6.6285	6.5999	6.5508

5.5 Conclusions

The following are the main finding of this chapter:

- Velocity decays upon increasing the Weissenberg, Prandtl and Reynold numbers.
- Larger convection parameter enhances the velocity.
- The temperature profile decreases by increasing Prandtl, Reynold, natural, Weissenberg numbers and convection parameter.
- The skin friction decreases by increasing Weissenberg and Renold numbers.
- The local Nusselt number increases when Prandtl number (fixed Weissenberg number) enhances or it decreases on increasing Weissenberg number (fixed Prandtl number).

Chapter 6

Boundary layer flow of Williamson nanofluid past a vertical exponentially stretching cylinder

6.1 Introduction

The boundary layer flow of Williamson nanofluid past an exponentially stretching surface is explored. The governing partial differential equations and the associated boundary conditions are reduced to nonlinear ordinary differential equations after using the boundary layer approximation and similarity transformation. The obtained system of nonlinear ordinary differential equations subject to the boundary conditions are solved numerically by employing Keller box method. The effects of different physical parameters (e.g. Reynold number Re , Schmidt number Sc , Prandtl number Pr , the natural convection parameter λ and Weissenberg number We , the buoyancy ratio N_r , the Brownian motion parameter N_b , the thermophoresis parameter N_t) on velocity, temperature and nano concentration profiles are presented through graphs. The skin friction coefficient and Nusselt number are also computed for different parameters.

6.2 Formulation

Consider the problem of natural convection and heat transfer of a Williamson nanofluid flowing past a vertical circular cylinder of radius a . Brownian motion thermophoresis are considered. The cylinder is stretched exponentially with velocity U_w . The temperature at the surface of the cylinder is assumed T_w and the uniform ambient temperature is taken as T_∞ . The flow under consideration is governed by

$$u_r + \frac{u}{r} + w_z = 0, \quad (6.1)$$

$$uw_r + ww_z = \frac{\nu}{r}(\Gamma w_r^2 + w_r) + \nu[w_{rr} + 2\Gamma w_{rr}w_r] + g\beta(T - T_\infty)(1 - \phi_\infty) + \frac{1}{\rho}(\rho^* - \rho)(\phi - \phi_\infty), \quad (6.2)$$

$$uT_r + wT_z = \alpha(T_{rr} + \frac{1}{r}T_r) + \frac{\rho^*c_p^*}{\rho c_p}(D_T T_r \phi_r + \frac{D_T}{T_\infty} T_r^2), \quad (6.3)$$

$$u\phi_r + w\phi_z = D_B(\phi_{rr} + \frac{1}{r}\phi_r) + \frac{D_T}{T_\infty}(T_{rr} + \frac{1}{r}T_r). \quad (6.4)$$

In above expression the velocity components along the (r, z) axes are (u, w) , ρ and ρ^* are the densities of the base fluid and the nanoparticle material respectively, k is the consistency coefficient, $\rho^*c_p^*$ is the effective heat capacity of the nanoparticle material and ρc_p is the effective heat capacity of the base fluid, g is the gravitational acceleration along the z -direction, D_B is Brownian diffusion coefficient, D_T is thermophoretic diffusion coefficient, β is the coefficient of thermal expansion, T is the temperature and α is the thermal diffusibility of base fluid. The corresponding boundary conditions can be written as

$$u(a, z) = 0, \quad w(a, z) = U_w \quad w(r, z) \longrightarrow 0 \text{ as } r \longrightarrow \infty, \quad (6.5)$$

$$T(a, z) = T_w(z), \quad T(r, z) \longrightarrow T_\infty \text{ as } r \longrightarrow \infty, \quad (6.6)$$

$$\phi(a, z) = \phi_w(z), \quad \phi(r, z) \longrightarrow \phi_\infty \text{ as } r \longrightarrow \infty, \quad (6.7)$$

in which $U_w = 2ake^{z/a}$ represents the fluid velocity at the surface of the cylinder.

6.3 Solution of the problem

Writing

$$u = -\frac{1}{2}U_w \frac{f(\eta)}{\sqrt{\eta}}, \quad w = U_w f'(\eta), \quad (6.8)$$

$$\theta = \frac{T - T_\infty}{T_w - T_\infty}, \quad \eta = \frac{r^2}{a^2}, \quad h = \frac{\phi - \phi_\infty}{\phi_w - \phi_\infty} \quad (6.9)$$

we have from Eqs. (6.1) to (6.4) as follows

$$\eta f''' (4We\sqrt{\eta}f'' + 1) + f'' (5We\sqrt{\eta}f'' + 1) + \text{Re}(ff'' - f'^2) + \text{Re} \lambda (1 - \phi_\infty)(\theta + N_r h) = 0, \quad (6.10)$$

$$\eta \theta'' + \theta' + \text{Re} \text{Pr}(f\theta' - f'\theta) + \eta \theta' (N_b h' + N_t \theta') = 0, \quad (6.11)$$

$$\eta h'' + h' + \frac{N_t}{N_b}(\eta \theta'' + \theta') + \text{Re} Sc(fh' - f'h) = 0. \quad (6.12)$$

in which $\lambda = g\beta a(T_w - T_\infty)/U_w^2$ is the natural convection parameter, $\text{Pr} = \nu/\alpha$ is the Prandtl number, $Sc = \nu/D_B$ is the Schmidt number, $We = 4\Gamma U_w/a$ is the Weissenberg number, $N_r = (\rho^* - \rho)(\phi_w - \phi_\infty)/\rho\beta(T_w - T_\infty)(1 - \phi_\infty)$ is the buoyancy ratio, $N_b = \rho^* C_p^* D_B(\phi_w - \phi_\infty)/\rho C_p \alpha$ is the Brownian motion parameter, $N_t = \rho^* C_p^* D_T(\phi_w - \phi_\infty)/\rho C_p \alpha T_\infty$ is the thermophoresis parameter and $\text{Re} = aU_w/4\nu$ is the Reynolds number. The boundary conditions can be expressed as

$$f(1) = 0, \quad f'(1) = 1, \quad \theta(1) = 1, \quad h(1) = 1, \quad (6.13)$$

$$f' \rightarrow 0, \quad \theta \rightarrow 0, \quad h \rightarrow 0, \quad \text{as } \eta \rightarrow \infty. \quad (6.14)$$

Flow quantities of interests are

$$\tau_w = \tau_{rz} |_{r=a}, \quad q_w = -k \tau_r |_{r=a}, \quad (6.15)$$

$$c_f = \frac{\tau_w}{\rho U_w^2}, \quad Nu_z = \frac{ae^{z/a} q_w}{k(T_w - T_\infty)} \quad (6.16)$$

The solutions of the resulting problems are obtained by using Keller box method.

6.4 Results and discussion

The problem of natural convection boundary layer flow of Williamson nanofluid past an exponentially stretched cylinder is studied. The solution of the problem is obtained numerically with the help of Keller box method. Effect of the various parameters such as the Reynolds number Re , the Weissenberg number We , the Schmidt number Sc , the Brownian motion parameter N_b , the thermophoresis parameter N_t , the buoyancy ratio parameter N_r , the Prandtl number Pr and the natural convection parameter λ on the nondimensional velocity, temperature and concentration profiles are presented graphically in Figs.6.1 – 6.10 and in Tables 6.1 – 6.4. From Figs.6.1 to 6.4 the velocity profiles are presented for different physical parameters. Fig.6.1 shows the effect of the buoyancy ratio parameter N_r on the velocity profile. It is observed that larger buoyancy ratio parameter N_r increases the velocity profile. Fig.6.2 reflects the influence of natural convection parameter λ on the velocity profile. It is noticed that when natural convection parameter λ increases then velocity profile rapidly increases. That is the natural convection parameter λ is directly proportional to the velocity. In Fig.6.3 the effects of the Weissenberg number We on the velocity profile are presented. Slight decrease in velocity profile is seen by increasing the values of Weissenberg number We . In Fig.6.4, with the increase of Reynold number Re , the velocity profile decreases. Figs.6.5 to 6.8 reflect the behavior of temperature profiles for different physical parameters. Fig.6.5 shows the influence of Prandtl number Pr on the temperature profile. By increasing the values of Prandtl number Pr , the temperature profile decreases. Fig.6.6 describes the influence of Brownian motion parameter N_b on the temperature profile. The temperature profile increases by increasing the values of Brownian motion parameter N_b . Fig.6.7 shows the effects of the Reynold number Re on the temperature profile. The temperature profile rapidly decreases by increasing the values of Reynold number Re . Fig.6.8 shows the influence of the thermophoresis parameter N_t over the temperature profile. By increasing the values of the thermophoresis parameter N_t , the temperature profile increases. Figs.6.9 and 6.10 highlight the nano concentration profile. In Fig.6.9 it is clear that by increasing the value of Schmidt number Sc the nano concentration profile decreases instantly.

In Fig.6.10 rising effect of Reynold number Re can be seen on nano concentration profile. By increasing the value of Reynolds number Re the nano concentration profile increases. Table 6.1 shows the boundary derivatives for the velocity profile at the surface of the cylinder that corresponds to the skin friction coefficient at the surface tabulated for different values of Re and λ . From table 6.1 it is observed that the magnitude of the boundary derivative increases with the increase in Re and it decreases by increasing the values of λ . Table 6.2 shows the boundary derivatives for the velocity profile at the surface of cylinder which corresponds to the skin friction coefficient at the surface tabulated for different values of N_r and λ . From table 6.2 it is observed that the magnitude of boundary derivative decreases by increasing both N_r and λ . Table 6.3 shows the values for local Nusselt numbers calculated for different values of N_b and Pr . From entries in the table it is noticed that with the increase in Pr , the local Nusselt number increases and it decreases by increasing N_b . Table 6.4 shows the values for local Nusselt numbers calculated for different values of N_t and Re . Tabulated values indicate that with the increase in Re the local Nusselt number increases and it decreases by increasing N_t .

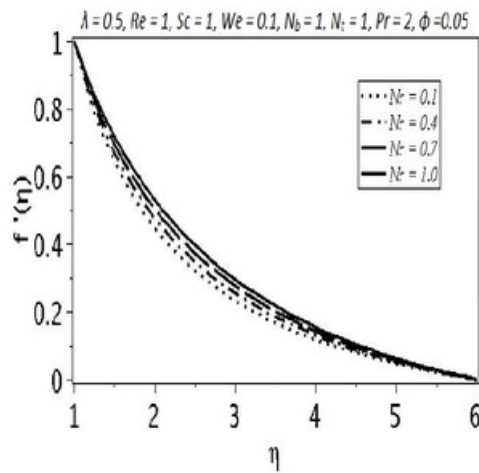


Fig.6.1 Influence of buoyancy ratio on velocity profile

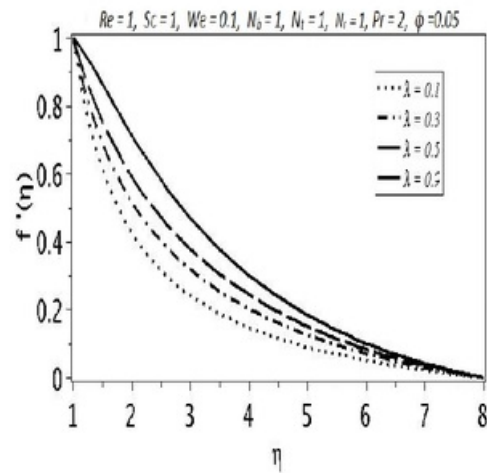


Fig.6.2 Influence of natural convection parameter on velocity profile

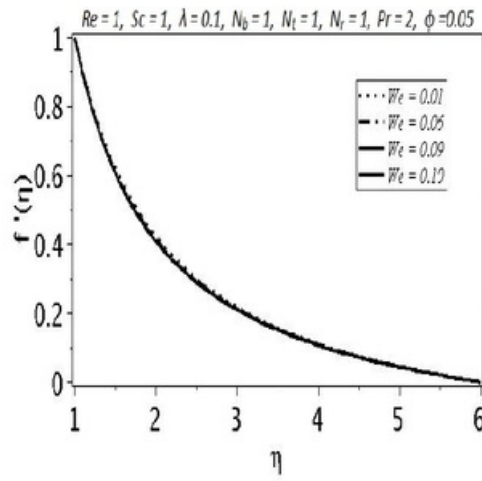


Fig.6.3 Influence of Weissenberg number on velocity profile

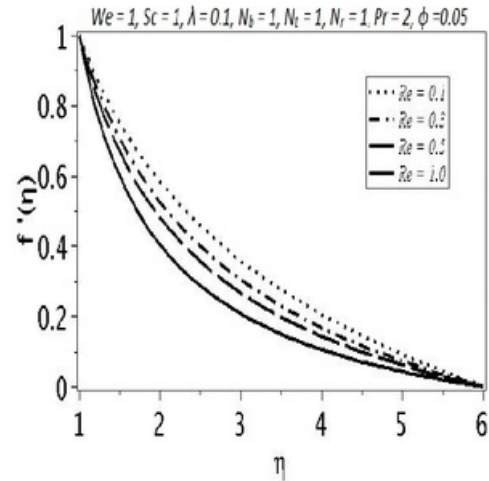


Fig.6.4 Influence of Reynolds number on velocity profile

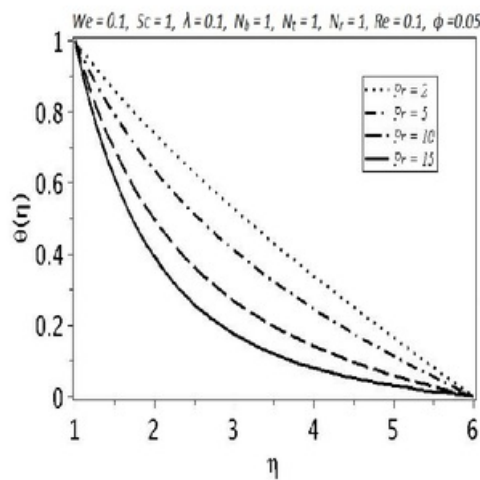


Fig.6.5 Influence of Prandtl number on temperature profile

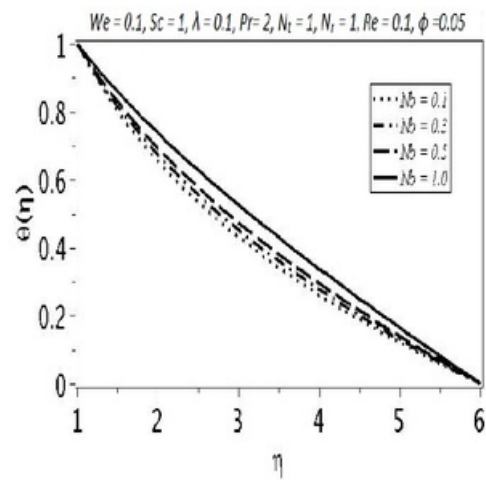


Fig 6.6 Influence of Brownian motion parameter on temperature profile

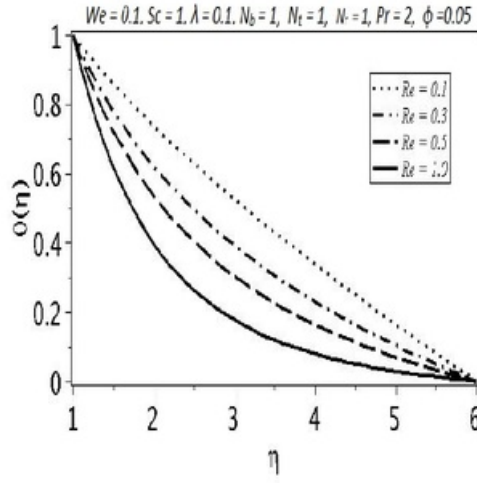


Fig.6.7 Influence of Reynold number on temperature profile

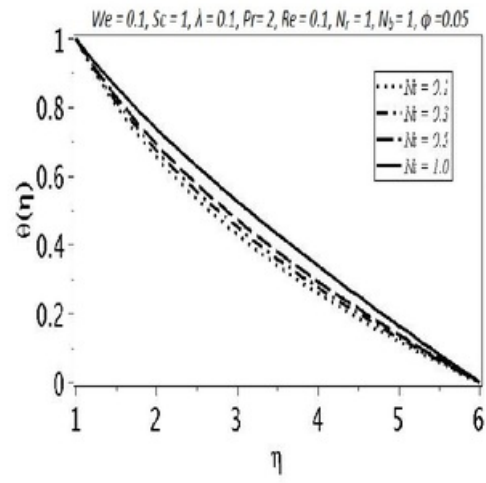


Fig.6.8 Influence of thermophoresis parameter on temperature profile

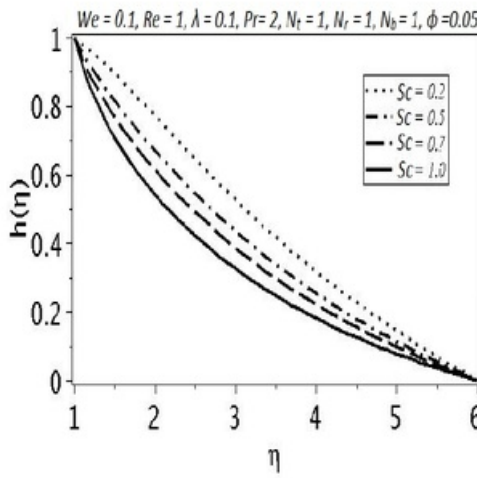


Fig.6.9 Influence of Schmidt number on concentration profile

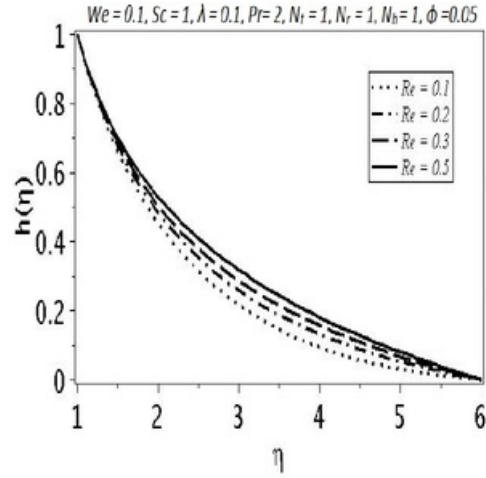


Fig.6.10 Influence of Reynold number on concentration profile

Table 6.1 : Skin friction coefficient at surface of the cylinder for $\lambda \backslash \text{Re}$.

$\lambda \backslash \text{Re}$	0.1	0.2	0.3	0.4	0.5	1.0
0.1	0.5417665	0.6472440	0.7405385	0.8256308	0.9048707	1.1877323
0.3	0.5047508	0.5878888	0.6638048	0.7338210	0.7991701	1.0823029
0.5	0.4685034	0.5308771	0.5911608	0.6478879	0.7011902	0.9304973
0.7	0.4329826	0.4759543	0.5220001	0.5667934	0.6093992	0.7926674
1.0	0.3809803	0.3970323	0.4237953	0.4526199	0.4810536	0.6052925

Table 6.2 : Skin friction coefficient at surface of the cylinder for $\lambda \backslash N_r$.

$\lambda \backslash N_r$	0.1	0.2	0.3	0.4	0.5	1.0
0.1	0.9225412	0.9170612	0.9115928	0.9061359	0.9006905	0.8736364
0.3	0.8274242	0.8119717	0.7966064	0.7813283	0.7661372	0.6914783
0.5	0.7389129	0.7145075	0.6903109	0.6663227	0.6425421	0.5267080
0.7	0.6557539	0.6231766	0.5909584	0.5590979	0.5275932	0.3752816
1.0	0.5391606	0.4954539	0.4523649	0.4098899	0.3680230	0.1674808

Table 6.3 : Local Nusselt numbers for different values of $\text{Pr} \backslash N_b$.

$\text{Pr} \backslash N_b$	0.1	0.2	0.3	0.4	0.5	1.0
1	0.3670232	0.3512651	0.3351202	0.3194159	0.3042953	0.2379131
3	0.5673555	0.5428482	0.5222006	0.5029387	0.4845972	0.4032442
5	0.7501875	0.7145851	0.6891727	0.6666279	0.6455541	0.5525502
10	1.1218606	1.0693323	1.0361168	1.0082439	0.9828072	0.8714786
15	1.4103439	1.3511575	1.3143805	1.2839238	1.2563011	1.1353196

Table 6.4 : Local Nusselt numbers for different values of $N_t \backslash \text{Re}$.

$N_t \backslash \text{Re}$	0.1	0.2	0.3	0.4	0.7	1.0
0.1	0.4577478	0.5829143	0.6903830	0.7851347	1.0196609	1.2079586
0.3	0.4197439	0.5424134	0.6478759	0.7408885	0.9709497	1.1553141
0.5	0.3846766	0.5047382	0.6081510	0.6994234	0.9251340	1.1057320
0.7	0.3524091	0.4697585	0.5710763	0.6606027	0.8820635	1.0590535
1.0	0.3089417	0.4220501	0.5201416	0.6070311	0.8222791	0.9941360

6.5 Conclusions

47

Keller box method is employed to find the numerical solution for flow of Williamson nanofluid past a vertical exponentially stretching cylinder. The main findings of the study are summarized below.

- The velocity profile increases upon increasing buoyancy ratio parameter and natural convection parameter but it decreases by increasing Weissenberg and Reynold numbers.
- The temperature profile ¹ increases for larger Brownian motion parameter N_b and thermophoresis parameter N_t .
- The nano concentration profile decreases upon increasing Schmidt number Sc and it increases by increasing Reynold number Re .
- Skin friction coefficient decreases upon increasing natural convection parameter λ and buoyancy ratio parameter N_r but it increases for increasing Reynold number Re .
- Local Nusselt number increases for larger Reynold and Prandtl numbers but it decreases when Brownian motion and thermophoresis parameters are increased.

Chapter 7

Dual stratified mixed convection flow of Eyring-Powell fluid past an inclined stretching cylinder with heat generation/absorption effect

7.1 Introduction

This chapter is proposed to study the effects of double stratified medium in the mixed convection boundary layer flow of Eyring-Powell fluid flow induced is by an inclined stretching cylinder. Flow analysis is studied ⁸ in the presence of heat generation/absorption. Temperature and concentration are assumed higher than ambient fluid across the surface of cylinder. The arising ² flow system of partial differential equations is primarily transformed into coupled ² non-linear ordinary differential equations with the aid of suitable transformations. Numerical solutions of resulting non-linear boundary value problem are computed successfully by utilizing fifth order Runge-Kutta algorithm with shooting technique. The velocity, temperature and concentration profiles are examined graphically. Further the numerical findings are obtained for two distinct cases namely, zero (plate) and non-zero (cylinder) values of curvature parameter and the behaviour are presented through graphs for skin-friction coefficient, Nusselt number and Sherwood

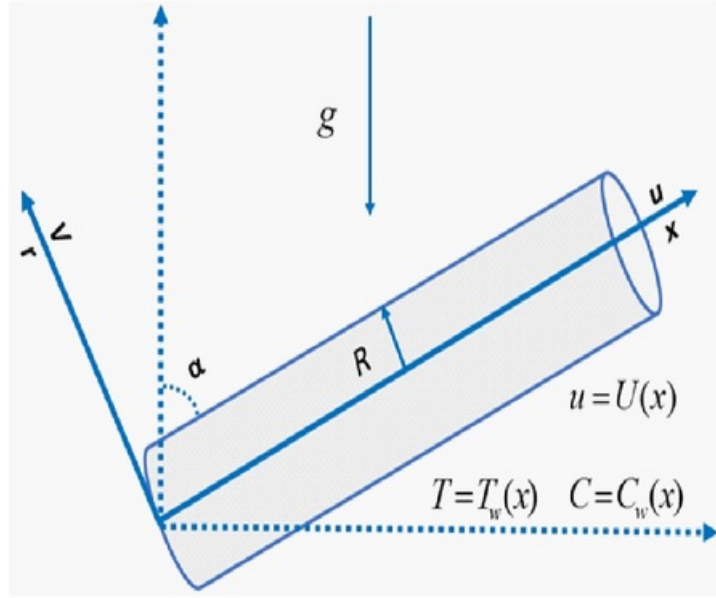


Figure 7-1: Fig. 7.1. Physical configuration and coordinate system.

number. The current analysis is validated by comparative analysis with previously published work.

7.2 Formulation

7.2.1 Flow analysis

Consider two dimensional and steady incompressible boundary layer flow of Eyring-Powell fluid by an inclined stretching cylinder. Flow analysis is taken with double stratification in the presence of mixed convection and heat generation/absorption. Temperature and concentration at the surface of cylinder are assumed at higher than the ambient fluid. The boundary layer approximation give rise to following expression:

$$\frac{\partial (ru)}{\partial x} + \frac{\partial (rv)}{\partial r} = 0, \quad (7.1)$$

$$u \frac{\partial u}{\partial x} + v \frac{\partial u}{\partial r} = \left(\nu + \frac{1}{\beta \rho c} \right) \frac{\partial^2 u}{\partial r^2} - \frac{1}{2\beta c^3 \rho} \left(\frac{\partial u}{\partial r} \right)^2 \frac{\partial^2 u}{\partial r^2} + \frac{1}{r} \left(\nu + \frac{1}{\beta \rho c} \right) \frac{\partial u}{\partial r} - \frac{1}{6\beta r \rho c^3} \left(\frac{\partial u}{\partial r} \right)^3 + g\beta_T (T - T_\infty) + g\beta_c (C - C_\infty) \cos \alpha. \quad (7.2)$$

The axial direction of cylinder is supposed as x - axis and r - axis is perpendicular to it. In the above expressions, the velocity components u and v are in the x and r direction respectively. Here ρ is the fluid density, ν is the kinematic viscosity, β_T is the coefficient of thermal expansion, β_c is the coefficient of concentration expansion and α is the inclination of cylinder with x - axis respectively. Note that β and c are the Eyring-Powell fluid parameters. The corresponding boundary conditions are

$$u(x, r) = U(x) = \frac{U_o}{L} x, \quad v(x, r) = 0, \quad \text{at } r = R, \quad \text{and } u(x, r) \rightarrow 0, \quad \text{as } r \rightarrow \infty, \quad (7.3)$$

Stream function satisfying continuity Eq. (7.1) is defined by the definition

$$u = \frac{1}{r} \left(\frac{\partial \psi}{\partial r} \right), \quad v = -\frac{1}{r} \left(\frac{\partial \psi}{\partial x} \right). \quad (7.4)$$

To trace out the solution of Eq. (7.2) under boundary conditions Eq. (7.3) we used following transformations

$$\eta = \frac{r^2 - R^2}{2R} \left(\frac{U}{\nu L} \right)^{\frac{1}{2}}, \quad \psi = \left(\frac{U_0 \nu}{L} x^2 \right)^{\frac{1}{2}} R f(\eta), \quad u = \frac{U_0}{L} x f'(\eta), \quad v = -\frac{R}{r} \sqrt{\frac{U_0 \nu}{L}} f(\eta), \quad (7.5)$$

where U_0 is the free stream velocity, L is the reference length, $f'(\eta)$ represents dimensionless variable and prime denotes differentiation with respect to η (similarity variable) that is the velocity of fluid past an inclined stretching cylinder having radius R . Incorporating Eqs. (7.4) – (7.5) into Eq. (7.2), we get

$$(1 + 2K\eta)(1 + M)f''' + ff'' - (f')^2 + 2K(1 + M)f'' - \frac{4}{3}\lambda MK(1 + 2K\eta)(f'')^3$$

$$-M\lambda(1+2K\eta)^2(f'')^2 f''' + \lambda_m(\theta + N\phi)\cos\alpha = 0, \quad (7.6)$$

with

$$f'(0) = 1, \quad f(0) = 0, \quad f'(\infty) \rightarrow 0 \quad (7.7)$$

Here K , M , λ , λ_m , and N denote curvature parameter, fluid parameters, mixed convection parameter and ratio of thermal to concentration buoyancy forces respectively. These definitions are

$$K = \frac{1}{R} \sqrt{\frac{\nu}{a}}, \quad M = \frac{1}{\mu\beta c}, \quad \lambda = \frac{ax^3}{2c^2\nu}, \quad \lambda_m = \frac{Gr}{Re_x^2}, \quad N = \frac{Gr}{Gr^*} \quad \text{and} \quad a = \frac{U_0}{L} \quad (7.8)$$

where Gr and Gr^* denotes Grashof number due to temperature and concentration respectively as

$$Gr^* = \frac{g\beta_T(T_w - T_0)x^3}{\nu^2}, \quad Gr = \frac{g\beta_C(C_w - C_0)x^3}{\nu^2} \quad (7.9)$$

The skin friction coefficient at the surface of cylinder is considered as

$$C_f = \frac{\tau_w}{\rho \frac{U^2}{2}}, \quad (7.10)$$

$$\tau_w = \left[\mu \left(\frac{\partial u}{\partial r} \right) + \frac{1}{\beta c} \frac{\partial u}{\partial r} - \frac{1}{6\beta c^3} \left(\frac{\partial u}{\partial r} \right)^3 \right]_{r=R}, \quad (7.11)$$

where μ denotes dynamic viscosity of fluid and τ is the shear stress. The dimensionless form of skin friction coefficient is given by

$$C_f Re_x^{1/2} = 2(1+M)f''(0) - \frac{2M\lambda}{3}[f''(0)]^3, \quad (7.12)$$

with $Re_x = U_0^2 x / \nu L$ is local Reynolds number.

7.2.2 Heat and mass transfer analysis

Heat transfer analysis is carried out in the presence of heat generation/absorption. The destruction of fluctuation velocity gradients by action of viscous stresses in a laminar boundary layer flow of Eyring-Powell fluid is assumed small so the viscous dissipation is neglected. Thun under boundary layer approximation, the energy and concentration equations take the forms

$$u \frac{\partial T}{\partial x} + v \frac{\partial T}{\partial r} = \frac{K}{\rho C_P} \frac{\partial}{\partial r} \left(r \frac{\partial T}{\partial r} \right) + \frac{Q_0(T - T_\infty)}{\rho C_P}. \quad (7.13)$$

$$u \frac{\partial C}{\partial x} + v \frac{\partial C}{\partial r} = \frac{D}{r} \frac{\partial}{\partial r} \left(r \frac{\partial C}{\partial r} \right). \quad (7.14)$$

where K denotes thermal conductivity, C_P is specific heat at constant pressure, D the mass diffusivity and Q_0 the heat generation and absorption coefficient. Temperature and concentration boundary conditions for the fluid flow problem are

$$\begin{aligned} T(x, r) &= T_w(x) = T_0 + \frac{b}{L}x, \quad C(x, r) = C_w(x) = C_0 + d\frac{x}{L} \text{ at } r = R, \\ T(x, r) &\rightarrow T_\infty(x) = T_0 + \frac{c}{L}x, \quad C(x, r) \rightarrow C_\infty(x) = C_0 + e\frac{x}{L}, \text{ as } r \rightarrow \infty, \end{aligned} \quad (7.15)$$

where $T_w(x)$, $C_w(x)$, $T_\infty(x)$, $C_\infty(x)$, T_0 , C_0 denotes prescribed surface temperature, surface concentration, variable ambient temperature, variable ambient concentration, reference temperature and reference concentration respectively. Here b , c , d and e are positive constants. To find out the dimensionless forms of Eqs. (7.13) and Eq. (7.14) under boundary conditions i-e Eq. (7.15), we define

$$\eta = \frac{r^2 - R^2}{2R} \left(\frac{U_0}{\nu L} \right)^{\frac{1}{2}}, \quad \theta(\eta) = \frac{T - T_\infty}{T_w - T_0}, \quad \phi(\eta) = \frac{C - C_\infty}{C_w - C_0}, \quad (7.16)$$

After substituting Eq. (7.16) in Eqs. (7.13) – (7.14), the dimensionless form of energy and concentration equations is given by

$$(1 + 2K\eta)\theta'' + 2K\theta' + \text{Pr} \left(f\theta' - f'\theta - f'\epsilon_1 + \delta_H\theta \right) = 0. \quad (7.17)$$

$$(1 + 2K\eta)\phi'' + 2K\phi' + Sc \left(f\phi' - f'\phi - f'\epsilon_2 \right) = 0. \quad (7.18)$$

subject to the transformed boundary conditions

$$\theta = 1 - \epsilon_1, \quad \phi = 1 - \epsilon_2 \quad \text{at} \quad \eta = 0, \quad \theta \rightarrow 0, \quad \phi \rightarrow 0, \quad \text{as} \quad \eta \rightarrow \infty \quad (7.19)$$

where Pr , ϵ_1 , δ_H , Sc and ϵ_2 denote Prandtl number, thermal stratification parameter, heat generation/absorption parameter, Schmidt number and solutal stratification parameter respectively. These have definitions

$$\text{Pr} = \frac{\rho C_P}{K}, \quad \epsilon_1 = \frac{c}{b}, \quad \delta_H = \frac{LQ_0}{U_0 \rho C_P}, \quad Sc = \frac{\nu}{D}, \quad \epsilon_2 = \frac{e}{d} \quad (7.20)$$

103

The local Nusselt and Sherwood numbers are defined as

$$Nu_x = \frac{xq_w}{k(T_w - T_\infty)}, \quad q_w = -k \left(\frac{\partial T}{\partial r} \right)_{r=R} \quad (7.21)$$

$$Sh = \frac{-xj_w}{D(C_w - C_0)}, \quad j_w = -D \left(\frac{\partial C}{\partial r} \right)_{r=R} \quad (7.22)$$

in dimensionless form, these quantities are

$$Nu_x \text{Re}_x^{-1/2} = -\theta'(0), \quad Sh \text{Re}_x^{-1/2} = -\phi'(0), \quad (7.23)$$

7.3 Results and discussion

7.3.1 Numerical solution

The systems of governing coupled non-linear ordinary differential equations i.e Eqs. (7.6), (7.17) and (7.18) subject to boundary conditions (7.7) and (7.19) are solved by employing shooting method with the aid of fifth order Runge-Kutta scheme. Firstly, reduction has been done in a

system of seven first order simultaneous equations by letting

$$\begin{aligned} Z_2 &= f', \\ Z_3 &= Z_2' = f'', \\ Z_5 &= \theta', \\ Z_6 &= \phi'. \end{aligned}$$

Then the equivalent form of Eqs. (7.6), (7.17) and (7.18) under new variables is given by:

$$\begin{aligned} Z_1' &= Z_2, \\ Z_2' &= Z_3, \\ Z_3' &= \frac{(Z_2)^2 - Z_1 Z_3 - 2K(1+M)Z_3 + \frac{4}{3}\lambda MK(1+2K\eta)Z_3^3 - \lambda_m(Z_4 + NZ_6)\cos\alpha}{(1+2K\eta)(1+M) - M\lambda(1+2K\eta)^2 Z_3^2}, \\ Z_4' &= Z_5, \\ Z_5' &= \frac{\text{Pr}(Z_2 Z_4 + \epsilon_1 Z_2 - Z_1 Z_5 - \delta_H Z_4) - 2K Z_5}{1+2K\eta}, \\ Z_6' &= Z_7, \\ Z_7' &= \frac{\text{Sc}(Z_2 Z_6 + \epsilon_2 Z_1 - Z_1 Z_7) - 2K Z_7}{1+2K\eta}. \end{aligned} \tag{7.24}$$

The corresponding boundary conditions in new variables are given as follows

$$\begin{aligned} 123 \\ Z_1(0) &= 0, \\ Z_2(0) &= 1, \\ Z_3(0) &= \text{unknown}, \\ Z_4(0) &= 1 - \epsilon_1, \\ Z_5(0) &= \text{unknown}, \\ Z_6(0) &= 1 - \epsilon_2, \\ Z_7(0) &= \text{unknown}. \end{aligned} \tag{7.25}$$

In order to integrate Eq. (7.25) as an initial value problem, we required values for $Z_3(0)$ i.e. $f''(0)$, $Z_5(0)$ i.e. $\theta'(0)$ and $Z_7(0)$ implies $\phi'(0)$. The initial conditions $Z_3(0)$, $Z_5(0)$, $Z_7(0)$ are not given but we have additional boundary conditions

$$\begin{aligned} Z_2(\infty) &= 0, \\ Z_4(\infty) &= 0, \\ Z_6(\infty) &= 0. \end{aligned} \quad (7.26)$$

2

K	Pr	M	$\frac{1}{2}C_f Re_x^{1/2} = (1+M)f''(0) - \frac{M\lambda}{3}[f''(0)]^3$
0.1	1.1	0.1	-0.9809
0.2	-	-	-1.0254
0.3	-	-	-1.0694
0.1	1.1	0.1	-0.9809
-	1.2	-	-0.9825
-	1.3	-	-0.9839
0.1	1.1	0.1	-0.9809
-	-	0.2	-1.0268
-	-	0.3	-1.0779

By choosing favourable guessed values of $f''(0)$, $\theta'(0)$ and $\phi'(0)$ the integration of system of first order differential equations are carried out in such a way that the boundary conditions given in Eq. (7.27) holds absolutely. The step size $\Delta\eta = 0.05$ is used to obtain the numerical solution with four decimal accuracy as convergence criteria.

Tables 7.1 and 7.2 are constructed to indicate the influence of embedded physical parameters symbolically, K , Pr , M , λ , Sc , ϵ_1 , ϵ_2 on skin friction coefficient. Adopted parametric values are mixed convection parameter $\lambda_m = 0.1$, ratio of buoyancy forces $N = 0.1$, inclination angle $\alpha = 30^\circ$ and heat generation/absorption parameter $\delta_H = 0.1$. It is revealed that skin friction coefficient increases (in absolute sense) for higher values of curvature parameter K , thermal stratification parameter ϵ_1 , solutal stratification parameter ϵ_2 fluid parameter M , Prandtl

number Pr and Schmidt number Sc . Skin friction coefficient shows declined effect on fluid parameters λ .

Table – 7.2 : Numerical values of skin friction coefficient for λ , Sc , ϵ_1 and ϵ_2 .				
λ	Sc	ϵ_1	ϵ_2	$\frac{1}{2}C_f Re_x^{1/2} = (1 + M)f''(0) - \frac{M\lambda}{3}[f''(0)]^3$
0.1	1.1	0.1	0.1	-0.9809
0.2	-	-	-	-0.9760
0.3	-	-	-	-0.9738
0.1	1.1	0.1	0.1	-0.9809
-	1.2	-	-	-0.9850
-	1.3	-	-	-0.9893
0.1	1.1	0.1	0.1	-0.9809
-	-	0.2	-	-0.9868
-	-	0.3	-	-0.9937
0.1	0.2	0.1	0.1	-0.9809
-	-	-	0.2	-0.9887
-	-	-	0.3	-0.9995

Tables 7.3–7.4 show the influence of different physical parameters on heat and mass transfer rate for fluid parameters $\lambda = 0.1$ and $M = 0.1$, mixed convection parameter $\lambda_m = 0.1$, ratio of buoyancy forces $N = 0.1$, inclination angle $\alpha = 30^\circ$ and heat generation/absorption parameter $\delta_H = 0.1$. Particularly, Table 7.3 shows the variation of heat transfer rate against frequent values of curvature parameter K , Prandtl number Pr and thermal stratification parameter ϵ_1 . Table 7.4 shows the rate variation of mass transfer for different values of curvature parameter K , Schmidt number Sc and solutal stratification parameter ϵ_2 . It is examined that the heat and mass transfer rate increases for larger values of curvature parameter, Prandtl number Pr and Schmidt number Sc , respectively. Heat and mass transfer rates exhibit decreasing behavior towards thermal stratification parameter and solutal stratification parameter respectively. By having Eqs. (7.6) and (7.17) the flow problem can be identified by Ishak and Nazar [55]. Furthermore, in the absence of curvature parameter (i-e $K = 0$)

Table – 7.3 : Temperature gradient at the surface of cylinder
for various values of K , Pr and ϵ_1 .

K	Pr	ϵ_1	$-\theta'(0)$
0.1	1.1	0.1	1.0983
0.2	-	-	1.1306
0.3	-	-	1.1632
0.1	1.1	0.1	1.0983
-	1.2	-	1.1553
-	1.3	-	1.2101
0.1	1.1	0.1	1.0983
-	-	0.2	1.0567
-	-	0.3	1.0144

Table – 7.4 : Mass transfer rate at outer surface of cylinder
for different values of K , Sc and ϵ_2 .

K	Sc	ϵ_2	$-\phi'(0)$
0.1	0.2	0.1	0.4500
0.2	-	-	0.5020
0.3	-	-	0.5512
0.1	0.2	0.1	0.4500
-	0.3	-	0.5220
-	0.4	-	0.6068
0.1	0.2	0.1	0.4500
-	-	0.2	0.4013
-	-	0.3	0.3711

For $M = 0$, $\lambda = 0$, $\lambda_m = 0$, $\alpha = 0^\circ$, $\epsilon_1 = 0$, and $\delta_H = 0$, Eqs. (7.6) and (7.17) reduce to the flow problem given by Grubka and Bobba [56]. Table 7.5 is constructed to compare the heat transfer rate for various values of Prandtl number Pr in a limited sense. An excellent agreement has been found which leads to conformity of present work.

Table – 7.5 : Comparision of heat transfer rate for different values of Prandtl number Pr			
Pr	Grubka and Bobba [56]	Ishak and Nazar [55]	Present study
0.72	0.8086	0.8086313	0.8089
1.00	1.0000	1.0000000	1.0000
3.00	1.9237	1.9236825	1.9239
10.0	3.7207	3.7206739	3.7208

7.3.2 Velocity profiles

Figs. 7.2 – 7.8 illustrate the effects of flow controlling parameters on non-dimensional velocity profiles. Fig. 7.2 shows that an increase in thermal stratification parameter ϵ_1 leads to decrease in velocity profile. This effect is due to drop of convective potential between surface of cylinder and ambient temperature. Fig. 7.3 identifies that an increase in mixed convection parameter λ_m yields an increase in fluid velocity. Physically, this is due to enhancement of thermal buoyancy force. Higher values of mixed convection parameter λ_m lead to an increase in velocity within a boundary layer. The behaviour of an inclination α on velocity is depicted in Fig. 7.4. It is noticed that for higher values of an inclination α the velocity profile declines. Because by increasing an inclination α relative to x -axis the influence of gravity is reduced which results decline in velocity within a boundary layer. Fig. 7.5 illustrates that for larger values of curvature parameter K the radius of cylinder decreases and fluids motion accelerates. This is due to reduction of contact surface area of cylinder with fluid which offers less resistance to fluid flow. So increase in curvature parameter K causes increase in velocity profile within the boundary layer. The effect of solutal stratification parameter ϵ_2 on velocity is displayed in Fig. 7.6. It is observed that the fluid velocity decreases within boundary layer for the increasing values of solutal stratification parameter ϵ_2 . Fig. 7.7 evidents that the velocity profile increases against increasing value of fluid parameter M . Because fluid parameter M has inverse relation with viscosity so higher values of fluid parameter M brings fluid to be less viscous which results increase in rate of deformation. Fig. 7.8 is sketched to examine the effects of ratio of buoyancy forces N on velocity profile. As N is the ratio of concentration to the thermal buoyancy forces, so larger values of buoyancy forces N reflects dominancy in concentration buoyancy force which yield an increase in velocity distribution within a boundary layer.

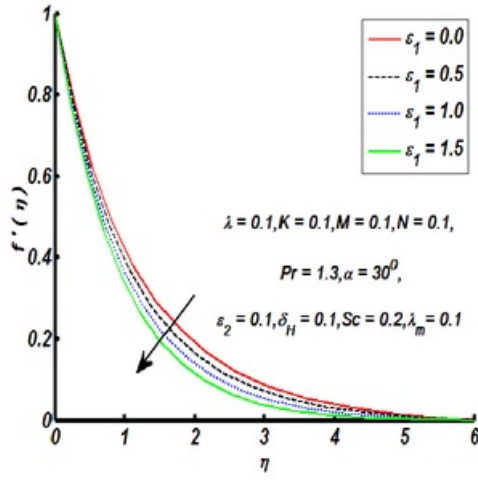


Fig. 7.2. Effect of thermal stratification parameter ϵ_1 on velocity profile.

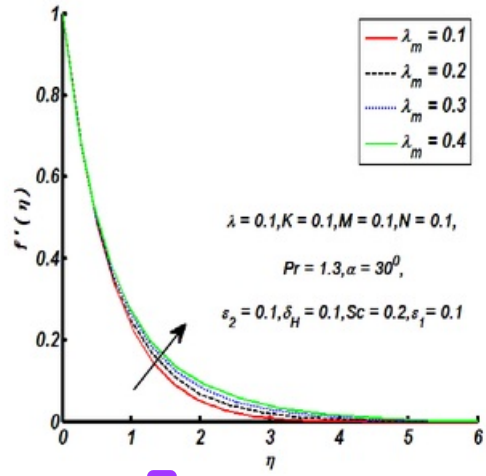


Fig. 7.3. Effect of mixed convection parameter on velocity profile.

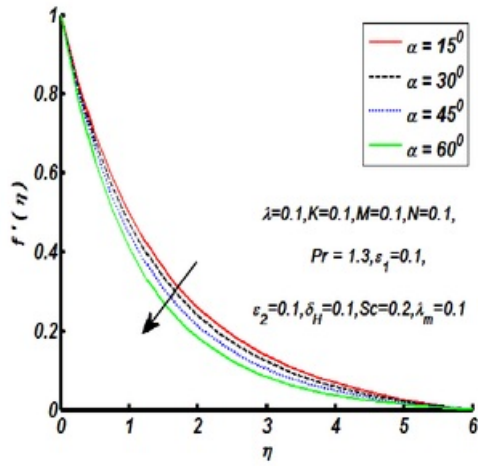


Fig. 7.4. Effect of an inclination on velocity profile.

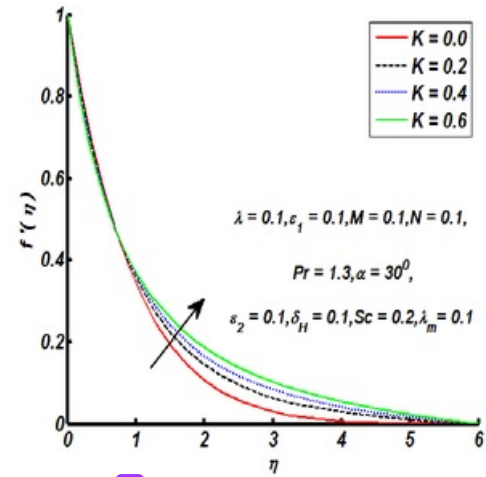


Fig. 7.5. Effect of curvature parameter K on velocity profile.

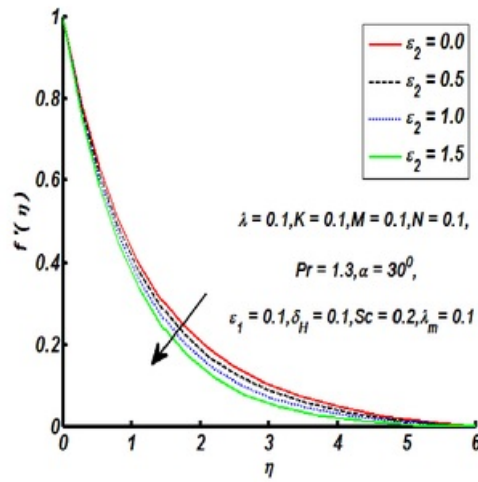


Fig. 7.6. Effect of solutal stratification parameter on velocity profile.

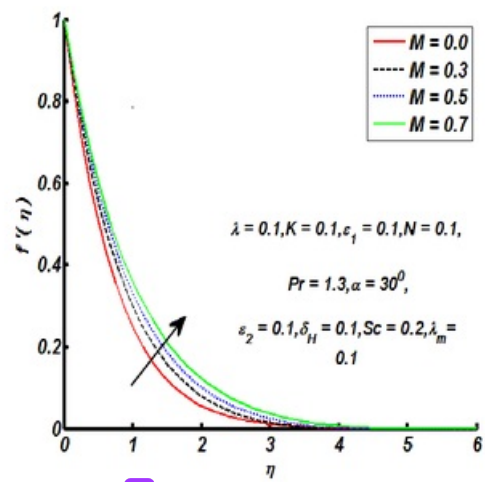


Fig. 7.7. Effect of fluid parameter M on velocity profile.

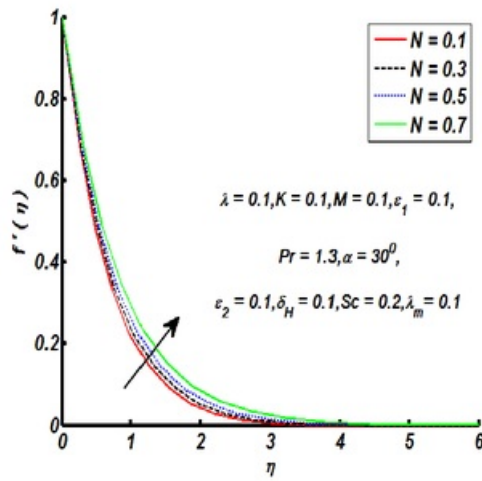


Fig. 7.8. Effect of ratio of buoyancy forces N on velocity profile.

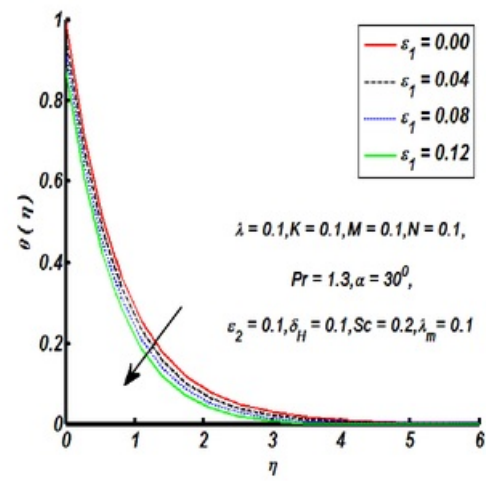


Fig. 7.9. Effect of thermal stratification parameter on temperature profile.

7.3.3 Temperature profile

Figs. 7.9–7.14 reflect the impacts of different physical flow parameters on temperature profiles. Influence of thermal stratification parameter ϵ_1 on temperature profile is given by Fig. 7.9. It is prominent from figure that the temperature distribution decreases for increasing values of thermal stratification parameter ϵ_1 . This outcome is due to declined in temperature difference between surface of cylinder and ambient fluid. Hence temperature profile decreases within thermal boundary layer. Fig. 7.10 provides the influence of an inclination α against temperature distribution. It is noticed that an increase in inclination α shows enhancement in temperature within a boundary layer. This fact is due to gravity effect. For larger values of an inclination α the gravity effect reduces. It shows decrease in rate of heat transfer. Therefore temperature distribution increases. Fig. 7.11 elaborates the influence of heat generation/heat absorption parameter δ_H on temperature distribution. It is explored that increase in heat generation/heat absorption parameter δ_H causes increase in temperature of fluid. Here significant heat is produced during heat generation phenomena which results an increase in temperature distribution. Fig. 7.12 illustrates that the temperature distribution increases due to larger curvature parameter K . Temperature is stated as an average kinetic energy so, when we increase curvature parameter K of cylinder, velocity of the fluid increases which results increase in kinetic energy and due to which temperature increases. Note that temperature profile decreases adjacent to the surface of cylinder and it increases away from it. It is clearly seen that an increase in intensity of buoyancy forces shows an increase in temperature of fluid. Fig. 7.13 indicates that the temperature distribution increases for higher values of solutal stratification parameter ϵ_2 . Fig. 7.14 presents the influence of Prandtl number Pr on temperature profile. Prandtl number Pr has inverse relation towards thermal conductivity, fluid with higher Prandtl number Pr . Hence an increase in Prandtl number Pr causes a strong reduction in temperature of the fluid which results thinner thermal boundary layer. Sometimes we may have overshoot in the thermal boundary layer due to higher thermal conductivity. That effect can be controlled by introducing heat sink which helps to moderate the temperature.

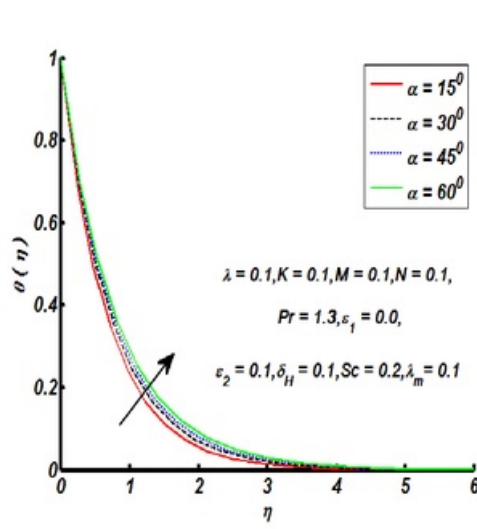


Fig. 7.10. Effect of an inclination on temperature profile.

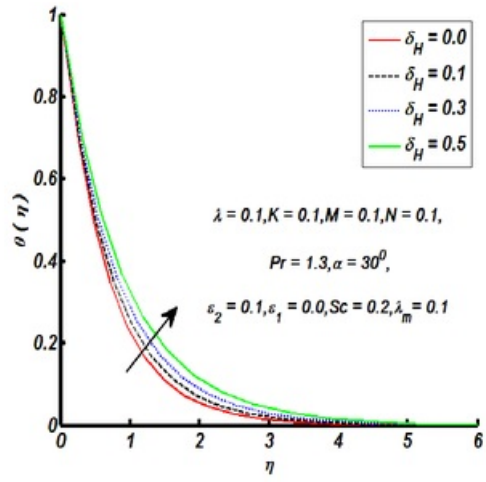


Fig. 7.11. Effect of heat generation/absorption parameter on temperature profile

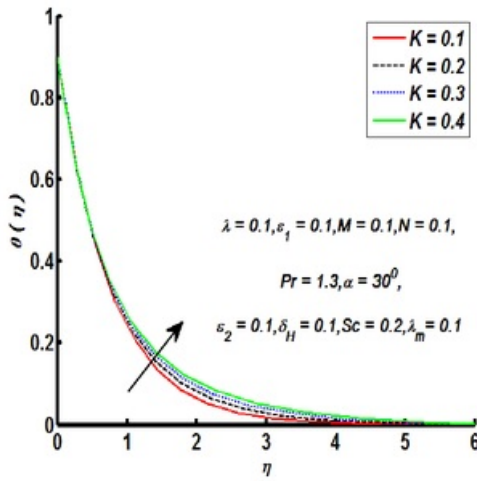


Fig. 7.12. Effect of curvature parameter K on temperature profile.

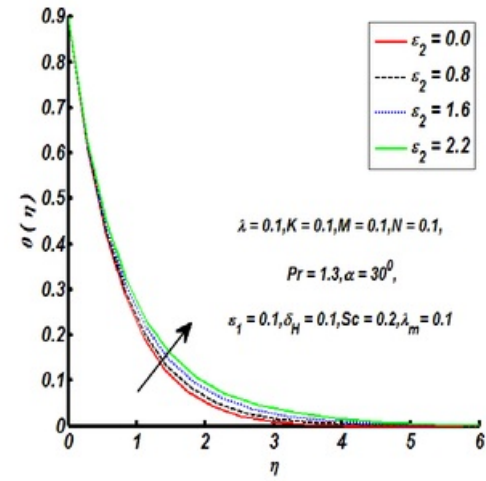


Fig. 7.13. Effect of solutal stratification parameter on temperature profile.

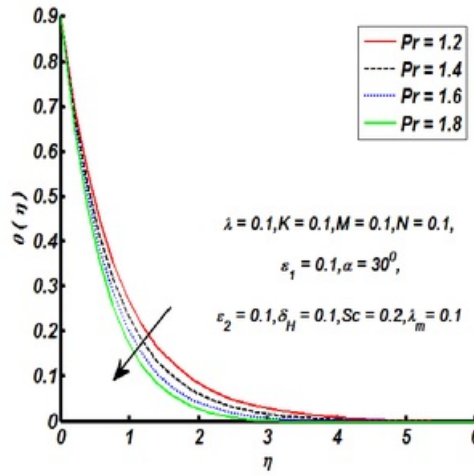


Fig. 7.14. Effect of Prandtl number Pr on temperature profile.

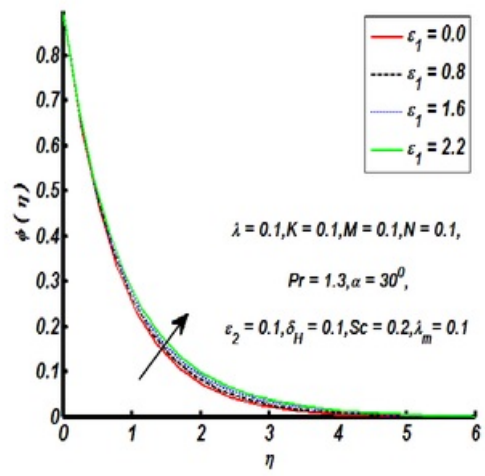


Fig. 7.15. Effect of thermal stratification parameter on concentration profile.

7.3.4 Concentration profile

Figs. 7.15 – 7.20 include the effects of several involved parameters over concentration profile. Fig. 7.15 demonstrates the impact of thermal stratification parameter ϵ_1 on concentration profile. An increase in thermal parameter ϵ_1 brings inciting in fluid concentration across the surface of cylinder. From Fig. 7.16, it is witnessed that the concentration boundary layer decreases by increasing Schmidt number Sc . Since this effect is similar to Pr verses thermal boundary layer. As Sc has inverse proportional behavior towards mass diffusivity. Thus higher values of Schmidt number Sc bring thinning in the concentration boundary layer. As a result concentration distribution decreases. Influence of solutal stratification parameter ϵ_2 is described through Fig. 7.17 over concentration profile. It is clear that concentration, the boundary layer thickness decreases for higher values of solutal stratification coefficient ϵ_2 . Influence of an inclination α and mixed convection parameter λ_m on skin friction coefficient for both plate and cylinder is sketched in Fig. 7.18. It is acknowledged that for increasing values of an inclination α the skin friction coefficient increases whereas it shows opposite effect for mixed convection parameter λ_m . Further, the magnitude of skin friction coefficient is higher for cylinder when compared with plate. Fig. 7.19 witnesses that mass transfer rate decreases for larger values

of an inclination α and heat generation/absorption parameter δ_H . It is also noticed that the strength of mass transfer rate is slightly larger for cylinder than plate. Fig. 7.20 is constructed to examine the behaviour of mixed convection λ_m and ratio of thermal to concentration buoyancy forces N on mass transfer rate. It is analyzed that for larger values of both mixed convection parameter λ_m and ratio of buoyancy forces N , the mass transfer rate increases. The magnitude of mass transfer rate for cylinder is more when compared to plate.

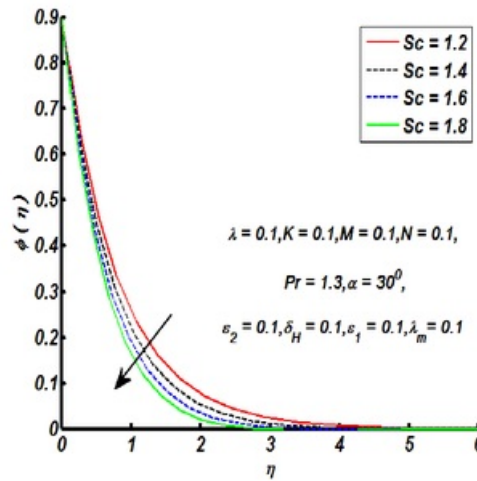


Fig. 7.16. Effect of Schmidt number Sc on concentration profile.

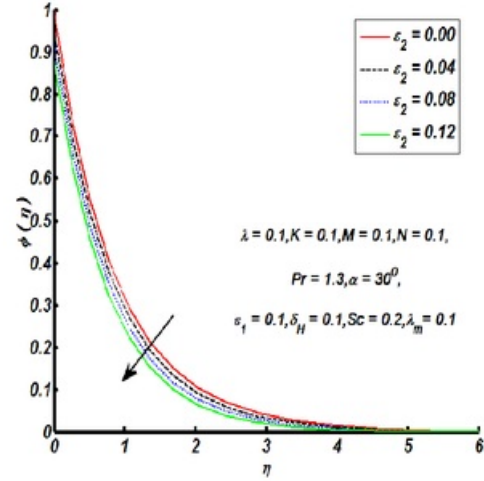


Fig. 7.17. Effect of solutal stratification parameter on concentration profile.

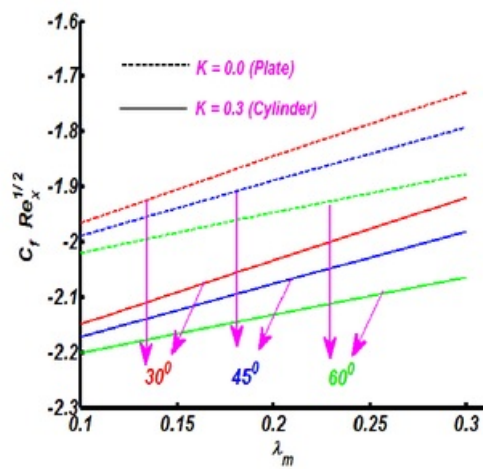


Fig. 7.18. Effect of an inclination and mixed convection on skin friction.

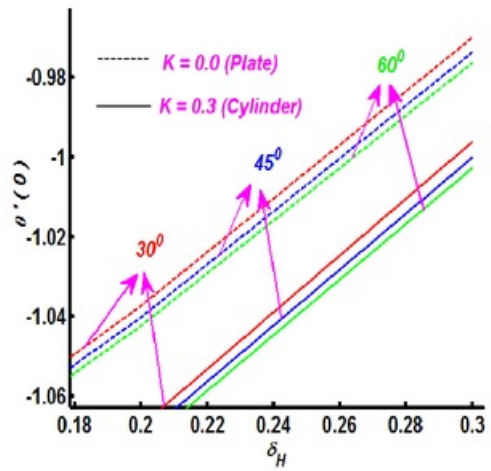


Fig. 7.19. Effect of an inclination and heat generation parameter on local Nusselt number.

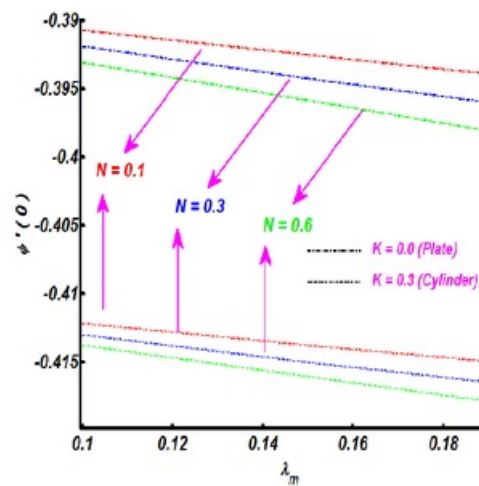


Fig. 7.20. Effect of mixed convection and ratio of buoyancy forces N on local Sherwood number.

7.4 Conclusion

Double stratified mixed convection boundary layer flow of Eyring-Powell fluid ⁶¹ induced by an inclined stretching cylinder is reported. Flow analysis is carried out with heat generation process. The findings of present study are listed as follows:

- The fluid velocity increases significantly for larger values of curvature parameter K , fluid parameter M , mixed convection parameter λ_m and ratio of buoyancy forces N . However velocity profile shows opposite variation for thermal stratification parameter ϵ_1 , solutal stratification parameter ϵ_2 and an inclination α .
- The fluid temperature is increasing function of solutal stratification parameter ϵ_2 , curvature parameter K , an inclination α and heat generation/absorption parameter δ_H . Temperature decays for thermal stratification parameter ϵ_1 and Prandtl number Pr .
- The concentration profile increases for increasing values of thermal stratification parameter ϵ_1 while it decreases for solutal stratification parameter ϵ_2 and Schmidt number Sc .
- Skin friction coefficient expressively enriches for cylinder in comparison to plate regarding an inclination α and it reduces for mixed convection parameter λ_m .
- Higher values of an inclination α and heat generation/absorption parameter δ_H shows reduction in heat transfer rate.
- ²⁷ • Mass transfer rate considerably increases for both mixed convection parameter λ_m and ratio of buoyancy forces N .

Chapter 8

8 Boundary layer flow of second grade fluid past a vertical exponentially stretching cylinder

8.1 Introduction

In this chapter we obtained the similarity solution for the boundary layer flow of a second grade fluid past a vertical cylinder stretching exponentially along its radial direction. Heat transfer is also analyzed. The resulting boundary layer problems are solved. The obtained system of equations subject to the boundary conditions are solved with the help of homotopy analysis method (HAM). The effects of the different parameters including Reynolds numbers, Prandtl numbers and the natural convection parameter are presented through graphs. The skin friction coefficient and Nusselt numbers are studied for different parameters.

8.2 Mathematical formulation

Consider the problem of natural convection boundary layer flow of a second grade fluid flowing over a vertical circular cylinder of radius a . The cylinder is assumed to be stretched exponentially with velocity U_w . The temperature at the surface of the cylinder is T_w and the uniform ambient temperature is taken as T_∞ such that $T_w - T_\infty > 0$ in case of the assisting flow, while

$T_w - T_\infty < 0$ for opposing flow, respectively. Under these assumptions the boundary layer equations of motion and heat transfer are

$$u_r + \frac{u}{r} + w_z = 0, \quad (8.1)$$

$$uw_r + ww_z = \nu(w_{rr} + \frac{1}{r}w_r) + \frac{\alpha_1}{\rho}[uw_{rrr} + ww_{rrz} + w_{rr}w_z - w_ru_{rr} + \frac{1}{r}(uw_{rr} + ww_{rz} + w_rw_z - w_ru_z)] + g\beta(T - T_\infty), \quad (8.2)$$

$$uT_r + wT_z = \alpha(T_{rr} + \frac{1}{r}T_r), \quad (8.3)$$

where the velocity components along the (r, z) axes are (u, w) , ρ is density, ν is the kinematic viscosity, p is pressure, g is the gravitational acceleration along the z - direction, β is the coefficient of thermal expansion, T is the temperature and α is the thermal diffusivity. The corresponding boundary conditions for the problem are

$$u(a, z) = 0, \quad w(a, z) = U_w \quad w(r, z) \longrightarrow 0 \text{ as } r \longrightarrow \infty, \quad (8.4)$$

$$T(a, z) = T_w(z), \quad T(r, z) \longrightarrow T_\infty \text{ as } r \longrightarrow \infty, \quad (8.5)$$

where $U_w = 2ake^{z/a}$ is the fluid velocity at the surface of the cylinder.

8.3 Solution of the problem

By considering the following similarity transformations:

$$u = -\frac{1}{2}U_w \frac{f(\eta)}{\sqrt{\eta}}, \quad w = U_w f'(\eta), \quad (8.6)$$

$$\theta = \frac{T - T_\infty}{T_w - T_\infty}, \quad \eta = \frac{r^2}{a^2}, \quad (8.7)$$

The Eqs. (8.1) to (8.3) take the form

$$\begin{aligned} \eta f''' + f'' + \text{Re}(ff'' - f'^2) - 2A(\eta f f^{iv} + 2f f''') \\ - 2\eta f' f''' - \eta f''^2 - 2f' f'' + \text{Re } \lambda \theta = 0, \end{aligned} \quad (8.8)$$

$$\eta\theta'' + \theta' + \frac{1}{2} \text{Re Pr}(f\theta' - f'\theta) = 0, \quad (8.9)$$

in which $\lambda = g\beta a(T_w - T_\infty)/U_w^2$ is the natural convection parameter, $\text{Pr} = \nu/\alpha$ is the Prandtl number, $A = \alpha_1 U_w / 2a\nu\rho$ is second grade fluid parameter and $\text{Re} = aU_w/4\nu$ is the Reynolds number. The boundary conditions in nondimensional form become

$$f(1) = 0, \quad f'(1) = 1, \quad \theta(1) = 1, \quad (8.10)$$

$$f' \rightarrow 0, \quad \theta \rightarrow 0, \quad \text{as } \eta \rightarrow \infty. \quad (8.11)$$

The important physical quantities such as the shear stress at the surface τ_w , the skin friction coefficient c_f , the heat flux at the surface of the cylinder q_w and the local Nusselt number Nu_z are

$$\tau_w = \tau_{rz}|_{r=a}, \quad q_w = -k\tau_r|_{r=a}, \quad (8.12)$$

$$c_f = \frac{\tau_w}{\rho U_w^2}, \quad Nu_z = \frac{ae^{z/a}q_w}{k(T_w - T_\infty)} \quad (8.13)$$

8.4 Homotopy solution

In order to develop solutions we employ the homotopic technique suggested by Liao [58]. The HAM is preferred due to the following facts. (i) The HAM does not require any small/large parameters in the problem. (ii) It gives us a way to verify the convergence of the developed series solutions. (iii) It is useful in providing incredible flexibility in the developing equation type of linear functions of solutions.

The initial guesses and linear operator are:

$$f_0(\eta) = (1 - e^{1-\eta}), \quad \theta_0(\eta) = \exp(1 - \eta), \quad (8.14)$$

and linear operators satisfying the properties

$$\mathcal{L}_f = f''' - f', \quad \mathcal{L}_\theta = \theta'' + \theta', \quad (8.15)$$

$$\mathcal{L}_f(C_1 + C_2e^\eta + C_3e^{-\eta}) = 0, \quad \mathcal{L}_g(C_4 + C_5e^{-\eta}) = 0, \quad (8.16)$$

where C_i ($i = 1 - 5$) indicate the arbitrary constants.

8.4.1 Zeroth-order deformation problems

The corresponding problems at the zeroth order are presented in the following forms:

$$(1 - q) \mathcal{L}_f [\hat{f}(\eta; q) - f_0(\eta)] = q \hbar_f \mathcal{N}_f [\hat{f}(\eta; q)], \quad (8.17)$$

$$(1 - q) \mathcal{L}_\theta [\hat{\theta}(\eta; q) - \theta_0(\eta)] = q \hbar_\theta \mathcal{N}_\theta [\hat{f}(\eta; q), \hat{\theta}(\eta, q)], \quad (8.18)$$

$$\begin{aligned} \hat{f}(1; q) &= 0, \quad \hat{f}'(1; q) = 1, \quad \hat{\theta}(0, q) = 1, \\ \hat{\theta}(\infty, q) &= 0, \quad \hat{f}'(\infty; q) = 0. \end{aligned} \quad (8.19)$$

$$\begin{aligned} \mathcal{N}_f[\hat{f}(\eta, q), \hat{\theta}(\eta, q)] &= \eta \frac{\partial^3 \hat{f}(\eta, q)}{\partial \eta^3} + \frac{\partial^2 \hat{f}(\eta, q)}{\partial \eta^2} + \text{Re} \left(\hat{f}(\eta, q) \frac{\partial^2 \hat{f}(\eta, q)}{\partial \eta^2} - \left(\frac{\partial \hat{f}(\eta, q)}{\partial \eta} \right)^2 \right) - 2A \left(\eta \hat{f}(\eta, q) \frac{\partial^4 \hat{f}(\eta, q)}{\partial \eta^4} + 2\hat{f}(\eta, q) \frac{\partial^3 \hat{f}(\eta, q)}{\partial \eta^3} \right) \\ &\quad - 2\eta \frac{\partial \hat{f}(\eta, q)}{\partial \eta} \frac{\partial^3 \hat{f}(\eta, q)}{\partial \eta^3} - \eta \left(\frac{\partial^2 \hat{f}(\eta, q)}{\partial \eta^2} \right)^2 - 2 \frac{\partial \hat{f}(\eta, q)}{\partial \eta} \frac{\partial^2 \hat{f}(\eta, q)}{\partial \eta^2} + \text{Re} \lambda \hat{\theta}(\eta, q) \end{aligned} \quad (8.20)$$

$$\mathcal{N}_\theta[\hat{f}(\eta, q), \hat{\theta}(\eta, q)] = \eta \frac{\partial^2 \hat{\theta}(\eta, q)}{\partial \eta^2} + \frac{\partial \hat{\theta}(\eta, q)}{\partial \eta} + \frac{1}{2} \text{Re Pr} \left(\hat{f}(\eta, q) \frac{\partial \hat{\theta}(\eta, q)}{\partial \eta} - \frac{\partial \hat{f}(\eta, q)}{\partial \eta} \hat{\theta}(\eta, q) \right). \quad (8.21)$$

Here q is an embedding parameter, \hbar_f and \hbar_θ the non-zero auxiliary parameters and \mathcal{N}_f and \mathcal{N}_θ indicate the nonlinear operators.

8.4.2 mth-order deformation problems

$$\mathcal{L}_f [f_m(\eta) - \chi_m f_{m-1}(\eta)] = \hbar_f R_m^f(\eta), \quad (8.22)$$

$$\mathcal{L}_\theta [\theta_m(\eta) - \chi_m \theta_{m-1}(\eta)] = \hbar_\theta R_m^\theta(\eta), \quad (8.23)$$

$$\begin{aligned} f'_m(1) &= 0, \quad f_m(1) = 0, \quad \theta_m(1) = 0, \\ f'_m(\infty) &= 0, \quad \theta_m(\infty) = 0, \end{aligned} \quad (8.24)$$

$$R_m^f(\eta) = \eta f_{m-1}''' + f_{m-1}'' + \operatorname{Re} \sum_{k=0}^{m-1} (f_{m-1-k} f_k'' - f_{m-1-k}' f_k') - 2A \sum_{k=0}^{m-1} (\eta f_{m-1-k} f_k'''' + 2f_{m-1-k} f_k''') - 2\eta \sum_{k=0}^{m-1} (f_{m-1-k}' f_k''') - \eta \sum_{k=0}^{m-1} (f_{m-1-k}'' f_k'') - 2 \sum_{k=0}^{m-1} (f_{m-1-k}' f_k'') + \operatorname{Re} \lambda \theta_{m-1}', \quad (8.25)$$

$$R_j^\theta(\eta) = \eta \theta_{j-1}'' + \theta_{j-1}' + \frac{1}{2} \operatorname{Re} \operatorname{Pr} \sum_{k=0}^{m-1} (f_{m-1-k} \theta_k' - f_{m-1-k}' \theta_k). \quad (8.26)$$

$$\chi_m = \begin{cases} 0, & m \leq 1, \\ 1, & m > 1. \end{cases} \quad (8.27)$$

The general solutions (f_m, θ_m) consisting of special solutions (f_m^*, θ_m^*) are

$$f_m(\eta) = f_m^*(\eta) + C_1 + C_2 e^\eta + C_3 e^{-\eta}, \quad (8.28)$$

$$\theta_m(\eta) = \theta_m^*(\eta) + C_4 + C_5 e^{-\eta}, \quad (8.29)$$

in which the values of $C_i (i = 1 - 5)$ are

$$\begin{aligned} C_1 &= \left(-\frac{\partial f_m^*(\eta)}{\partial \eta} - f_m^*(\eta) \right)_{\eta=0}, \quad C_2 = 0, \quad C_3 = \frac{\partial f_m^*(\eta)}{\partial \eta}, \quad C_4 = -\theta_m^*(\eta), \\ C_5 &= 0. \end{aligned} \quad (8.30)$$

8.5 Discussion

In this section the homotopic solutions are analyzed for the effect of various parameters such as the Reynolds number Re , the second grade parameter A , the Prandtl number Pr and the natural convection parameter λ on the nondimensional velocity and temperature. Here *Fig.8.1* shows the effect of Prandtl number Pr on the velocity profile f' . From *Fig.8.1* it is observed that by increasing Prandtl number Pr the velocity profile decreases. *Fig.8.2* shows the influence of the natural convection parameter λ on the velocity profile f' . Clearly when natural convection parameter λ increases then velocity profile also increases. That is, the natural convection parameter λ is directly proportional to the velocity profile f' . Similar characteristics are observed for second grade fluid parameter A in the *Figs. 8.3* and *8.4*. By increasing the value of Reynold number Re the velocity profile decreases. In *Fig.8.5* the h-curves of velocity profile for different

values of Reynold number are displayed when $Pr = 10, \lambda = 1, A = 0.5$. *Fig.8.6* shows that after increasing Prandtl number Pr the temperature profile decreases. *Fig.8.7* shows opposite behaviour of temperature profile upon increasing natural convection parameter λ . The temperature profile rapidly decreases by increasing the value of second grade parameter A (see *Fig.8.8*) and similar behaviour of temperature profile is examined by increasing the values of Reynold number Re (see *Fig.8.9*). *Fig.8.10* shows the convergence region for temperature profile through h-curves for different values of Prandtl number Pr when $\lambda = 1, Re = 2, A = 0.5$.

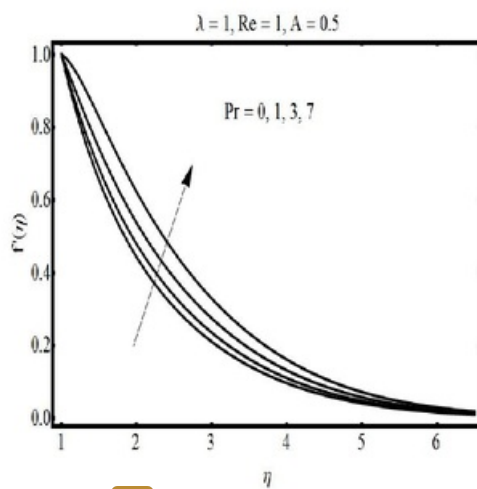


Fig.8.1 Influence of Prandtl number on velocity profile

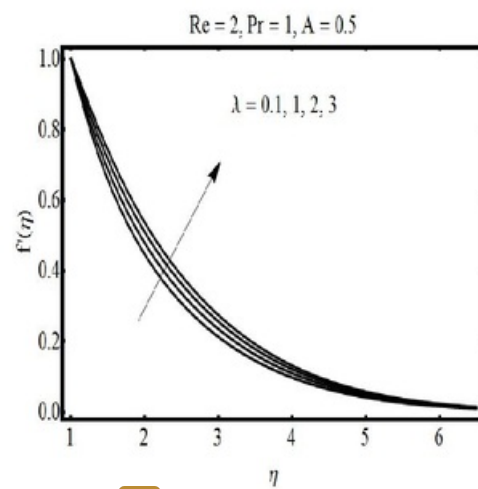


Fig.8.2 Influence of natural convection parameter on velocity profile

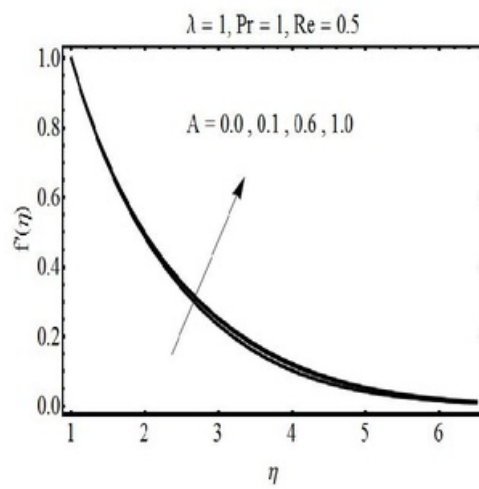


Fig.8.3 Influence of second grade parameter on velocity profile

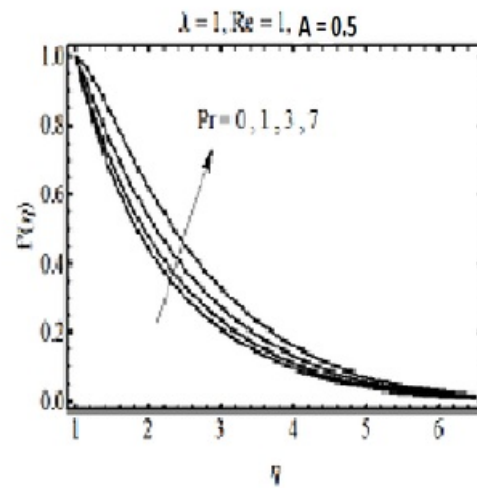


Fig.8.4 Influence of Reynolds number on velocity profile

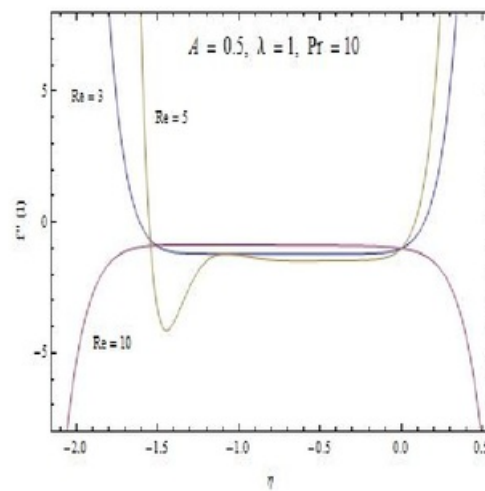
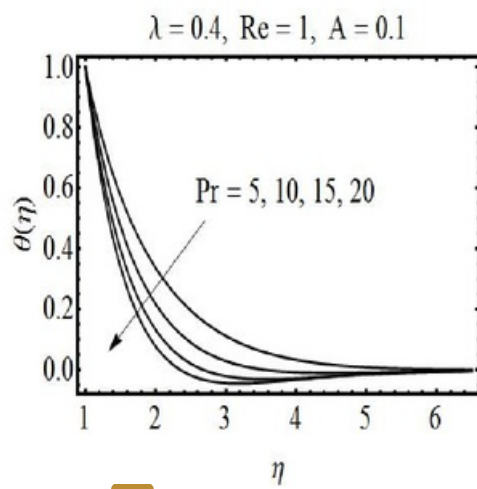
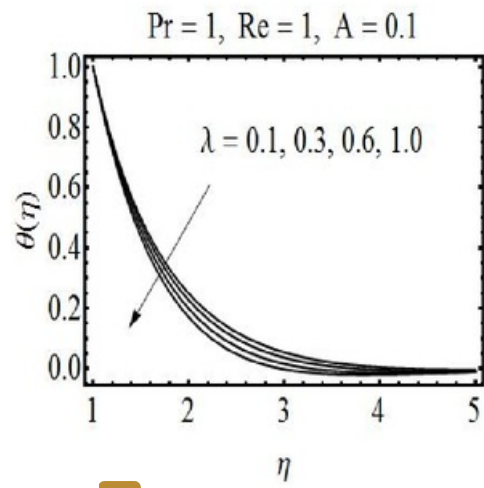


Fig.8.5 h-curve for velocity profile



30
Fig.8.6 Influence of Prandtl number on temperature profile



30
Fig.8.7 Influence of natural convection on temperature profile

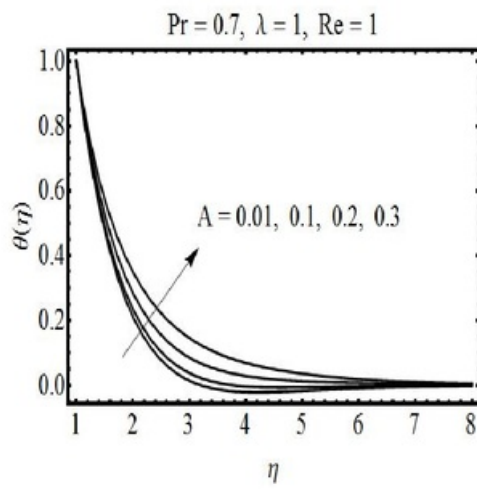


Fig.8.8 Influence of second grade parameter on temperature profile

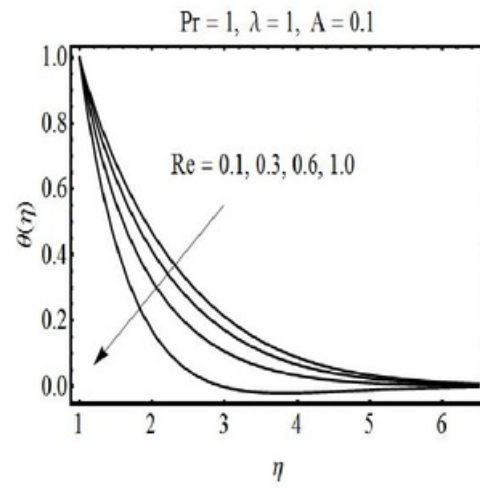


Fig.8.9 Influence of Reynolds number on temperature profile

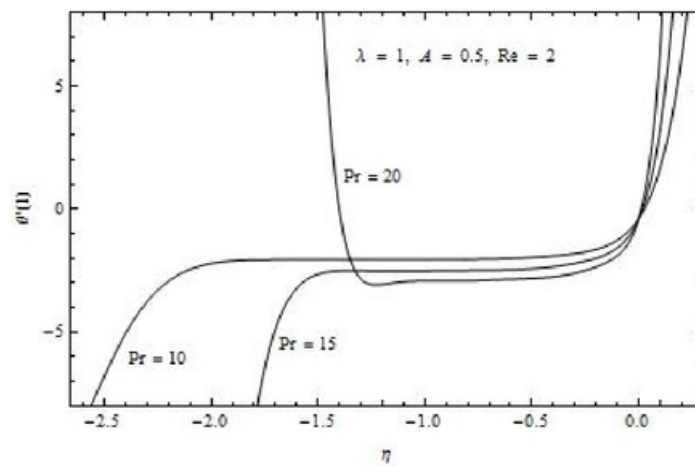


Fig.8.10 h-curve for temperature profile

Table 8.1 : Skin friction coefficient at the surface of the cylinder.

Re\Pr	0.7	1.0	7.0	10.0	15.0
0.5	0.331799	0.362456	0.843729	1.01324	1.1986
1.0	0.398152	0.457414	1.20143	1.4362	1.76274
1.5	0.459415	0.537164	1.4491	1.73577	2.13661
2.0	0.516379	0.612262	1.67114	2.0068	2.46585
2.5	0.568956	0.679781	1.86795	2.243470	2.689060

Table 8.2 : Local Nusselt numbers.

Re\λ	0.0	0.5	1.0	1.5	2.0
0.5	0.853004	0.823586	0.794351	0.765297	0.736421
1.0	1.00715	0.95683	0.907285	0.858489	0.810423
3.0	1.47889	1.38199	1.28968	1.20125	1.11607
5.0	1.83133	1.70796	1.59150	1.48009	1.37257
10.0	2.47349	2.32467	2.16570	2.01174	1.86475

8.6 Conclusions

The homotopy analysis method is employed to study the natural convection boundary layer flow of second grade fluid past an exponentially stretched cylinder. The main findings of the study are summarized as below:

- The velocity profile increases for larger Prandtl number, natural convection parameter and second grade parameter but it decreases by increasing Reynold number.
- The temperature profile increases on increasing Reynold number, natural convection parameter and Prandtl number but it decreases by increasing second grade parameter.
- Skin friction coefficient is an increasing function of Reynold and Prandtl numbers.
- Local Nusselt number enhances upon increasing natural convection parameter but it decreases by increasing Reynold number.

Bibliography

- [1] L. Prandtl, Über Flüssigkeitsbewegungen bei sehr kleiner Reibung, Verhandlg. III Intern. Math. Kongr. Heidelberg, (1904) 484-491.
- [2] H. Blasius, Grenzschichten in Flüssigkeiten mit kleiner Reibung, Z. Math. Phys. 56(1) (1908) 1-37.
- [3] M. S. Abel, M. M. Nandeppanavar, S. B. Malipatil, Heat transfer in a second grade fluid through a porous medium from a permeable stretching sheet with non-uniform heat source/sink, Int. J. Heat Mass Tran. 53 (2010) 1788-1795.
- [4] B. Sahoo, Y. Do, Effects of slip on sheet-driven flow and heat transfer of a third grade fluid past a stretching sheet, Int. Comm. Heat Mass Tran. 37 (2010) 1064-1071.
- [5] B. Sahoo, S. Poncet, Blasius flow and heat transfer of fourth-grade fluid with slip, App. Math. Mech. 34(12) (2013) 1465-1480.
- [6] S. Nadeem, R. Haq, N. S. Akbar, Z. H. Khan, MHD three-dimensional Casson fluid flow past a porous linearly stretching sheet, Alexandria Eng. J. 52(4) (2013) 577-582.
- [7] N. A. Khan, H. Khan, A boundary layer flows of non-Newtonian Williamson fluid, Non-linear Eng. 3(2) (2014) 107-115.
- [8] S. A. M. Tonekaboni, R. Abkar, R. Khoeilar, On the Study of Viscoelastic Walters' B Fluid in Boundary layer flows, Math. Prob. Eng. (2012), Article ID 861508.
- [9] T. Hayat, Z. Iqbal, M. Qasim, S. Obaidat, Steady flow of an Eyring Powell fluid over a moving surface with convective boundary conditions, Int. J. Heat Mass Tran. 55 (2012) 1817-1822.

- [10] Abdul Rehman, S. Nadeem, Mixed convection heat transfer in micropolar nanofluid over a vertical slender cylinder, *Chin. Phys. Lett.* 29(12) (2012) 124701.
- [11] C. Wang, C. Chen, Mixed convection boundary layer flow of non-Newtonian fluids along vertical wavy plates, *Int. J. Heat Fluid Flow*, 23 (2002) 831-839.
- [12] N. A. Khan, F. Riaz, F. Sultan, Effects of chemical reaction and magnetic field on a couple stress fluid over a non-linearly stretching sheet, *Eur. Phys. J. Plus* 129(18) (2014) 1-12.
- [13] S. Nadeem, R. Haq, Z. H. Khan, Numerical study of MHD boundary layer flow of a Maxwell fluid past a stretching sheet in the presence of nanoparticles, *J. Taiwan Ins. Che. Eng.* 45 (2014) 121-126.
- [14] N. S. Akbar, S. Nadeem, R. Haq. Z. H. Khan, Numerical solutions of Magnetohydrodynamic boundary layer flow of tangent hyperbolic fluid towards a stretching sheet, *Indian J. Phys.* 87(11) (2013) 1121-1124.
- [15] R. Malik, M. Khan, A. Munir, W. A. Khan, Flow and heat transfer in Sisko fluid with convective boundary condition, *Plos One*, 9(10) (2014) e107989.
- [16] T. Hayat, S. Asad, M. Mustafa, A. Alsaedi, Boundary layer flow of Carreau fluid over a convectively heated stretching sheet, *App. Math. Comp.* 246 (2014) 12-22.
- [17] M. A. A. Hamad, S. M. AbdEl-Gaied, W. A. Khan, Thermal jump effects on boundary layer flow of a Jeffrey fluid near the stagnation point on a stretching/shrinking sheet with variable thermal conductivity, *J. Fluids*, (2013) Article ID 749271.
- [18] T. Hayat, S. Mumtaz, Resonant oscillations of plate in an electrically conducting rotating Johnson-Segalman fluid, *Comp. Math. App.* 50 (2005) 1669-1676.
- [19] N. Phan-Thien, Stagnation flows for the Oldroyd-B fluid, *Rheologica Acta* , 23(2) (1984) 172-176.
- [20] P. Ravindran, J. M. Krishnan, K. R. Rajagopal , A note on the flow of a Burgers' fluid in an orthogonal rheometer, *Int. J. Eng. Sci.* 42(20) (2004) 1973-1985.

- [21] R. G. Pai, A. Kandasamy, Entrance region flow of Herschel-Bulkley fluid in an annular cylinder, *App. Math.* 5 (2014) 1964-1976.
- [22] N. Nirmalkar, R. P. Chhabra, R. J. Poole, On creeping flow of a Bingham plastic fluid past a square cylinder, *J. Non-Newtonian Fluid Mech.* 171 (2012) 17-30.
- [23] L. J. Crane, Flow past a stretching plate. *J. Appl. Math. Phys. (ZAMP)*. 21 (1970) 645-647.
- [24] D. Pal, Mixed convection heat transfer in the boundary layers on an exponentially stretching surface with magnetic field. *Appl. Math. Comp.* 217 (2010) 2356-2369.
- [25] T. R. Mahapatra, A. S. Gupta, Heat transfer in stagnation-point flow towards a stretching sheet, *Heat Mass Transfer* 38 (2002) 517-521.
- [26] N. Bachok, A. Ishak, I. Pop, Stagnation-point flow over a stretching/shrinking sheet in a nanofluid, *Nanoscale Res. Lett.* 6 (2011) 623.
- [27] T. C. Chiam, Magnetohydrodynamic heat transfer over a non-isothermal stretching sheet, *Acta Mech.* 122 (1997) 169-179.
- [28] M. Z. Salleh, R. Nazar, I. Pop, Boundary layer flow and heat transfer over a stretching sheet with Newtonian heating, *J. Taiwan Ins. Che.Eng.* 41 (2010) 651-655.
- [29] S. Mukhopadhyay, Slip effects on MHD boundary layer flow over an exponentially stretching sheet with suction/blowing and thermal radiation, *Ain Shams Eng. J.* 4 (2013) 485-491.
- [30] S. Mukhopadhyay, MHD boundary layer flow and heat transfer over an exponentially stretching sheet embedded in a thermally stratified medium, *Alexandria Eng. J.* 52 (2013) 259-265.
- [31] T. Fang, Y. Zhong, Viscous flow over a shrinking sheet with an arbitrary surface velocity, *Commun Nonlinear Sci Numer Simulat* 15 (2010) 3768-3776.
- [32] R. Bhargava, S. Sharma, H. S. Takhar, O. A. Beg, P. Bhargava, Numerical Solutions for Micropolar Transport Phenomena over a Nonlinear Stretching Sheet, *Nonlinear Analysis: Modelling and Control*, 12(1) (2007) 45-63.

- [33] T. Fang, S. Yao, J. Zhang, Abdul Aziz, Viscous flow over a shrinking sheet with a second order slip flow model, *Commun Nonlinear Sci Numer Simulat* 15 (2010) 1831-1842.
- [34] J. H. Merkin, V. Kumaran, The unsteady MHD boundary-layer flow on a shrinking sheet, *European Journal of Mechanics B/Fluids* 29 (2010) 357-363.
- [35] N. A. Yacob, A. Ishak, I. Pop, Melting heat transfer in boundary layer stagnation-point flow towards a stretching/shrinking sheet in a micropolar fluid, *Computers & Fluids* 47 (2011) 16-21.
- [36] L. Zheng, J. Niu, X. Zhang, L. Ma, Dual solutions for flow and radiative heat transfer of a micropolar fluid over stretching/shrinking sheet, *International Journal of Heat and Mass Transfer* 55 (2012) 7577-7586.
- [37] A. Ishak, R. Nazar, I. Pop, Uniform suction/blowing effect on flow and heat transfer due to a stretching cylinder, *Applied Mathematical Modelling* 32 (2008) 2059-2066.
- [38] A. Ishak, MHD boundary layer flow due to an exponentially stretching sheet with radiation effect, *Sains Malaysiana* 40(4) (2011) 391-395.
- [39] K. Govardhan, N. Kishan, Unsteady MHD boundary layer flow of an incompressible micropolar fluid over a stretching sheet, *Journal of Applied Fluid Mechanics*, 5(3) (2012) 23-28.
- [40] A. Ahmad, S. Asghar, Flow of a second grade fluid over a sheet stretching with arbitrary velocities subject to a transverse magnetic field, *Applied Mathematics Letters* 24 (2011) 1905-1909.
- [41] P. D. Weidman, E. Magyari, Generalized Crane flow induced by continuous surfaces stretching with arbitrary velocities, *Acta Mech* 209 (2010) 353-362.
- [42] J. Phakirappa, P. H. Veena, V. K. Pravin, Boundary layer flow and heat transfer flow past stretching sheet with temperature gradient dependent heat sink and internal heat eneration, *Int. J. of Mod. Eng. Res. (IJMER)*, 2(5) (2012) 3298-3305.

- [43] M. A. A. Mahmoud, M. Abd-Elaty Mahmoud, S. E. Waheed, Hydromagnetic boundary layer micropolar fluid flow over a stretching surface embedded in a non-Darcian porous medium with radiation, *Math. Prob. in Eng.*, Article ID 39392 (2006) 1–10.
- [44] F. T. Gang, Z. Ji, Z. Y. Fang, T. Hua, Unsteady viscous flow over an expanding stretching cylinder, *Chin. Phys. Lett.* 28(12) (2011) 124707.
- [45] H. A. Attia, Heat transfer in a stagnation point flow of a micropolar fluid over a stretching surface with heat generation/absorption, *Tamk. J. of Sci. and Eng.*, 9(4) (2006) 299–305.
- [46] B. Bidin, R. Nazar, Numerical solution of the boundary layer flow over an exponentially stretching sheet with thermal radiation, *Eur. J. of Sci. Res.* 33(4) (2009) 710–717.
- [47] H. Rosali, A. Ishak, I. Pop, Micropolar fluid flow towards a stretching/shrinking sheet in a porous medium with suction, *Int. Comm. in Heat and Mass Tran.* 39 (2012) 826–829.
- [48] M. Turkyilmazoglu, MHD fluid flow and heat transfer due to a stretching rotating disk, *Int. J. of Ther. Sci.* 51 (2012) 195–201.
- [49] M. A. Seddeek, Effects of Hall and ion-slip currents on magneto-micropolar fluid and heat transfer over a non-isothermal stretching sheet with suction and blowing, *Proc. R. Soc. Lond. A* (2001) 457, 3039–3050.
- [50] P.K. Kameswaran, S. Shaw, P. Sibanda, P.V.S.N. Murthy, Homogeneous–heterogeneous reactions in a nanofluid flow due to a porous stretching sheet, *Int. J. of Heat and Mass Trans.* 57 (2013) 465–472.
- [51] W. Ibrahim, B. Shankar, MHD boundary layer flow and heat transfer of a nanofluid past a permeable stretching sheet with velocity, thermal and solutal slip boundary conditions, *Comp. & Fluids* 75 (2013) 1–10.
- [52] N. Bachok, A. Ishak, Flow and heat transfer over a stretching cylinder with prescribed surface heat flux, *Malaysian Journal of Mathematical Sciences* 4(2) (2010) 159–169.
- [53] O.D. Makinde, W.A. Khan, Z.H. Khan, Buoyancy effects on MHD stagnation point flow and heat transfer of a nanofluid past a convectively heated stretching/shrinking sheet, *International Journal of Heat and Mass Transfer* 62 (2013) 526–533.

- [54] W. Ibrahim, B. Shankar, M. M. Nandeppanavar, MHD stagnation point flow and heat transfer due to nanofluid towards a stretching sheet, *International Journal of Heat and Mass Transfer* 56 (2013) 1-9.
- [55] A. Ishak and R. Nazar, Laminar boundary flow along a stretching cylinder, *European Journal of Scientific Research* 36 (2009) 22-29.
- [56] L.G. Grubka and K.M. Bobba, Heat transfer characteristics of a continuous stretching surface with variable temperature, *Journal of Heat Transfer* 107 (1985) 248-250.
- [57] S. Nadeem, S. Akram, Peristaltic transport of a hyperbolic tangent fluid model in an asymmetric channel, *Z. Naturforsch.* 64a (2009) 559-567.
- [58] S. J. Liao, *Beyond Perturbation: Introduction to Homotopy Analysis Method*, Chapman and Hall, CRC Press, Boca Raton, 2003.

Numerical study of non-Newtonian fluids past a stretching cylinder

ORIGINALITY REPORT

%**19**

SIMILARITY INDEX

%**7**

INTERNET SOURCES

%**17**

PUBLICATIONS

%**5**

STUDENT PAPERS

PRIMARY SOURCES

1

Submitted to Higher Education Commission
Pakistan

Student Paper

%**2**

2

Nazar, R.. "Stagnation point flow of a micropolar fluid towards a stretching sheet", International Journal of Non-Linear Mechanics, 200409

Publication

%**1**

3

Abel, S.. "Non-Newtonian magnetohydrodynamic flow over a stretching surface with heat and mass transfer", International Journal of Non-Linear Mechanics, 200409

Publication

%**1**

4

Olajuwon, B.. "Convection heat and mass transfer in a hydromagnetic flow of a second grade fluid in the presence of thermal radiation and thermal diffusion", International Communications in Heat and Mass Transfer, 201103

Publication

<%**1**

5	doiserbia.nb.rs Internet Source	<% 1
6	Hayat, T., M. Ijaz Khan, M. Farooq, Tabassam Yasmeeen, and A. Alsaedi. "Stagnation point flow with Cattaneo-Christov heat flux and homogeneous-heterogeneous reactions", <i>Journal of Molecular Liquids</i> , 2016. Publication	<% 1
7	Submitted to Universiti Teknologi Malaysia Student Paper	<% 1
8	Sandeep, Naramgari, Chalavadi Sulochana, and Animasaun Isaac Lare. "Stagnation-Point Flow of a Jeffrey Nanofluid over a Stretching Surface with Induced Magnetic Field and Chemical Reaction", <i>International Journal of Engineering Research in Africa</i> , 2015. Publication	<% 1
9	Nadeem, S., S. T. Hussain, and Changhoon Lee. "Flow of a Williamson fluid over a stretching sheet", <i>Brazilian Journal of Chemical Engineering</i> , 2013. Publication	<% 1
10	HAYAT, T, M WAQAS, S A SHEHZAD, and A ALSAEDI. "Stretched flow of Carreau nanofluid with convective boundary condition", <i>Pramana</i> , 2015. Publication	<% 1
11	Submitted to National Chiao-Tung University	

12

Submitted to International Islamic University
Malaysia

Student Paper

<% 1

13

Malik, M.Y., T. Salahuddin, Arif Hussain, and
S. Bilal. "MHD flow of tangent hyperbolic fluid
over a stretching cylinder: Using Keller box
method", Journal of Magnetism and Magnetic
Materials, 2015.

Publication

<% 1

14

Mustafa, Irfan, Tariq Javed, and Abid
Majeed. "MHD mixed convection stagnation
point flow of a nanofluid over a vertical plate
with viscous dissipation", Canadian Journal of
Physics, 2015.

Publication

<% 1

15

jyoung.im.ntu.edu.tw

Internet Source

<% 1

16

Munir, Asif, Azeem Shahzad, and Masood
Khan. "Convective Flow of Sisko Fluid over a
Bidirectional Stretching Surface", PLoS ONE,
2015.

Publication

<% 1

17

International Journal of Numerical Methods
for Heat & Fluid Flow, Volume 19, Issue 3-4
(2009-05-17)

Publication

<% 1

18

mecano.gme.usherbrooke.ca

Internet Source

<% 1

19

International Journal of Numerical Methods for Heat & Fluid Flow, Volume 25, Issue 3 (2015)

Publication

<% 1

20

Paliwal, B.. "Power law fluid flow past a square cylinder: momentum and heat transfer characteristics", Chemical Engineering Science, 200312

Publication

<% 1

21

Ibrahim, Wubshet, and Bandari Shankar. "MHD boundary layer flow and heat transfer of a nanofluid past a permeable stretching sheet with velocity, thermal and solutal slip boundary conditions", Computers & Fluids, 2013.

Publication

<% 1

22

Yuan-Hsiang Chu. "MIXED CONVECTION OF MICROPOLAR FLUIDS ALONG A VERTICAL WAVY SURFACE WITH A DISCONTINUOUS TEMPERATURE PROFILE", Numerical Heat Transfer Part A Applications, 11/15/2002

Publication

<% 1

23

Cheng, C.Y.. "Non-Darcy natural convection heat and mass transfer from a vertical wavy surface in saturated porous media", Applied Mathematics and Computation, 20061115

Publication

<% 1

- | | | |
|----|--|------|
| 24 | Kumari, M.. "MHD flow over a wedge with large blowing rates", International Journal of Engineering Science, 19980201
Publication | <% 1 |
| 25 | pkukmweb.ukm.my
Internet Source | <% 1 |
| 26 | Das, S., S. Chakraborty, R. N. Jana, and O. D. Makinde. "Entropy analysis of unsteady magneto-nanofluid flow past accelerating stretching sheet with convective boundary condition", Applied Mathematics and Mechanics, 2015.
Publication | <% 1 |
| 27 | Bhattacharyya, Krishnendu, G C Layek, and G S Seth. "Soret and Dufour effects on convective heat and mass transfer in stagnation-point flow towards a shrinking surface", Physica Scripta, 2014.
Publication | <% 1 |
| 28 | Nandy, Samir Kumar. "Unsteady flow of Maxwell fluid in the presence of nanoparticles toward a permeable shrinking surface with Navier slip", Journal of the Taiwan Institute of Chemical Engineers, 2015.
Publication | <% 1 |
| 29 | www.m-hikari.com
Internet Source | <% 1 |

30

Eckert, E.R.G.. "Heat transfer - a review of 1996 literature", International Journal of Heat and Mass Transfer, 20000415

Publication

<% 1

31

Iqbal, Z., M. Qasim, M. Awais, T. Hayat, and S. Asghar. "Stagnation-Point Flow by an Exponentially Stretching Sheet in the Presence of Viscous Dissipation and Thermal Radiation", Journal of Aerospace Engineering, 2015.

Publication

<% 1

32

Shateyi, S., and O. D. Makinde. "Hydromagnetic Stagnation-Point Flow towards a Radially Stretching Convectively Heated Disk", Mathematical Problems in Engineering, 2013.

Publication

<% 1

33

S. Hussnain. "Three-dimensional channel flow of second grade fluid in rotating frame", Applied Mathematics and Mechanics, 03/2012

Publication

<% 1

34

Patil, P.M.. "Unsteady effects on mixed convection boundary layer flow from a permeable slender cylinder due to non-linearly power law stretching", Computers and Fluids, 20120315

Publication

<% 1

35

Internet Source

<% 1

36

Mahmoud, Mostafa A.A. Mahmoud,
Mahmoud A. "Hydromagnetic boundary layer
micropolar fluid flow over a stretching
surface embedded in a non-Darci",
Mathematical Problems in Engineering,
Annual 2006 Issue

Publication

<% 1

37

Zheng, Liancun, Jiajia Niu, Xinxin Zhang, and
Lianxi Ma. "Dual solutions for flow and
radiative heat transfer of a micropolar fluid
over stretching/shrinking sheet", International
Journal of Heat and Mass Transfer, 2012.

Publication

<% 1

38

Marinca, V., and N. Herişanu. "On the flow of
a Walters-type B' viscoelastic fluid in a
vertical channel with porous wall",
International Journal of Heat and Mass
Transfer, 2014.

Publication

<% 1

39

www.hrpub.org

Internet Source

<% 1

40

ethesis.nitrkl.ac.in

Internet Source

<% 1

41

Submitted to University of Witwatersrand

Student Paper

<% 1

Patrick D. Weidman. "Generalized Crane flow

42 induced by continuous surfaces stretching with arbitrary velocities", Acta Mechanica, 06/21/2009 $< \% 1$
Publication

43 Dessie, Hunegnaw, and Naikoti Kishan. "Unsteady MHD Flow of Heat and Mass Transfer of Nanofluids over Stretching Sheet with a Non-Uniform Heat/Source/Sink Considering Viscous Dissipation and Chemical Reaction", International Journal of Engineering Research in Africa, 2015. $< \% 1$
Publication

44 l3ux02.univ-lille3.fr $< \% 1$
Internet Source

45 ne.nikkeibp.co.jp $< \% 1$
Internet Source

46 Hayat, T., Sadia Asad, and A. Alaseadi. "MHD Mixed Convection Flow of Burgers' Fluid in a Thermally Stratified Medium", Journal of Aerospace Engineering, 2016. $< \% 1$
Publication

47 Ibrahim, Wubshet, and O.D. Makinde. "The Effect of Double Stratification on Boundary-Layer Flow and Heat Transfer of Nanofluid over a Vertical Plate", Computers & Fluids, 2013. $< \% 1$
Publication

48 Khan, Junaid Ahmad, M. Mustafa, T. Hayat, $< \% 1$

M. Sheikholeslami, and A. Alsaedi. "Three-Dimensional Flow of Nanofluid Induced by an Exponentially Stretching Sheet: An Application to Solar Energy", PLoS ONE, 2015.

Publication

- 49 Khader, M. M., and A. M. Megahed. "Differential transformation method for studying flow and heat transfer due to stretching sheet embedded in porous medium with variable thickness, variable thermal conductivity, and thermal radiation", Applied Mathematics and Mechanics, 2014. <% 1
- Publication
-

- 50 Noreen Sher Akbar. "Endoscopic Effects on Peristaltic Flow of a Nanofluid", Communications in Theoretical Physics, 10/2011 <% 1
- Publication
-

- 51 Nadeem, S., and Rizwan UI Haq. "MHD Boundary Layer Flow of a Nano Fluid past a Porous Shrinking Sheet with Thermal Radiation", Journal of Aerospace Engineering, 2012. <% 1
- Publication
-

- 52 Makanda, Gilbert Makinde, O.D. Sibanda, . "Natural convection of viscoelastic fluid from a cone embedded in a porous medium with viscous dissip", Mathematical Problems in <% 1

53

Uddin, Md Jashim, N H Md Yusoff, O Anwar Bdg, and Ahamd Izani Ismail. "Lie group analysis and numerical solutions for non-Newtonian nanofluid flow in a porous medium with internal heat generation", *Physica Scripta*, 2013.

Publication

<% 1

54

Hayat, Tasawar, Maria Imtiaz, Ahmed Alsaedi, and Saleh Almezal. "On Cattaneo–Christov heat flux in MHD flow of Oldroyd-B fluid with homogeneous–heterogeneous reactions", *Journal of Magnetism and Magnetic Materials*, 2016.

Publication

<% 1

55

T. Ray Mahapatra. "Heat transfer in stagnation-point flow towards a stretching sheet", *Heat and Mass Transfer*, 06/01/2002

Publication

<% 1

56

Akilu, S., and M. Narahari. "Effects of Heat Generation or Absorption on Free Convection Flow of a Nanofluid Past an Isothermal Inclined Plate", *Advanced Materials Research*, 2014.

Publication

<% 1

57

www.waset.org

Internet Source

<% 1

58

Alsaedi, and Raana Mansoor.

"Magnetohydrodynamic Three-Dimensional Flow of Nanofluid by a Porous Shrinking Surface", Journal of Aerospace Engineering, 2015.

Publication

<% 1

59

nsp.naturalspublishing.com

Internet Source

<% 1

60

Butt, Adnan Saeed Ali, Asif. "Analysis of entropy generation effects in flow and heat transfer of viscous fluid through a porous m", International Journal of Exergy, Nov 7 2015 Issue

Publication

<% 1

61

Hayat, T., S. A. Shehzad, and A. Alsaedi. "MHD Three-Dimensional Flow by an Exponentially Stretching Surface with Convective Boundary Condition", Journal of Aerospace Engineering, 2014.

Publication

<% 1

62

paper

Student Paper

<% 1

63

Mustafa, Irfan, Tariq Javed, and Abuzar Ghaffari. "Heat transfer in MHD stagnation point flow of a ferrofluid over a stretchable rotating disk", Journal of Molecular Liquids, 2016.

Publication

<% 1

64

Eldabe, N.T.. "Chebyshev finite difference method for MHD flow of a micropolar fluid past a stretching sheet with heat transfer", Applied Mathematics and Computation, 20050114

Publication

<% 1

65

eprints.aston.ac.uk

Internet Source

<% 1

66

Salleh, M.Z.. "Boundary layer flow and heat transfer over a stretching sheet with Newtonian heating", Journal of the Taiwan Institute of Chemical Engineers, 201011

Publication

<% 1

67

eprints.utm.my

Internet Source

<% 1

68

Khan, Junaid Ahmad, M. Mustafa, T. Hayat, and A. Alsaedi. "Numerical study on three-dimensional flow of nanofluid past a convectively heated exponentially stretching sheet", Canadian Journal of Physics, 2015.

Publication

<% 1

69

Sarif, N.M., M.Z. Salleh, and R. Nazar. "Numerical Solution of Flow and Heat Transfer over a Stretching Sheet with Newtonian Heating using the Keller Box Method", Procedia Engineering, 2013.

Publication

<% 1

70

M. A. Antar. "Steady and transient liquid

sphere heating in a convective gas stream",
Heat and Mass Transfer, 04/07/2000

Publication

<% 1

71

Goldstein, R.J.. "Heat transfer - a review of
1999 literature", International Journal of Heat
and Mass Transfer, 200110

Publication

<% 1

72

P. M. Patil. "Effects of surface mass transfer
on unsteady mixed convection flow over a
vertical cone with chemical reaction", Heat
and Mass Transfer, 05/08/2011

Publication

<% 1

73

Sajid, M., and T. Hayat. "Influence of thermal
radiation on the boundary layer flow due to
an exponentially stretching sheet",
International Communications in Heat and
Mass Transfer, 2008.

Publication

<% 1

74

Submitted to King Saud University

Student Paper

<% 1

75

metrarail.com

Internet Source

<% 1

76

Khan, Masood, and Azeem Shahzad. "On
axisymmetric flow of Sisko fluid over a
radially stretching sheet", International
Journal of Non-Linear Mechanics, 2012.

Publication

<% 1

77

M. Z. Salleh. "Numerical solutions of free

convection boundary layer flow on a solid sphere with Newtonian heating in a micropolar fluid", Meccanica, 11/16/2011

Publication

<% 1

78

Liu, I.C.. "Heat transfer over a bidirectional stretching sheet with variable thermal conditions", International Journal of Heat and Mass Transfer, 20080715

Publication

<% 1

79

Majeed, Abid, Tariq Javed, and Sumayya Shami. "Numerical Analysis of Walters-B Fluid Flow and Heat Transfer over a Stretching Cylinder", Canadian Journal of Physics, 2016.

Publication

<% 1

80

M. A. Hossain. "Free convection from a vertical permeable circular cone with non-uniform surface heat flux", Heat and Mass Transfer, 04/27/2001

Publication

<% 1

81

www.usbr.gov

Internet Source

<% 1

82

Ghalambaz, M. Izadpanahi, E. Noghrehabad. "Study of the boundary layer heat transfer of nanofluids over a stretching sheet: passive control of ", Canadian Journal of Physics, July 2015 Issue

Publication

<% 1

Bikash Sahoo. "Flow and heat transfer of an

83

electrically conducting third grade fluid past an infinite plate with partial slip", *Meccanica*, 10/16/2009

Publication

<% 1

84

International Journal of Numerical Methods for Heat & Fluid Flow, Volume 24, Issue 7 (2014-09-16)

Publication

<% 1

85

Kothandapani, M., and J. Prakash. "Effects of thermal radiation parameter and magnetic field on the peristaltic motion of Williamson nanofluids in a tapered asymmetric channel", *International Journal of Heat and Mass Transfer*, 2015.

Publication

<% 1

86

Prasad, V. Ramachandra, S. Abdul Gaffar, E. Keshava Reddy, and O. Anwar Bég. "Numerical study of non-Newtonian Jeffreys fluid from a permeable horizontal isothermal cylinder in non-Darcy porous medium", *Journal of the Brazilian Society of Mechanical Sciences and Engineering*, 2014.

Publication

<% 1

87

Turkyilmazoglu, Mustafa. "Three dimensional MHD stagnation flow due to a stretchable rotating disk", *International Journal of Heat and Mass Transfer*, 2012.

Publication

<% 1

88

Nirmalkar, N., R. P. Chhabra, and R. J. Poole.

"Numerical Predictions of Momentum and Heat Transfer Characteristics from a Heated Sphere in Yield-Stress Fluids", Industrial & Engineering Chemistry Research, 2013.

Publication

<% 1

89

Ajibade, Abiodun O., and Ayuba M. Umar. "Effect of chemical reaction and radiation absorption on the unsteady MHD free convection Couette flow in a vertical channel filled with porous materials", Afrika Matematika, 2015.

Publication

<% 1

90

Hayat, T., Z. Iqbal, M. Mustafa, and A. Alsaedi. "Momentum and heat transfer of an upper-convected Maxwell fluid over a moving surface with convective boundary conditions", Nuclear Engineering and Design, 2012.

Publication

<% 1

91

Ferdows, M., Md. Jashim Uddin, and A.A. Afify. "Scaling group transformation for MHD boundary layer free convective heat and mass transfer flow past a convectively heated nonlinear radiating stretching sheet", International Journal of Heat and Mass Transfer, 2013.

Publication

<% 1

92

Seddeek, M.A.. "Analytical solution for the effect of radiation on flow of a magneto-micropolar fluid past a continuously moving

<% 1

93

SRINIVAS, S., P. B. A. REDDY, and B. S. R. V. PRASAD. "EFFECTS OF CHEMICAL REACTION AND THERMAL RADIATION ON MHD FLOW OVER AN INCLINED PERMEABLE STRETCHING SURFACE WITH NON-UNIFORM HEAT SOURCE/SINK: AN APPLICATION TO THE DYNAMICS OF BLOOD FLOW", Journal of Mechanics in Medicine and Biology, 2014.

Publication

<% 1

94

Abbas, Z. Sheikh, Mariam Sajid, M.. "Hydromagnetic stagnation point flow of a micropolar viscoelastic fluid towards a stretching/shrinkin", Canadian Journal of Physics, Oct 2014 Issue

Publication

<% 1

95

www.sciencepubco.com

Internet Source

<% 1

96

Patel, S.A., and R.P. Chhabra. "Steady flow of Bingham plastic fluids past an elliptical cylinder", Journal of Non-Newtonian Fluid Mechanics, 2013.

Publication

<% 1

97

Submitted to Universiti Sains Malaysia

Student Paper

<% 1

98	Hayat, Tasawar, Maria Imtiaz, and Ahmed Alsaedi. "MHD 3D flow of nanofluid in presence of convective conditions", Journal of Molecular Liquids, 2015. Publication	<% 1
99	www.iteverywhere.com Internet Source	<% 1
100	Multidiscipline Modeling in Materials and Structures, Volume 9, Issue 4 (2013-11-02) Publication	<% 1
101	Abel, M.S.. "Numerical solution of the momentum and heat transfer equations for a hydromagnetic flow due to a stretching sheet of a non-uniform property micropolar liquid", Applied Mathematics and Computation, 20110215 Publication	<% 1
102	www.vkingpub.com Internet Source	<% 1
103	Sundaravadivelu, K.. "Double diffusive nonlinear convection in a square cavity", Fluid Dynamics Research, 200011 Publication	<% 1
104	www.fao.org Internet Source	<% 1
105	www.theflatnet.de Internet Source	<% 1

- | | | |
|--|---|----------------|
| <div style="background-color: #6b8e23; color: white; padding: 2px 5px; display: inline-block;">106</div> | <p>Zhu, Jing, Liu Zheng, Liancun Zheng, and Xinxin Zhang. "Second-order slip MHD flow and heat transfer of nanofluids with thermal radiation and chemical reaction", Applied Mathematics and Mechanics, 2015.</p> <p>Publication</p> | <p><% 1</p> |
| <hr/> | | |
| <div style="background-color: #2c3e50; color: white; padding: 2px 5px; display: inline-block;">107</div> | <p>A S Gupta. "Effects of suction or blowing on the velocity and temperature distribution in the flow past a porous flat plate of a power-law fluid", Fluid Dynamics Research, 08/2003</p> <p>Publication</p> | <p><% 1</p> |
| <hr/> | | |
| <div style="background-color: #2980b9; color: white; padding: 2px 5px; display: inline-block;">108</div> | <p>Rana, Puneet, R. Bhargava, and O.A. BÃ©g. "Numerical solution for mixed convection boundary layer flow of a nanofluid along an inclined plate embedded in a porous medium", Computers & Mathematics with Applications, 2012.</p> <p>Publication</p> | <p><% 1</p> |
| <hr/> | | |
| <div style="background-color: #e74c3c; color: white; padding: 2px 5px; display: inline-block;">109</div> | <p>Rauf, A., M.K. Siddiq, F.M. Abbasi, M.A. Meraj, M. Ashraf, and S.A. Shehzad. "Influence of convective conditions on three dimensional mixed convective hydromagnetic boundary layer flow of Casson nanofluid", Journal of Magnetism and Magnetic Materials, 2016.</p> <p>Publication</p> | <p><% 1</p> |
| <hr/> | | |
| <div style="background-color: #e91e63; color: white; padding: 2px 5px; display: inline-block;">110</div> | <p>ccsenet.org</p> <p>Internet Source</p> | <p><% 1</p> |

111	manuscript.sciknow.org Internet Source	<% 1
112	www.boundaryvalueproblems.com Internet Source	<% 1
113	Munawar, Sufian, Ahmer Mehmood, and Asif Ali. "Three-dimensional squeezing flow in a rotating channel of lower stretching porous wall", Computers & Mathematics with Applications, 2012. Publication	<% 1
114	Makanda, Gilbert Shaw, Sachin Sibanda, P. "Diffusion of chemically reactive species in casson fluid flow over an unsteady stretching surface in", Mathematical Problems in Engineering, Annual 2015 Issue Publication	<% 1
115	Ritz, J.-B.. "Shear-induced particle migration in a short-dwell coater", Chemical Engineering Science, 200011 Publication	<% 1
116	www.ijmes.info Internet Source	<% 1
117	International Journal of Numerical Methods for Heat & Fluid Flow, Volume 7, Issue 4 (2006-09-19) Publication	<% 1
118	Raju, C.S.K., N. Sandeep, and M. Gnaneswara Reddy. "Effect of Nonlinear	<% 1

Thermal Radiation on 3D Jeffrey Fluid Flow in the Presence of Homogeneous–Heterogeneous Reactions", International Journal of Engineering Research in Africa, 2015.

Publication

-
- 119 Patil, P.M.. "Unsteady mixed convection flow from a moving vertical plate in a parallel free stream: Influence of heat generation or absorption", International Journal of Heat and Mass Transfer, 201010 <%1

Publication

-
- 120 Hayat, Tasawar, Sumaira Qayyum, Maria Imtiaz, Faris Alzahrani, and Ahmed Alsaedi. "Partial slip effect in flow of magnetite-Fe₃O₄ nanoparticles between rotating stretchable disks", Journal of Magnetism and Magnetic Materials, 2016. <%1

Publication

-
- 121 Ibrahim, Wubshet. "The Effect of Induced Magnetic Field and Convective Boundary Condition on MHD Stagnation Point Flow and Heat Transfer of Nanofluid Past a Stretching Sheet", IEEE Transactions on Nanotechnology, 2015. <%1

Publication

-
- 122 Yazdi, Mohammad H., Shahrir Abdullah, Ishak Hashim, and Kamaruzzaman Sopian. "Effects of Viscous Dissipation on the Slip <%1

MHD Flow and Heat Transfer past a Permeable Surface with Convective Boundary Conditions", Energies, 2011.

Publication

-
- | | | |
|------------|--|------|
| 123 | International Journal of Numerical Methods for Heat & Fluid Flow, Volume 7, Issue 2-3 (2007-05-06) | <% 1 |
|------------|--|------|

Publication

-
- | | | |
|------------|--|------|
| 124 | ddfe.curtin.edu.au | <% 1 |
|------------|--|------|

Internet Source

-
- | | | |
|------------|---|------|
| 125 | Patil, P.M., S. Roy, and E. Momoniat. "Thermal diffusion and diffusion-thermo effects on mixed convection from an exponentially impermeable stretching surface", International Journal of Heat and Mass Transfer, 2016. | <% 1 |
|------------|---|------|

Publication

-
- | | | |
|------------|--|------|
| 126 | www.sp-road.sp.hkd.mlit.go.jp | <% 1 |
|------------|--|------|

Internet Source

-
- | | | |
|------------|---|------|
| 127 | KOTHANDAPANI, M., and J. PRAKASH. "THE PERISTALTIC TRANSPORT OF CARREAU NANOFUIDS UNDER EFFECT OF A MAGNETIC FIELD IN A TAPERED ASYMMETRIC CHANNEL: APPLICATION OF THE CANCER THERAPY", Journal of Mechanics in Medicine and Biology, 2014. | <% 1 |
|------------|---|------|

Publication

-
- | | | |
|------------|--|------|
| 128 | docslide.us | <% 1 |
|------------|--|------|

Internet Source

129	glass.phys.uniroma1.it Internet Source	<% 1
130	S. S. Motsa. "The Effects of Chemical Reaction, Hall, and Ion-Slip Currents on MHD Micropolar Fluid Flow with Thermal Diffusivity Using a Novel Numerical Technique", Journal of Applied Mathematics, 2012 Publication	<% 1
131	www.ijar.lit.az Internet Source	<% 1
132	ejde.math.txstate.edu Internet Source	<% 1
133	Submitted to University of Stellenbosch, South Africa Student Paper	<% 1
134	maxwellsci.com Internet Source	<% 1
135	Wong, Sin Wei, M. A. Omar Awang, Anuar Ishak, and Ioan Pop. "Boundary Layer Flow and Heat Transfer over an Exponentially Stretching/Shrinking Permeable Sheet with Viscous Dissipation", Journal of Aerospace Engineering, 2014. Publication	<% 1
136	Lee, H.R.. "Non-parallel thermal instability of forced convection flow over a heated, non-	<% 1

137

Engineering Computations, Volume 29, Issue
6 (2012-08-18)

Publication

<% 1

138

Qasim, Muhammad, Ilyas Khan, and
Sharidan Shafie. "Heat Transfer in a
Micropolar Fluid over a Stretching Sheet with
Newtonian Heating", PLoS ONE, 2013.

Publication

<% 1

139

Hayat, T., M. Bilal Ashraf, and A. Alsaedi.
"Small-Time Solutions for the Thin Film Flow
of a Casson Fluid Due to a Suddenly Moved
Plate", Journal of Aerospace Engineering,
2013.

Publication

<% 1

140

Khan, Masood, and Waqar Azeem Khan.
"Three-dimensional flow and heat transfer to
burgers fluid using Cattaneo-Christov heat
flux model", Journal of Molecular Liquids,
2016.

Publication

<% 1

141

Bachok, N.. "Melting heat transfer in
boundary layer stagnation-point flow towards
a stretching/shrinking sheet", Physics Letters
A, 20100906

Publication

<% 1

Misra, J.C.. "Flow and heat transfer of a MHD

- | | | |
|-----|---|------|
| 142 | viscoelastic fluid in a channel with stretching walls: Some applications to haemodynamics", Computers and Fluids, 200801
Publication | <% 1 |
| 143 | Aziz, Asim, Yasir Ali, Taha Aziz, and J. I. Siddique. "Heat Transfer Analysis for Stationary Boundary Layer Slip Flow of a Power-Law Fluid in a Darcy Porous Medium with Plate Suction/Injection", PLoS ONE, 2015.
Publication | <% 1 |
| 144 | Labropulu, F.. "Non-orthogonal stagnation-point flow towards a stretching surface in a non-Newtonian fluid with heat transfer", International Journal of Thermal Sciences, 201006
Publication | <% 1 |
| 145 | Wang, C.C.. "Mixed convection boundary layer flow of non-Newtonian fluids along vertical wavy plates", International Journal of Heat and Fluid Flow, 200212
Publication | <% 1 |
| 146 | Bartel, J., and K. Bencheikh. "Nuclear mean fields through self-consistent semiclassical calculations", The European Physical Journal A, 2002.
Publication | <% 1 |
| 147 | Imtiaz, Maria, Tasawar Hayat, Ahmed Alsaedi, and Aatef Hobiny. "Homogeneous- | <% 1 |

heterogeneous reactions in MHD flow due to an unsteady curved stretching surface", Journal of Molecular Liquids, 2016.

Publication

148 Siddiqui, A.M.. "Magnetohydrodynamics flow of a Burgers@? fluid in an orthogonal rheometer", Applied Mathematical Modelling, 201010 ≤ 1

Publication

149 Mitrovic, B.M.. "On the Prandtl or Schmidt number dependence of the turbulent heat or mass transfer coefficient", Chemical Engineering Science, 200402 ≤ 1

Publication

150 Wang, C.Y.. "Review of similarity stretching exact solutions of the Navier-Stokes equations", European Journal of Mechanics / B Fluids, 201109/10 ≤ 1

Publication

151 Lesage, F.. "Boundary element method in modelling of momentum transport and liquid-to-wall mass transfer in a packed-bed reactor", Chemical Engineering Science, 200001 ≤ 1

Publication

152 Hayat, T., Zakir Hussain, M. Farooq, and A. Alsaedi. "Effects of homogeneous and heterogeneous reactions and melting heat in the viscoelastic fluid flow", Journal of ≤ 1

-
- 153 de la Macorra, A.. "Interacting dark energy: Decay into fermions", *Astroparticle Physics*, 200710

Publication

-
- 154 H. S. Takhar. "Unsteady compressible boundary layer flow in the stagnation region of a sphere with a magnetic field", *Archive of Applied Mechanics (Ingenieur Archiv)*, 10/23/1997

Publication

-
- 155 M. A. Seddeek. "Effects of Hall and ion-slip currents on magneto-micropolar fluid and heat transfer over a non-isothermal stretching sheet with suction and blowing", *Proceedings of The Royal Society A Mathematical Physical and Engineering Sciences*, 12/08/2001

Publication

-
- 156 Hussain, Tariq, Sabir Ali Shehzad, Tasawar Hayat, Ahmed Alsaedi, Falleh Al-Solamy, and Muhammad Ramzan. "Radiative Hydromagnetic Flow of Jeffrey Nanofluid by an Exponentially Stretching Sheet", *PLoS ONE*, 2014.

Publication

-
- 157 Seyed Ali Madani Tonekaboni. "On the Study of Viscoelastic Walters' B Fluid in Boundary

Layer Flows", Mathematical Problems in Engineering, 2012

Publication

EXCLUDE QUOTES	OFF	EXCLUDE MATCHES	< 3 WORDS
EXCLUDE BIBLIOGRAPHY	ON		